INERTIAL STABILITY AND MESOSCALE CONVECTIVE SYSTEMS

by

KERRY ANDREW EMANUEL

S.B., Massachusetts Institute of Technology

(1976)

SUBMITTED IN PARTIAL FULFILLMENT

OF THE REQUIREMENTS FOR THE

DEGREE OF

DOCTOR OF PHILOSOPHY

at the

MASSACHUSETTS INSTITUTE OF TECHNOLOGY

(MAY, 1978)

Signature of Author. .....

Certified by.....
Thesis Supervisor

Accepted by.....
Chairman, Departmental Committee

INERTIAL STABILITY AND MESOSCALE CONVECTIVE SYSTEMS

by

KERRY ANDREW EMANUEL

Submitted to the Department of Meteorology
on 5 May 1978 in partial fulfillment of the
requirements for the Degree of Doctor of Philosophy

ABSTRACT

A clear understanding of the dynamics of cumulus convection in the atmosphere continues to evade atmospheric scientists. Although it has been recognized that persistent organized convection depends upon circulations of a length scale much greater than that of the cumulus cloud, the nature of these circulations and their interaction with cumuli remains enigmatic. These motions may be driven by the convection, as appears to be the case in tropical cyclones; in other cases the circulations may result from an instability of the larger scale flow. This paper addresses the latter possibility.

Observations of intense convective lines in temperate latitudes indicate that conditional instability and strong vertical shear of the horizontal wind are necessary prerequisites for the development of organized convection. We speculate that the large vertical shears are conducive to the mesoscale circulations associated with the convection, and on this basis proceed to carry out an investigation of the stability of shear flow to disturbances oriented parallel to the shear. It is found that as the Richardson number of the flow decreases below a critical value dependent on the diffusive characteristics and depth of the fluid, circulations of a length scale commensurate with those of observed convective lines occur. The ensuing flow patterns and pressure distributions are also comparable with those observed in connection with squall lines.

It is found that the basic mechanism of the instability is an imbalance of the Coriolis and pressure forces within the fluid, a state traditionally defined as inertial instability. Additionally, we present evidence that this instability mechanism may also account for diverse forms of banded overturning motions in the atmosphere, ranging from cirrus streaks in the jet stream to a type of Ekman Layer instability.

Thesis Supervisor: Jule G. Charney, Professor of Meteorology

ERRATA

1.) Discussions concerning the possibility that inertial instability sets in as standing oscillations are incorrect, although the conclusion that instability of this type is impossible stands. The reader is referred to Walton (1975) for a discussion of oscillatory instability in fluids with small diffusion.

2.) Page 125 does not exist.

ACKNOWLEDGEMENTS

I am most sincerely grateful for the assistance afforded me by many of the students, faculty, and staff of the Department of Meteorology. In particular, I would like to thank Professor Jule Charney for his many helpful suggestions and comments; David Andrews and Professors Frederick Sanders and Peter Stone for reading and improving the original manuscript; Steven Ricci and Isabelle Kole for their quick and artful work in drafting the figures; and Debbie Schmitt for typing the thesis. Many thanks are due Neil Gordon, with whom I engaged in numerous spirited conversations on the nature of convection, and Eddie Nelson, Linda Notzelman, Virginia Mills, and Jane McNabb who put up with me.

This research was made possible by the National Science Foundation, under grant 76-20070 ATM.

TABLE OF CONTENTS

TABLE OF CONTENTS (continued)

LIST OF FIGURES

LIST OF FIGURES (continued)

LIST OF FIGURES (continued)

"The local storm is isolated, but its behavior is intimately related to the large-scale properties of the atmosphere, and hence some of its aspects can be treated by the weather forecaster, though not the details of the complicated processes at work in the small region where water is condensed and evaporated."

-- F. H. Ludlam

"Big whirls have little whirls that feed on their velocity, and little whirls have lesser whirls and so on to viscosity."

-- L. F. Richardson

INTRODUCTION

A sound knowledge of the nature of cumulus convection and associated mesoscale circulations is essential to the further development of meteorology as an applied science. Despite the great advances in the understanding and prediction of synoptic scale weather systems that have occurred over the last three decades, the improvement in the skill of forecasting weather for a given location has lagged considerably, in part because of the influence of small scale processes. Since it cannot be hoped that microscale phenomena may be explicitly predicted by operational numerical models, their occurrence must be forecast indirectly by identifying, directly or statistically, those dynamic aspects of the large scale circulation conducive to their development. If such features may be successfully identified, then they may be used to predict the development of small scale disturbances, and further, to parameterize their effect on the large scale dynamics.

Although cumulus convection may occur whenever the atmosphere is conditionally unstable, it has been demonstrated that persistent, organized convection, which is of great dynamic importance and forecasting interest, depends on moisture convergence occurring on a scale much larger

than that of the cumulus cloud. In some circulations, such as tropical cyclones, the cumulus themselves indirectly provide the necessary moisture convergence through their collective effect on the large scale flow. In the case of extratropical convective systems, however, it is not always clear whether the mesoscale flow is purely a consequence of the convection, or whether such flow initiates and organizes the convection. It is generally recognized that the intensity of convection is related to characteristics of the large scale wind field, as well as the vertical distributions of temperature and moisture, but most investigators of severe local storms have attributed this relationship to a direct interaction between the cumulus and the synoptic-scale environment (e.g. Newton, 1966). The organization of intense convection, where it is not obviously related to surface fronts or similar features, is usually attributed to the pattern of synoptic-scale forcing. It is significant that the utilization of statistical relations of the occurrence of severe convection with synoptic-scale features has proven to be quite successful in forecasting the former. The apparent validity of such relations suggests the existence of a dynamical link between the synoptic- and micro-scales.

It is the premise of this paper that the intensity and

persistence of organized convection are determined by the susceptibility of the synoptic-scale temperature, moisture, and wind fields to mesoscale circulations - whether or not the latter result from or initiate the cumulus. We assert that while conditional instability is necessary for any convection, its presence may not be sufficient to allow mesoscale circulations to develop. On the other hand, certain large scale distributions of velocity and density may be unstable to mesoscale perturbations in a convectively unstable atmosphere. The degree of this instability, together with the amount of buoyant energy available to cumulus, determines the intensity of the convection. The conditional instability allows the convection to occur in the first place; the synoptic-scale environment facilitates the development of mesoscale circulations which in turn support the convection.

In order to assess the stability of the large scale flow to mesoscale disturbances, it is nescessary to take into account several parameters normally neglected on the cumulus scale, such as the absolute vorticity of the flow. Analytic examination of mesoscale flows is hampered by the inability to apply simplifying assumptions on the basis of scale; the motion fields are too small to be considered inviscid and quasi-geostrophic, but too large to neglect

rotation. Fortunately, many extratropical convective systems are organized into lines and hence the mesoscale flow, in these cases, may be considered to be two-dimensional. In particular, pre-coldfrontal squall lines comprise an interesting class of convection on which to test the abovementioned premise, as their organization on the mesoscale is apparently simple, and as they have received much attention in observational studies of intense convection. With this in mind, the approach taken here will be as follows:

(a) Examine observations of extratropical convective lines in order to ascertain the general properties of the associated large scale velocity and density fields.

(b) Perform a stability analysis on an idealized flow field based on such observations, and determine the criteria for instability in this flow.

(c) Compare the results of the stability analysis with observations of convective lines.

Following this format, Chapter 1 is directed toward an examination of line convection as observed in the atmosphere and in laboratory experiments. The properties

of the kinematic and thermodynamic environment of squall lines, as revealed by observational studies and as reflected in operational forecasting criteria, are investigated. It is found that intense convective lines occur in environments characterized by conditional instability and strong vertical shear of the horizontal wind. On this basis, a stability analysis of shear flow in a rotating viscous fluid is proposed.

The classical theoretical investigations of shear flow in rotating fluids are reviewed in Chapter 2. These studies indicate that three forms of instability are possible in an adiabatic, stably stratified, baroclinic fluid: baroclinic instability, characterized by wavelengths on the order of the radius of deformation of the fluid; inflectional (or Rayleigh) instability which can occur only if the gradient of absolute vorticity changes sign within the fluid; and "symmetric" instability characterized by waves of great length in the direction of the shear, but vanishing length (in the inviscid theory) in the direction normal to the shear.

The baroclinic instability mechanism has received great attention as it is associated with the majority of synoptic scale weather phenomena. The other two forms of instability are generally regarded as very small scale

activity confined to localized regions such as the planetary boundary layer. Of these, however, the symmetric instability has recently been related to the development of such mesoscale phenomena as squall lines and banded overturning motions observed in some planetary atmospheres. Unlike baroclinic instability, symmetric motions are critically influenced by the presence of viscosity in the fluid; thus the inviscid theory is inadequate for examining their complete structure. A need therefore arises for a comprehensive treatment of shear instability in rotating, diffusive fluids.

This need is addressed in Chapter 3, in which a complete linear stability analysis of shear flow in a rotating, diffusive fluid is presented. The propagating characteristics of the instability are also discussed therein.

Chapter 4 details the method of solution of the perturbation equations developed in Chapter 3, and is so constructed that the casual reader may skip, without loss of continuity, directly to Chapter 5 which presents solutions of the equations for various boundary conditions and fluid scale properties.

In Chapter 6, the structures of the disturbances, as well as the conditions under which they may occur, are

compared in detail with observations of convective mesosystems. We explore those processes in the atmosphere that lead to a state of inertial instability, and speculate upon the effects of convection on the inertially induced mesoscale circulation. Finally, we discuss the possible role of inertial stability in certain forms of boundary layer roll vortices and other banded circulations in the atmosphere.

CHAPTER 1

OBSERVATIONS OF CONVECTIVE LINES

The organization of convection into lines has received considerable attention from investigators of thunderstorm phenomena. The first systematic investigation of line thunderstorms in the United States is embodied in the Thunderstorm Project of 1946-47 (Byers and Braham, 1949). Of 56 thunderstorms observed in Ohio during this project, 32 were imbedded in lines; only six of which were clearly associated with fronts. Andre (1949) found that most thunderstorms and the vast majority of tornadoes observed in the United States occur within the warm sector of extratropical cyclones, well ahead (at least 100 mi) of the attendant cold fronts. Many of the pre-frontal thunderstorms occur within squall lines; when such lines are present, thunderstorms are highly concentrated along the lines.

Line convection is also observed in the tropics, although its predominance over other forms of convection is not obvious. Houze (1975) finds that many of the convective systems observed during the GATE consist of lines that are typically 25 to 40 km wide and $\sim$150 km long.

Byers (1951) notes that squall lines are generally more persistent than other forms of convection, lasting as

long as 24 hours. A few lines observed during the Thunderstorm Project contained as many as 50 individually identifiable thunderstorms. Convective storms occurring within squall lines appear to be structurally similar to other thunderstorms, but tend to be more severe.

The oft observed lack of pre-existing density or wind discontinuities at the surface is perhaps the most striking characteristic of the line squall. Although some lines appear to form along recognized fronts and thereafter propagate away from the latter (Newton, 1950), many convective lines develop well ahead of surface discontinuities (Fulks, 1951). In these instances, the origin of mesoscale circulations associated with the development of the squall lines is uncertain.

(a) Kinematic and Thermodynamic Environment

The synoptic environment of the mid-latitude convective line is characterized by strong vertical shear of the horizontal wind and marked convective instability. Newton (1950 and 1963), Fulks (1951), Breiland (1958), Boucher and Wexler (1961), Browning and Ludlam (1962), Skaggs (1967), and Carlson and Ludlam (1968) all emphasize the relationship of severe storms, in general, and squall lines in particular to vertical wind shear. Ramaswamy

(1956) finds that strong vertical wind shear also characterizes line squalls in India, and Breiland (1958) notes the association of instability lines with the downward extension of a strong vertical shear zone in the middle and upper troposphere.

The mechanism by which vertical wind shear influences convection has been speculated upon extensively. Newton (1950) proposed that the destruction of mean shear by convective processes gives rise to a solenoidal circulation, as the actual shear is set out of balance with the thermal wind. Such motions favor upward flow to the right of the convection (with respect to the shear vector) and thereby encourage the systematic development of new cumuli in such locations that the line appears to propagate to the right of the mean flow. In a later paper, Newton (1963) discusses the effects of dynamically induced pressure gradients that result from direct cumulus-shear interaction on the development of new cumulus cells, and concludes that the resulting vertical pressure gradients exert an upward acceleration comparable in magnitude with the buoyancy forces within the clouds. Moncrieff and Miller (1976) show that a component of shear normal to convective lines may enhance the relative inflow and outflow velocities and hence serves to intensify the system as well as cause

it to propagate. Observations of squall lines in mid-latitudes, however, reveal that their orientation is more nearly along the shear (Newton, 1950), and theoretical studies (e.g. Keuttner, 1971) indicate that any curvature of the wind profile with height acts to suppress convection except when it occurs in lines parallel to the shear.

It is apparent from these investigations that the presence of shear is critical to the development of intense convection. But most of these studies have dealt with the short time scale direct interaction between shear and cumuli, and have not addressed the question of an intermediate scale interplay occurring over a longer interval of time. Yet, the existence of circulations much larger than the cumulus scale is strongly implied in the case of intense, persistent convection. Cotton, et.al. (1976) find that mesoscale circulations modify convection by enhancing the convergence of moisture and momentum in the planetary boundary layer, as well as deepening the latter, and by altering the vertical shear of the horizontal wind.

Direct evidence of mesoscale circulations is scant, though the association of convection with the seabreeze circulations in Florida studied by Cotton (ibid) is clear. A strong mesoscale circulation associated with a frontal

thunderstorm line was deduced by Sanders and Paine (1975) from mesonet data obtained by the National Severe Storms Laboratory.

The thermodynamic conditions accompanying mid-latitude squall lines vary a great deal among individual lines, but nevertheless show certain common features. In most instances, a shallow layer of moist air near the surface overlain by drier air of small static stability precedes the passage of a line. Breiland (1958) finds that convective lines favor an environment of convective instability in which the moist layer at low levels is capped by an inversion and overlain by very dry air. Eisen (1972) notes that a stable layer at about 750 mb precedes the development of an intense squall line in Oklahoma. The juxtaposition of moist and dry air is also a common observation in association with line squalls in India (Ramaswamy, 1956).

Conditional instability appears to be a necessary but insufficient condition for intense convection. The tropics are frequently characterized by a state of conditional instability, but the occurrence of severe, organized convection is relatively rare. A few outbreaks of severe convection in middle latitudes, on the other hand, occur in an atmosphere that is only marginally unstable (Hoxit and

Chappell, 1975).

In addition to characteristic vertical distributions of density and moisture discussed above, the environment in which intense line convection occurs often exhibits prominent horizontal gradients of moisture. The development of thunderstorms along the "dry line" of the Plains States is a most striking example in this respect, but many squall lines are observed to form along the western periphery of moist tongues occasionally observed in the warm sectors of developing cyclones. Fulks (1951), for example, finds that squall line thunderstorms are more likely to occur within or to the west of anomalies in the moisture field than east of them. In the case of the dry line, storms appear to develop in the region of the strongest moisture gradient.

(b) Structure, Orientation, and Movement

Most squall lines are defined by a general linear arrangement of discrete convective cells, although there have been observed cases of a nearly continuous band of precipitation. The line thunderstorms recorded on radar during the Thunderstorm Project of 1946-47 were spaced up to 15 km apart; a single line was generally composed of between 5 and 50 such cells (Byers, 1949). The motion of

the individual radar echoes within convective lines is generally rapid and directed along the line, with a tendency to move more slowly than the line in the direction of propagation of the latter often observed. (Cells form in the right-rear quadrant of the line (with respect to the shear vector), and decay in the left-front quadrant.) Pestaina-Haynes and Austin (1976) find that the motion of cells in squall lines is usually faster than the mean environmental wind in the cloud layer, in contrast to isolated supercell thunderstorms which move more slowly than and to the right of the mean cloud layer wind.

Newton (1950) notes that squall lines are nearly parallel to the 500 mb flow, and tend to move, as entities, to the right of the mean wind. Byers (1951), Boucher and Wexler (1961), and Pestana-Haynes and Austin (1976) observe that mid-latitude convective line movement is best correlated with the component of 700 mb flow normal to the lines, and Byers (1949) finds that lines are generally oriented 10-15° counterclockwise from the wind vector at this level. The intense and devastating squall lines of 3-4 April 1974 were nearly parallel to the flow at all levels; the environmental wind exhibited little directional shear with height (Hoxit and Chappell, 1975). At the height of the activity on these dates, as many as five squall lines were

in progress simultaneously. These appeared to be more or less parallel, and spaced roughly 100 km apart. Although an outbreak of this magnitude is uncommon, it is not unusual to observe two or three squall lines during outbreaks of severe weather.

The pressure variations accompanying squall lines were first observed in detail during the Ohio phase of the Thunderstorm Project (Byers and Braham, 1949) and later examined by Fujita (1955). Typically, the surface pressure falls - sometimes rapidly - for an hour or so preceding the onset of precipitation, at which time there occurs an abrupt pressure rise accompanied by strong, gusty winds. Following the passage of thunderstorms, the pressure often falls again in response to the passage of a "wake low" (Fujita, 1955). Finally, the pressure returns to roughly the pre-storm value along with a less rapid recovery of surface temperature. A typical barogram recorded during the passage of a squall line is reproduced in Figure 1.

Mesoscale pressure variations such as those discussed above are most likely a hydrostatic consequence of temperature changes forced by vertical motion and latent heating and cooling. Fujita (1955) attributes the "thunderstorm high" to sub-cloud cooling induced by evaporating precipitation, and Clark and List (1971) have

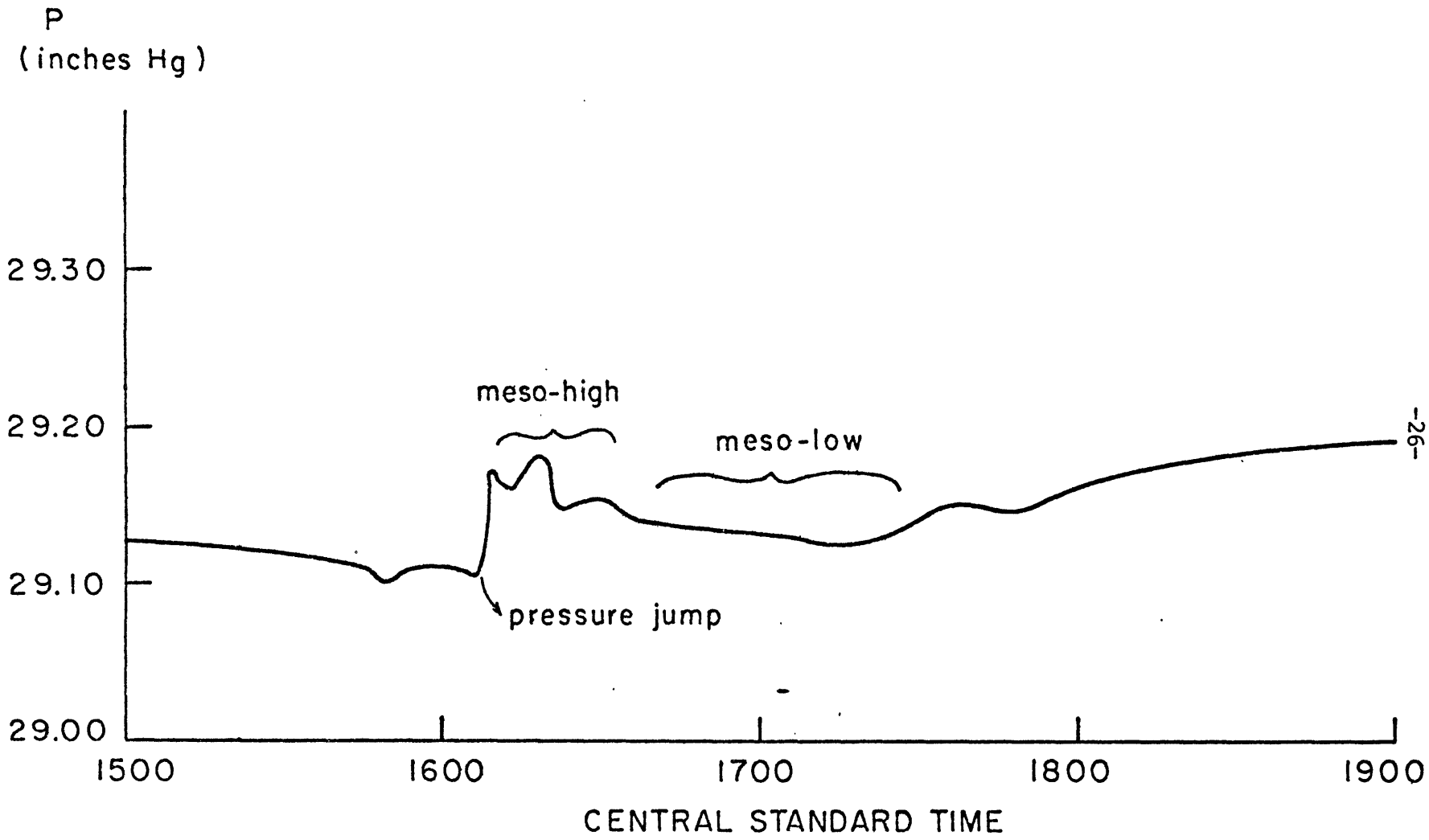

Figure 1: Barogram from Minco City, Oklahoma on 26 April, 1969 (Data from the National Severe Storms Laboratory)

shown that high concentrations of liquid water and ice found within thunderstorms may force a substantial vertical pressure gradient. The pressure falls prior and subsequent to the passage of thunderstorm lines may be attributed to adiabatic warming within sub-saturated downdrafts. Observations of squall lines within the network of the National Severe Storms Laboratory in Oklahoma reveal intense downdrafts ahead of the radar echoes, and broader descent to the rear of the lines (Fankhauser, 1969; Sanders and Paine, 1975; Stokes, 1976).

The general features of air flow in convective lines have been investigated on both the observational and theoretical levels. The results of these studies suggest the presence of a sloping updraft-downdraft pair with warm air entering the front of the system and rising back over a cold downdraft entering from the rear at mid-levels and driven by evaporative cooling. The anvil clouds of extratropical squall systems are most often observed to flow out ahead of the line (Ludlam, 1963); it is usually assumed that this feature reflects the outflow pattern aloft. The mesoscale circulation deduced by Newton (1963) from a time series of rawinsonde observations during the Thunderstorm Project is shown in Figure 2.

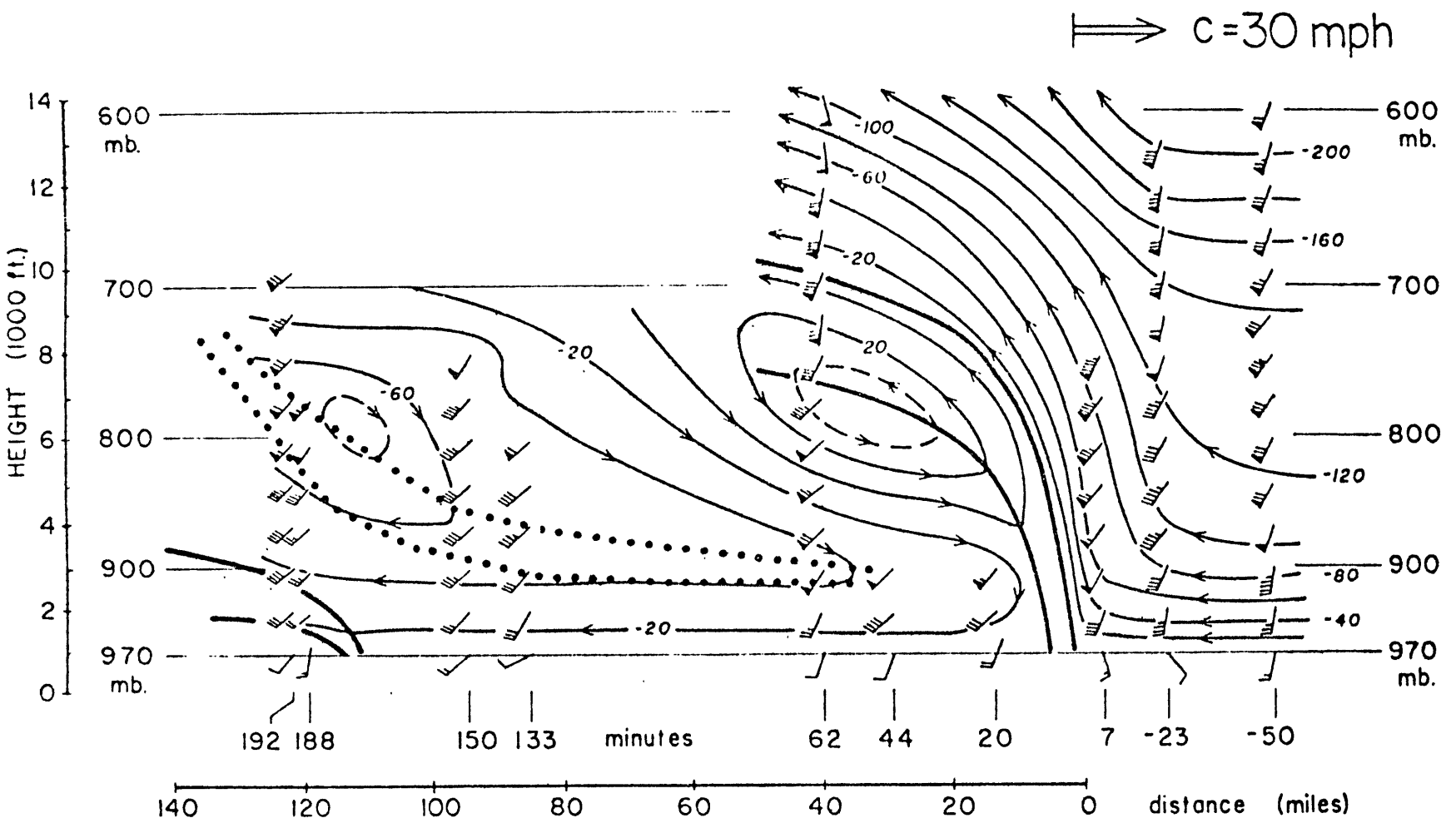

Figure 2: Streamlines relative to a moving squall line as deduced from a time series of wind observations. (From Newton, 1963)

(c) Boundary Layer Roll Vortices

Lines of low-level cumulus clouds are frequently observed during windy conditions. Glider pilots find that extended bands of upward and downward motion exist under certain conditions, and are observed to lie parallel to the wind direction (Woodcock, 1941). These bands do not always contain visible cloud.

Cloud streets over the tropical Atlantic were observed frequently during the BOMEX. Winds in the vicinity of the bands appeared to increase with altitude, but with little directional shear. The lines are parallel to the wind direction within the boundary layer, and are spaced at distances of typically two to four times their depth (Kuettner, 1971).

Tank experiments with Ekman flow reveal two distinct forms of boundary layer roll vortices. As the Reynolds number of the flow is increased, the first type appears as rolls of large spacing (25 to 33 times the Ekman layer depth), oriented along or slightly clockwise from the geostrophic flow above the boundary layer. At higher Reynolds numbers, a second form appears with smaller spacing (12 times the Ekman depth) and an orientation about 15° counterclockwise from the geostrophic flow (Tatro and Mollo-Christensen, 1967). This latter class of boundary

layer rolls is likely a form of inflectional instability, but the first type is not well understood (Greenspan, 1968, p. 286). Lilly (1966) was able to determine the critical Reynolds numbers characterizing the onset of both forms of instability by numerically solving the linear eigenvalue equations governing Ekman flow. His results are in excellent agreement with the observations of Tatro and Mollo-Christensen (1967). Lilly notes that the "Class A" or low Reynolds number instability is directly dependent on the presence of rotation in the fluid and, unlike inflectional instabilities, the Class A variety has been observed to completely penetrate the interior flow in tank experiments.

(d) Summary of Observations

The observations reviewed here strongly suggest a relationship between organized mesoscale overturning motions in fluids and the presence of shear. While many studies of intense convection have emphasized a direct interaction between macroscale flow and individual cumulus elements, the possibility that convection is indirectly coupled with the large scale shear through mesoscale circulations must also be considered. Any theoretical investigation of mesoscale motions associated with organized convection must

by broadly compatible with observations such as those discussed within this chapter.

CHAPTER 2

THE STABILITY OF SHEAR FLOW: CLASSICAL THEORY

The intimate association of banded convection and vertical wind shear, noted in Chapter 1, leads one to examine in detail the types of instability that may occur in fluid flows exhibiting shear. Shearing instability has been of great interest to fluid dynamicists beginning with Rayleigh who first described the physical mechanism of shearing instability in inviscid parallel flows (Rayleigh, 1880). Since then, much has been learned about this phenomenon; it is the purpose of this chapter to briefly review the current understanding of such processes.

Broadly, the forms of unstable motion that occur in adiabatic shear flow may be classified according to their energetic characteristics. Those motions which derive kinetic energy from the available potential energy of a statically stable initial state will be classified as baroclinic; those which arise due to an unstable arrangement of momentum in the initial state will be categorized according to the specific mechanism of the instability. If the transfer of kinetic energy from the mean flow to the eddies is direct, and does not involve the operation of centrifugal forces, the associated instability is of the inflectional type. This class, for example, includes

Kelvin-Helmholtz instability which is generally described in terms of the differential motion of two discrete layers of fluid of differing density; hence the instability must do work against gravity. Those disturbances which depend on the rotation of the fluid and originate from an unstable distribution of angular momentum will be classified as inertial motions. Convective instability resulting purely from a gravitationally unstable distribution of mass will not be dealt with specifically.

The classification of instability types according to their energetics is not always justified. Unstable waves in a baroclinic fluid, for example, may intensify due to both baroclinic and barotropic instability (Brown, 1969). Local convective instability may act indirectly to intensify much larger disturbances, including otherwise baroclinic waves (Tracton, 1973). Despite the presence of multiple energy sources in some growing disturbances, it is usually possible to distinguish one source that dominates the growth and structure of the system.

An exhaustive treatment of shear flow instability is not intended here; rather, we seek an understanding of those disturbances which tend to occur in the form of parallel rows and possess length scales comparable to those observed in connection with line convection in the atmosphere.

Motions resulting from diabatic, topographic, or frictional forcing are not dealt with here. The observed development of convective lines at night and over flat terrain implies that at least some such circulations are independent of diurnal heating and topography.

(a) Instabilities of Stably Stratified Rotating Fluids

Of the various instabilities observed in rotating fluids, the baroclinic instability has received the greatest attention as a consequence of its obvious connection to the migratory large scale pressure systems observed in the atmosphere. Charney (1947) was the first to examine the baroclinic mechanism analytically and present detailed information on the growth rates and structure of the instabilities. Characteristic growth rates of about $(1\ \text{day})^{-1}$ and length scales comparable to the fluid radius of deformation preclude the possibility that this mechanism is directly associated with mesoscale circulations.

Rayleigh instability, observed in rotating and non-rotating fluids, can occur only when an absolute velocity profile through the flow contains an inflection point. If the flow contains only vertical shear and is stably stratified, instability can develop only if the minimum

Richardson number somewhere within the fluid is less than 1/4. Instability will occur in horizontally sheared flow only when the absolute vorticity of the flow contains at least one maximum, as shown by Kuo (1949). Disturbances of this kind exhibit variations along the direction of the shear vector and show no tendency to align with the latter.

The last form of instability can only occur in rotating fluids and results from an unstable distribution of centrifugal and pressure forces within the fluid. The first investigation of the mechanism of inertial instability was conducted by Rayleigh (1916), who derived the stability criterion for a homogeneous, incompressible, and inviscid circular vortex flow. Later, Solberg (1933) extended Rayleigh's results to an inhomogeneous fluid. The fundamental conclusion of these analyses is that circular vortex flow is stable to axisymmetric disturbances as long as the square of the angular momentum of the flow increases with radius along an isentropic surface, otherwise it is unstable. Due to the symmetry of the disturbances in the circular vortex (there is no azimuthal variation of the perturbations), this class of disturbance has also been called symmetric instability. The alignment of the disturbance axis along the shear suggests an association

of this form of shear instability with line convection.

(b) Structure and Mechanism of Inertial Instability

In its simplest form, inertial motion may be understood by examining the forces acting upon a fluid ring displaced radially in a circular vortex of homogeneous inviscid fluid. The displaced ring conserves its angular momentum while it is acted upon by the pressure gradient characteristic of its new environment. If the resulting force acts to displace the parcel back towards its original position, the configuration is stable; otherwise, it is unstable.

If one displaces a fluid ring radially from point A to point B within a circular vortex, and it is assumed that the pressure gradients within the vortex are not changed by the displacement, then the radial momentum equation at point B may be written:

$$\left(\frac{dV}{dt}\right)_B = -\frac{1}{\rho}\left(\frac{\partial p}{\partial r}\right)_B + r_B\omega^2$$

where ω is the local angular velocity of the fluid, V is the radial velocity component, ρ is the density, and r_B the radius at point B. The above may also be written in

terms of the angular momentum M, where

$$M = \rho r^2 \omega$$

then

$$\left(\frac{dV}{dt}\right)_B = -\frac{1}{\rho}\left(\frac{\partial p}{\partial r}\right)_B + \frac{M_A^2}{r_B^3}\frac{1}{\rho^2}$$

Under the assumption that the radial pressure gradient is unaffected by the displacement,

$$-\frac{1}{\rho}\left(\frac{\partial p}{\partial r}\right)_B = -\frac{1}{\rho^2}\frac{M_B^2}{r_B^3}$$

The radial momentum equation may then be written:

$$\left(\frac{dV}{dt}\right)_B = \frac{1}{\rho^2 r_B^3}\left(M_A^2 - M_B^2\right)$$

If the displacement from A to B is outward, then there will be a restoring acceleration provided that

$$M_B^2 > M_A^2$$

Otherwise, the fluid ring will continue to accelerate outward. A necessary condition for instability in a homo-

geneous and inviscid circular vortex is then

$$\frac{\partial M^2}{\partial r} < 0$$

In an inhomogeneous fluid, with horizontal and vertical density gradients, the mechanism is similar. If, when a parcel is displaced along an isentropic surface, the sum of resulting centrifugal and pressure gradient accelerations does not act to return the parcel toward its initial position, then an instability may develop. Provided that the fluid motions may be considered hydrostatic, the necessary condition for instability in this instance is

$$\frac{1}{r^3}\left(\frac{\partial M^2}{\partial r}\right)_\theta < 0$$

where r is the absolute radius of curvature of the flow, and the subscript denotes displacement along an isentropic surface. In a rotating co-ordinate system, it may be shown that for a zonal current u in hydrostatic and geostrophic equilibrium,

$$\lim_{r\to\infty} \frac{1}{r^3}\left(\frac{\partial M^2}{\partial r}\right)_\theta \simeq f^2\rho^2\left(1 - \frac{1}{Ri} - \frac{1}{f}\frac{\partial u}{\partial y}\right)$$

where f is the Coriolis parameter and $Ri \equiv \frac{g(\partial \ln\theta/\partial z)}{(\partial u/\partial z)^2}$

For this special case, Stone (1966) discusses the growth rates

of symmetric disturbances in an inviscid flow with constant vertical shear and no horizontal velocity variation, and compares the characteristics of the unstable motions with those of other forms of instability. He finds that the disturbances arise in the form of overturning motions primarily along isentropic surfaces, with the largest growth rates occuring for rolls with vanishing width in a direction transverse to the shear. The dependence of the growth rate on the transverse wavelength is not great for small wavelengths, so that it is useful to define a maximum wavelength for instability. For the type of initial flow considered and for fluid bounded above and below by rigid horizontal plates, the symmetric instability sets in when the Richardson number (Ri, as previously defined) falls below unity. The expressions derived by Stone for the growth rate σ_i and maximum wavelength L_{max} are:

$$\sigma_i = f\left(\frac{1}{Ri} - 1\right)^{1/2}$$

$$L_{max} = 2\,\frac{\overline{U_z}H}{f}\,(1 - Ri)^{1/2}$$

where f is the Coriolis parameter, $\overline{U_z}$ is the constant shear value, and H is the depth of the fluid. The initial growth rates of symmetric disturbances are found to exceed

those of baroclinic and Kelvin-Helmholtz instabilities when the Richardson number lies between .25 and .95.

As discussed previously, the inertial instability draws energy from the kinetic energy of the mean flow; in so doing the inertial eddies transport momentum down gradient.

Yanai and Tokioka (1969) performed a numerical experiment in order to simulate meridional motions in an axially symmetric vortex. In this experiment, the nonlinear inviscid equations of motion are integrated in a domain bounded above and below by rigid boundaries. The results are in accord with the linear theory, but with horizontal wavelengths limited by the numerical grid size. An integration is also performed for a case in which the region of instability is restricted to a small area. It is found that the resulting motions do not penetrate far into the surrounding stable fluid.

The addition of viscosity to the linear symmetric stability problem greatly complicates its solution, as the resulting equations are of much higher order. The first attempt at solving the viscous system of equations governing symmetric instability in a baroclinic fluid was made by Kuo (1954). The linear problem is solved exactly for the case of non-oscillatory instability in fluid with neutral

stratification. Solutions are obtained for horizontally periodic disturbances, as well as for those confined, in the horizontal, between rigid free-slip walls separated by a distance equal to the depth; in both cases the fluid is bounded above and below by free-slip rigid plates.

Kuo finds that the flow becomes unstable when a parameter Q defined by

$$Q = T_o \frac{\overline{U_z}}{f} (1 + P)$$

exceeds a critical value dependent on the Taylor number

$$T_o = \frac{f^2 H^4}{\nu^2}$$

Here, $\overline{U_z}$ is the constant shear value, f is the Coriolis parameter, H is the fluid depth, and P is the Prandtl number ν/κ (the ratio of the coefficients of diffusion of momentum and heat). The horizontal wavelength of the marginally unstable disturbance is on the order of the fluid depth, unless the diffusion is very small ($T_o > 10^5$). Kuo's results for the critical value of Q are reproduced in Figure 3. The motions set in as overturning cells tilted down and to the right of the shear, quite similar to the pattern obtained by Yanai and Tokioka (1969), except

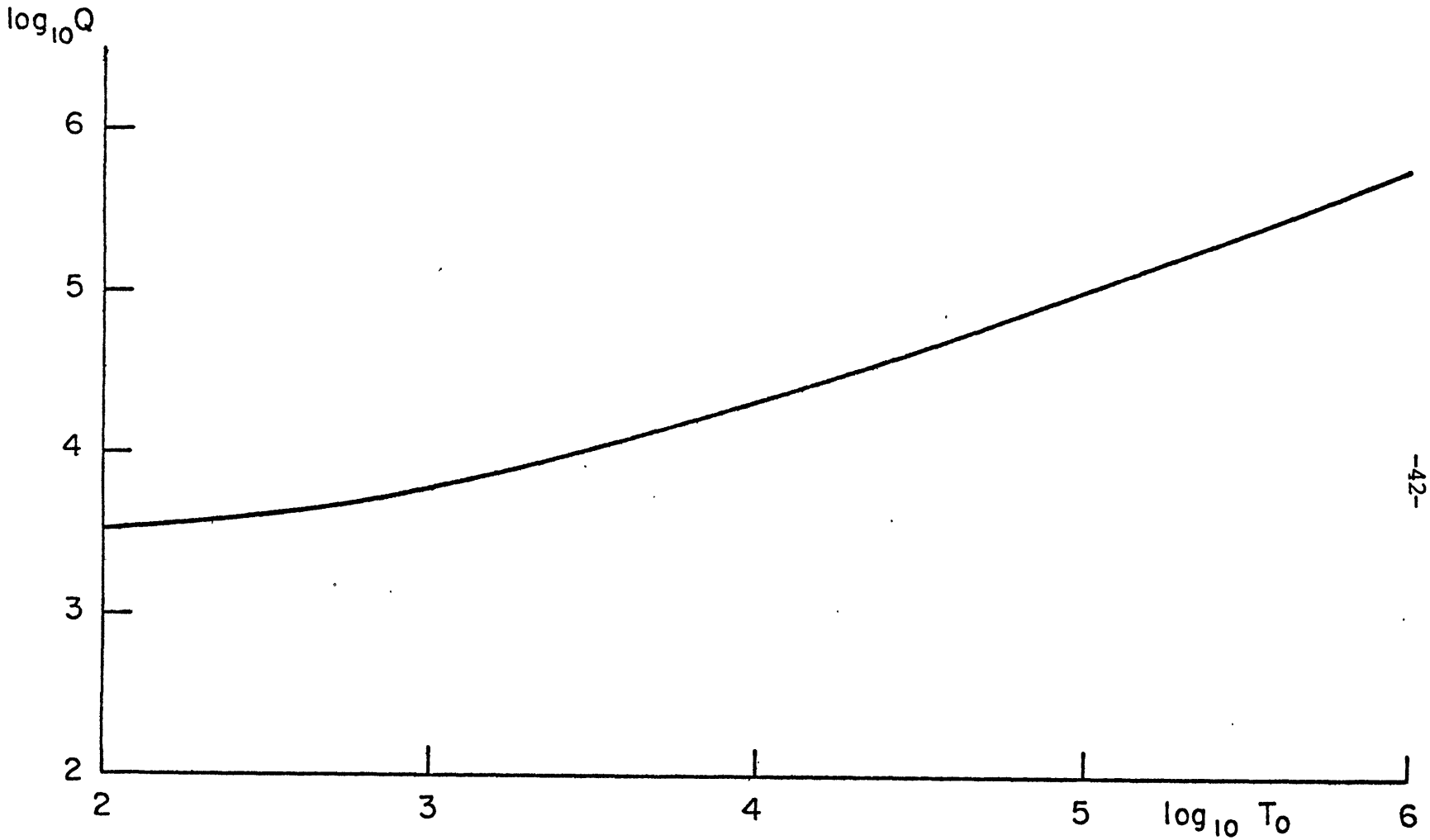

Figure 3: The critical value of Kuo's stability parameter Q as a function of the Taylor Number T_o, for a neutrally stratified fluid. (Kuo, 1954)

that the cells are tilted across the potential isotherms, which are vertical in this case, rather than being more or less aligned with them. This result coincides with Stone's (1971) finding that accelerations in the vertical cause the rolls to have a smaller slope than the potential isotherms. For large Taylor numbers, the momentum of the perturbation velocity component along the instability line is much greater than that of the transverse velocity component.

One interesting aspect of Kuo's result is the dependence of the flow stability on the Prandtl number, a phenomenon which is unaffected by letting T_o tend toward infinity - indicating that the behavior of disturbances with finite viscosity, however small, is fundamentally different from that displayed by fluid with no viscosity. This characteristic is also apparent in an analysis of McIntyre (1969) for viscous symmetric motions in an unbounded fluid with stratification and shear. In the limit as the diffusion parameters approach zero, monotonic instability sets in when

$$Ri < \frac{(1 + P)^2}{4P}$$

and oscillatory instability occurs when

$$Ri < \frac{(1 + 3P)^2}{8P(1 + P)}$$

As the former parameter is always larger than the latter (except when P=1 in which case it may be shown that oscillatory instability is not possible), monotonically growing disturbances will occur initially as the fluid is destabilized.*

An extension of this analysis to include small non-linearity and boundary effects (large Taylor number) was carried out by Walton (1975), who determined the critical Richardson number as a function of the inverse Taylor number and Prandtl number when the former is small. The fluid is bounded above and below by rigid, no-slip boundaries, and a perturbation expansion in $T_o^{-1/6}$ is used. The critical Richardson numbers derived by Walton for monotonic and overstable oscillations to second order in $T_o^{-1/6}$ are as follows:

$$\text{MONOTONIC:} \quad Ri_m = \frac{(1+P)^2}{4P}\left[1 - 3\left(\frac{\pi^2}{2}\right)^{2/3} T_{,}^{-1/3}\right]$$

---

* It will be demonstrated within Chapter 3 that McIntyre's criterion for oscillatory instability does not apply to bounded fluids.

$$\text{OSCILLATORY:}\quad Ri_o = \frac{(1+3P)^2}{8P(1+P)}\left\{1 - 3\left(\frac{\pi^2}{2}\right)^{2/3}\left(1+\frac{1}{P}\right)^{2/3} T_o^{-1/3}\right\}$$

(Comments in the previous footnote also apply to the second expression above.) These expressions are valid for $T_o^{-1} << \sim 10^{-3}$. In this range of Taylor numbers, the horizontal wavelength of the motion is a strong function of the diffusion; when the viscosity becomes sufficiently large, the wavelength is more dependent on the depth of the fluid and the slope of the potential isotherms (see Chapter 5). Walton also finds that the instability produces a secondary circulation that transports zonal momentum poleward, which is in the opposite sense to the first order eddy transport ($\overline{u'v'}$).

As might be expected, the effect of diffusion is to stabilize the fluid, for a constant Prandtl number. The inclusion of diffusive effects also imposes limits on the horizontal wavelength of the motions; Walton's results indicate that for values of the parameters typical of the atmosphere, the horizontal wavelength is on the order of 10 times the depth through which the fluid is unstable. Because of the limited Taylor numbers for which the theory is valid, this conclusion is applicable to the atmosphere only if this depth is greater than about 10 km.

(c) Speculation on the Role of Inertial Instability in Organized Convection

The properties of inertial stability, as here discussed, bear some semblance to mesoscale circulations associated with organized convection. The connection between convection and inertial effects was perhaps first perceived by Newton (1950) who, however, viewed the shear as a propagating rather than intensifying mechanism. Newton proposes that the reduction of shear by turbulent mixing within large cumulonimbi causes the actual momentum field to be out of balance with the mass field. The resulting solenoidal circulations favor the development of new convection to the right of the shear with respect to the existing convection. Essentially, this is a description of inertial overturning induced by diffusion.

Williams (1968) performed a numerical experiment similar to that of Yanai and Tokioka (1969) but allowed double diffusivity ($P \neq 1$). Williams notes the similarity of the inertial circulations with those occurring in a squall line depicted by Newton (1966). Inertial motions were thought to produce large downward fluxes of westerly momentum west of a squall line studied by McGinley and Sasaki (1975). In this instance, the strong solar heating of the desert regions of the southwestern United States produced large areas of low Richardson number. The westerly

momentum transport to the surface, induced by inertial instability, was thought to cause a line of strong convergence between eastward moving air from the deserts, and northward flowing air from the Gulf of Mexico. Paine and Kaplan (1976) find that severe meso- and micro-scale phenomena occur in regions where an imbalance of the macroscale mass and momentum fields is indicated by an analysis of the various components of the divergence equation. A direct association of the intense squall lines of 3-4 April 1974 with inertial circulations is proposed by Raymond (1977), who also finds that the wavelengths and orientation of the lines are comparable with those suggested by the existing theory of inertial instability.

Although these studies suggest an association of convection with inertial instability, the theory is not well enough defined to allow many conclusions. Clearly, a more general understanding of the nature of inertial circulations is needed to assess their relationship with organized convection. We must not only understand the structure and behavior of such systems under general atmospheric conditions, but we should identify those dynamical processes that induce within the atmosphere a state of inertial instability. As a first step in this direction, we proceed to extend the linear stability theory

to include diffusive effects in a more general way, and also to take into account the effects of horizontal shear and various boundary conditions. A more precise analysis of the stability criteria for inertial motions, as well as a better understanding of their structure, will make possible a better comparison of theory with the observations of organized convection.

CHAPTER 3

A LINEAR STABILITY ANALYSIS OF VISCOUS ROTATING FLOW WITH LINEAR SHEAR

In light of the observed association of squall lines with vertical shear, discussed in Chapter 1, we examine the stability of vertical shear flow in a rotating viscous fluid for two-dimensional displacements transverse to the shear. As an extension of previous investigations, horizontal shear is also included.

The equilibrium flow is taken to be a steady current with constant horizontal and vertical shears:

$$\bar{U} = \overline{U_z} z + \overline{U_y} y$$

in which $\overline{U_z}$ and $\overline{U_y}$ are constant vertical and horizontal shear values respectively. Similarly, the equilibrium density distribution may be written:

$$\ln\bar{\rho} = \frac{\partial \ln\bar{\rho}}{\partial y} y + \frac{\partial \ln\bar{\rho}}{\partial z} z$$

The condition of thermal wind balance is

$$f\overline{U_z} = g \frac{\partial \ln\bar{\rho}}{\partial y}$$

in which f is the Coriolis parameter and g is the acceleration

of gravity. The square of the Brunt-Väisälä frequency is defined for a Boussinesq fluid

$$N^2 = -g \frac{\partial \ln \rho}{\partial z} = \text{constant}$$

Using these relations, the density distribution may be expressed

$$g \ln \bar{\rho} = f\overline{U_z}\, y - N^2 z$$

The stability of this balanced initial state is explored by determining the time dependence of small perturbations superposed on the equilibrium state. If the perturbations do not grow with time, we define the initial state to be stable, otherwise such a state will not remain steady. Assuming that these perturbations are two-dimensional, there will be no variation in the zonal (or $\hat{x}$) direction. Denoting the perturbations by primes, the linearized adiabatic Boussinesq equations are:

$$(\frac{\partial}{\partial t} - \nu\nabla^2)u' + v'\overline{U_y} + w'\overline{U_z} = fv' \qquad (1)$$

$$(\frac{\partial}{\partial t} - \nu\nabla^2)v' = -\frac{1}{\rho_o}\frac{\partial p'}{\partial y} - fu' \qquad (2)$$

$$\alpha\left(\frac{\partial}{\partial t} - \nu\nabla^2\right)w' = -\frac{1}{\rho_o}\frac{\partial p'}{\partial z} - \frac{\rho'}{\rho_o}g \qquad (3)$$

$$\left(\frac{\partial}{\partial t} - \kappa\nabla^2\right)\frac{\rho'}{\rho_o} + \frac{f\overline{U}_z}{g}v' - \frac{N^2}{g}w' = 0 \qquad (4)$$

$$\frac{\partial v'}{\partial y} + \frac{\partial w'}{\partial z} = 0 \qquad (5)$$

The coefficients of momentum and heat diffusion are ν and κ respectively, and α is a tag set equal to zero or unity depending upon whether the flow is considered to be hydrostatic or not. The Coriolis parameter f is constant.

The flow in the y-z plane may be described in terms of a streamfunction by virtue of the form of the continuity Equation (5). Such a variable is here defined so that

$$v' \equiv -\frac{\partial \psi}{\partial z} \qquad\qquad w' \equiv \frac{\partial \psi}{\partial y}$$

Using this notation, the entire set of equations may be reduced to a single eighth-order equation for the streamfunction (details of the reduction may be found in Appendix 1):

$$\left(\frac{\partial}{\partial t} - \kappa\nabla^2\right)\left(\frac{\partial}{\partial t} - \nu\nabla^2\right)^2\left(\alpha\frac{\partial^2}{\partial y^2} + \frac{\partial^2}{\partial z^2}\right)\psi$$

$$= -\left(\frac{\partial}{\partial t} - \nu\nabla^2\right)\left(f\overline{U_z}\frac{\partial^2\psi}{\partial y\partial z} + N^2\frac{\partial^2\psi}{\partial y^2}\right) \qquad (6)$$

$$-\left(\frac{\partial}{\partial t} - \kappa\nabla^2\right)\left(f\overline{U_z}\frac{\partial^2\psi}{\partial y\partial z} + f\overline{\eta}\frac{\partial^2\psi}{\partial z^2}\right)$$

where $\overline{\eta}$ is the absolute vorticity of the flow:

$$\overline{\eta} \equiv f - \overline{U_y}$$

It is desired to obtain critical stability criteria from this analysis; that is, to find the relationship of the parameters describing the equilibrium state when the flow is marginally stable. Additionally, the structures of the perturbation mass and velocity fields that characterize this state are of interest. After some simplification, we will solve the equations analytically.

If an exponential time dependence is assumed and boundary conditions on the streamfunction are specified, then the relationship among the stability parameters, which appear as constant coefficients in Equation (6), are determined as characteristic values of the latter. The

time dependence may enter both as growth (or decay) and as oscillation. The marginal state is defined as no growth or decay, and may or may not permit non-amplifying oscillations. If neutral oscillations are solutions of the viscous equations, then the disturbances are said to begin as overstability.

The approach taken here will be to represent the perturbation streamfunction as a Fourier series in y and t, and to find that component wave which first becomes unstable as the fluid flow is destabilized. The domain is taken to be infinite in y and bounded above and below by rigid boundaries.

So that the analysis may be condensed, the following simplified cases will be examined individually:

i) Disturbances are hydrostatic ($\alpha=0$) and horizontal diffusion may be ignored ($\nabla^2 = \partial^2/\partial z^2$).

ii) Disturbances are non-hydrostatic ($\alpha=1$), the fluid is neutrally stratified ($N^2=0$), and horizontal diffusion is important ($\nabla^2 = \partial^2/\partial y^2 + \partial^2/\partial z^2$).

Each of the above cases will be analyzed for disturbances that begin as steady overturning as well as for those that begin as oscillations.

The degree to which both the hydrostatic assumption and the neglect of horizontal diffusion are valid depends on the ratio of the vertical to the horizontal length scales of the circulation; it can be shown that this ratio is determined by the slope of the potential isotherms, $f\overline{U}_z/N^2$. If this slope is small, one can neglect vertical acceleration and horizontal diffusion in the basic equations.

The boundaries at the top and bottom of the domain are taken to be rigid and frictionless (free-slip), and each boundary is considered to be perfectly conducting ($\rho' = 0$). From the hydrostatic equation, it follows that $\partial p/\partial z = 0$ on the boundaries. The free-slip boundary conditions are then:

$$\frac{\partial \psi}{\partial y}\ ,\ \frac{\partial^2 \psi}{\partial z^2}\ ,\ \frac{\partial u}{\partial z}\ ,\ \frac{\partial p}{\partial z} = 0 \quad \text{at boundaries}$$

In addition, Case (i) is solved for no-slip boundaries:

$$\frac{\partial \psi}{\partial y}\ ,\ \frac{\partial \psi}{\partial z}\ ,\ u,\ \frac{\partial p}{\partial z} = 0 \quad \text{at boundaries}$$

(a) Scaling

In both Cases (i) and (ii), the scaling of the space and time variables is found to reduce the number of parameters involved in the analysis to at most three. The following transformations are made in Case (i):

$$y \rightarrow y'H \frac{N^2}{f\overline{U}_z}$$

$$z \rightarrow z'H$$

where H is the depth of the fluid, and primes denote non-dimensional variables. Here, the horizontal dimension is scaled by the ratio of the fluid depth and the slope of the potential isotherms, $f\overline{U}_z/N^2$, while the vertical dimension is scaled simply by the fluid depth. In the inviscid case, the disturbances seek vanishing length scales, hence the reader may be surprised that the diffusive parameters do not appear in the scaling of the spacial dimensions. In effect, we assume that there is sufficient diffusion that the scale of the circulations is determined by the boundaries rather than by diffusion directly. These assumptions are not intrinsically important, since we do not neglect any terms in the governing equations, but they will nevertheless prove eminently justifiable in geophysical flows.

The appropriate time scale will prove to be the inverse of Coriolis parameter f, but in order to simplify the form of the equations, we choose a diffusive time scale:

$$t \to t' \frac{H^2}{\nu}$$

Using the indicated scaling for Case (i), Equation (6) becomes:

$$T\left(\frac{\partial}{\partial t'} - \frac{1}{P}\frac{\partial^2}{\partial z'^2}\right)\left(\frac{\partial}{\partial t'} - \frac{\partial^2}{\partial z'^2}\right)^2 \frac{\partial^2 \psi}{\partial z'^2}$$

$$= -\left(\frac{\partial}{\partial t'} - \frac{\partial^2}{\partial z'^2}\right)\left(R\frac{\partial^2 \psi}{\partial y' \partial z'} + R\frac{\partial^2 \psi}{\partial y'^2}\right)$$

$$- \left(\frac{\partial}{\partial t'} - \frac{1}{P}\frac{\partial^2}{\partial z'^2}\right)\left(R\frac{\partial^2 \psi}{\partial y' \partial z'} + \frac{\partial^2 \psi}{\partial z'^2}\right) \qquad (7)$$

The non-dimensional parameters are:

$T \equiv \frac{f}{\eta}\frac{\nu^2}{f^2 H^4}$ (a modified inverse Taylor number)

$R \equiv \frac{f}{\eta}\frac{1}{Ri}$ ($Ri = N^2/\overline{U_z}^2$)

$P \equiv \nu/\kappa$ (Prandtl number)

If the disturbances begin as stationary overturning, then $\partial/\partial t' = 0$ and Equation (7) may be integrated twice to obtain the sixth order equation

$$T \frac{\partial^6 \psi}{\partial z^6} = -R(1+P) \frac{\partial^2 \psi}{\partial y \partial z} - RP \frac{\partial^2 \psi}{\partial y^2} - \frac{\partial^2 \psi}{\partial z^2} \qquad (8)$$

(The two constants of integration vanish due to the boundary conditions, as shown in Appendix 1. Also, the primes have been dropped.) The above may be written in terms of only two non-dimensional parameters by again scaling:

$$y^* \rightarrow y \frac{P}{1+P}$$

in which y^* is the old independent variable, and defining

$$\chi_i \equiv R \frac{(1+P)^2}{P}$$

Then, Equation (8) becomes:

$$T \frac{\partial^6 \psi}{\partial z^6} = -\chi_i \frac{\partial^2 \psi}{\partial y \partial z} - \chi_i \frac{\partial^2 \psi}{\partial y^2} - \frac{\partial^2 \psi}{\partial z^2} \qquad (9)$$

For Case (ii), it may be expected that the horizontal and vertical length scales are similar. Equation (6) is transformed in this instance by the following scaling:

$$y \rightarrow y'H$$

$$z \rightarrow z'H$$

$$t \rightarrow t' \frac{\nu}{H^2}$$

The steady form of Equation (6) then becomes, after two integrations:

$$T(\nabla^2)^3\psi = - \frac{\overline{U_z}}{\overline{\eta}} (1+P) \frac{\partial^2\psi}{\partial y' \partial z'} - \frac{\partial^2\psi}{\partial z'^2} \qquad (10)$$

(Again, the two constants of integration vanish. See Appendix 1).

In neutrally stratified shear flow, the stability parameter is the ratio of the shear and the absolute vorticity. In this instance, the flow becomes increasingly unstable for larger values of P, while the disturbances in hydrostatic stratified flow are more unstable when the Prandtl number differs from unity in either direction. Presumably, the effect of heat conduction in a stably stratified fluid is to mitigate the effect of the stratification, while heat diffusion in neutrally stratified flow can only act to decrease the horizontal density gradient.

(b) Overstable Oscillations

It is easily shown that oscillatory instability is impossible under free-slip boundary conditions if P=1 (see Appendix 2); however, when the Prandtl number differs

from unity, neutral oscillations may occur, in which case the instability begins as travelling or standing waves. The criterion of oscillatory instability is generally not the same as that for stationary instability.

It is not possible to solve the partial differential equation governing oscillatory instability using the techniques to be demonstrated in Chapter 4; however, it is possible to obtain solutions in the special case where the instability sets in as a standing oscillation, so that the form of the streamfunction may be expressed:

$$\psi = \mathrm{Re}[e^{i\sigma t}\, \Psi(y,z)] \qquad (11)$$

where both σ and Ψ are constrained to be real. In fact, the above expression will be generally valid if it can be proven that a wave travelling one direction in y has the same properties as another travelling in the opposite direction; then the two linear waves may be superposed to yield a standing oscillation. Such a symmetry is not immediately evident on physical grounds, nor has it been possible to prove for the general case. Walton (1975), however, has shown the symmetry to exist in waves satisfying expansions of the governing equations to second order in $T_o^{-1/6}$. Assuming that (11) is valid in this range, it will

presently be shown that overstable oscillations will not be important when T_o^{-1} is much larger than 10^{-5}. This result may be interpreted in either of two ways: the neutral oscillations cannot occur at all for large diffusion, or asymmetry in the wave propagation (if it exists) prohibits standing oscillations when the diffusion is large. The former interpretation appears more reasonable in light of the lack of standing oscillations in the intermediate range ($T_o^{-1} \sim 10^{-4}$) where Walton's results are still valid, and also in consideration of the lack of overstability in the Bénard convection problem in rotating flow when $T_o^{-1} \gtrsim \sim 10^{-3}$ (see Chandrasekhar, 1961).

If the standing wave form (11) is substituted into Equation (7), governing hydrostatic instability, and real and imaginary parts are separated, two equations result:

$$T\sigma\left[\sigma^2 \frac{\partial^2\Psi}{\partial z^2}\right] = \sigma\left[T\left(1+\frac{2}{P}\right)\frac{\partial^6\Psi}{\partial z^6} + 2R\frac{\partial^2\Psi}{\partial y\partial z} + R\frac{\partial^2\Psi}{\partial y^2} + \frac{\partial^2\Psi}{\partial z^2}\right] \tag{12a}$$

$$T\sigma^2[1+2P]\frac{\partial^2\Psi}{\partial z^2} = T\frac{\partial^6\Psi}{\partial z^6} + (1+P)R\frac{\partial^2\Psi}{\partial y\partial z} + PR\frac{\partial^2\Psi}{\partial y^2} + \frac{\partial^2\Psi}{\partial z^2} \tag{12b}$$

The trivial solution $(\partial/\partial t - \partial^2/\partial z^2)\Psi = 0$ has been integrated out of Equation (12b). Comparing the two terms involving $\partial^2\Psi/\partial z^2$ in each equation, it is noted that

$$T\sigma^2 \sim O(1)$$

Referring to the original time scale, ν/H^2, it will be seen that dimensionally,

$$\sigma \sim O(f)$$

hence, the time scale is determined by the rotation rate of the fluid.

One solution of Equation (12a) is $\sigma=0$, in which case (12b) reduces to the steady form (8). Otherwise, the quantity $\sigma^2 T\, \partial^2\Psi/\partial z^2$ may be eliminated between (12a) and (12b), yielding an expression governing neutral oscillations:

$$2T \frac{(1+P)^2}{P} \frac{\partial^6\psi}{\partial z^6} + R(1+3P) \frac{\partial^2\psi}{\partial y \partial z} + R(1+P) \frac{\partial^2\psi}{\partial y^2}$$

$$+ 2P \frac{\partial^2\psi}{\partial z^2} = 0$$

Applying the transformation:

$$y \to y' \frac{1+P}{1+3P}$$

the above becomes:

$$T(1+\frac{1}{P})^2 \frac{\partial^6\Psi}{\partial z^6} + \frac{1}{2}R\frac{(3+1/P)^2}{1+1/P}\frac{\partial^2\Psi}{\partial y'\partial z}$$

$$+ \frac{1}{2}R\frac{(3+1/P)^2}{1+1/P}\frac{\partial^2\Psi}{\partial y'^2} + \frac{\partial^2\Psi}{\partial z^2} = 0 \qquad (13)$$

Equation (13) has exactly the same form as (9), with the first term multiplied by $(1+1/P)^2$ and $\chi_i = \frac{1}{2}R\,[(3+\frac{1}{P})^2/(1+\frac{1}{P})]$. Without solving the equation, it is immediately apparent that, as the fluid is destabilized, oscillatory instability never occurs before stationary motions when the fluid is hydrostatic ($f\overline{U_z}/N^2 \ll 1$), since

(a) The diffusion parameter is always larger in the case of oscillatory instability;

(b) The shear parameter χ_i is always smaller in the oscillatory case, except when P=1 in which instance oscillations are not possible (see Appendix 2).

In fact, these conditions are sufficient to eliminate the possibility of hydrostatic standing waves in the linear theory altogether, when the boundaries are free-slip. This is proven as follows: In the limit as $\sigma \to 0$, both

Equations (9) and (13) must be satisfied. This condition is met when the critical stability curves in the T-R plane defining the marginal states of each form of instability intersect. We have shown that this never occurs, so that σ^2 must be of one sign. We can prove that in the special case P=1, $\sigma^2 < 0$:

Eliminating the term involving $\partial^2\Psi/\partial y\partial z$ between (12a) and (12b), we have:

$$T\sigma^2[1+3P]\frac{\partial^2\Psi}{\partial z^2} = -T\left[\frac{P^2+P+2}{P}\right]\frac{\partial^6\Psi}{\partial z^6}$$

$$- R(1-P)\frac{\partial^2\Psi}{\partial y^2} + (1-P)\frac{\partial^2\Psi}{\partial z^2}$$

Multiplying through by Ψ and integrating between the boundaries in the vertical and over one wavelength in the horizontal we have for the case P=1:

$$T\sigma^2\int_0^L\int_0^1 \Psi\,\frac{\partial^2\Psi}{\partial z^2}\,dydz = -T\int_0^L\int_0^1 \Psi\,\frac{\partial^6\Psi}{\partial z^6}\,dydz$$

Employing free-slip boundary conditions (Ψ, $\partial^2\Psi/\partial z^2$, $\partial^4\Psi/\partial z^4 = 0$ at the boundaries) and integrating by parts, the preceding is equivalent to:

$$T\sigma^2\int_0^L\int_0^1 \left(\frac{\partial\Psi}{\partial z}\right)^2 dydz = -T\int_0^L\int_0^1 \left(\frac{\partial^3\Psi}{\partial z^3}\right)^2 dydz$$

Evidently, $\sigma^2 < 0$ in this case; since by the preceding arguments σ^2 never vanishes, it must always be negative. This violates the separation, via (11), of the governing equations into real and imaginary parts; hence, this branch of the solution does not exist. The marginal state for oscillatory instabiltiy is therefore impossible under hydrostatic conditions when the boundaries are free-slip.

By a procedure similar to that employed in deriving Equation (13), the relation governing oscillatory instability for Case (ii) may be derived:

$$T\left(1+\frac{1}{P}\right)^2 (\nabla^2)^3 \Psi = -\frac{1}{2}\left(3+\frac{1}{P}\right) \frac{\overline{U_z}}{\overline{\eta}} \frac{\partial^2 \Psi}{\partial y \partial z} - \frac{\partial^2 \Psi}{\partial z^2} \qquad (14)$$

Again, this has the same form as the steady instability Equation (10), except that the diffusion term is multiplied by $(1 + 1/P)^2$, and the shear term by $\frac{1}{2}(3 + 1/P)$ instead of 1+P.

The diffusion parameter is always greater in the oscillatory case, and when $P > 1$ the shear term is always smaller; however, if $P < 1$, the latter is larger and the initial dominance of one or the other instability form is not obvious. In order to ascertain which form of instability sets in first as the fluid is destabilized, it is necessary to solve Equation (14).

(c) Summary

For convenience, the scaled equations governing the onset of steady and oscillatory instability in stably stratified and neutrally stratified fluid are summarized here, as well as the scaling relevant to each and the two forms of boundary conditions to be applied in their solution:

Case (i) - Hydrostatic disturbances in fluid with stable stratification:

Steady Overturning:

$$T \frac{\partial^6 \Psi}{\partial z^6} = -\chi_i \frac{\partial^2 \Psi}{\partial y \partial z} - \chi_i \frac{\partial^2 \Psi}{\partial y^2} - \frac{\partial^2 \Psi}{\partial z^2} \qquad (9)$$

$$T \equiv \frac{f}{\eta} \frac{\nu^2}{f^2 H^4} \qquad \chi_i \equiv \frac{f}{\eta} \frac{1}{Ri} \frac{(1+P)^2}{P}$$

$$z^* \rightarrow zH \qquad y^* \rightarrow yH \frac{N^2 P}{f \overline{U_z} (1+P)}$$

(asterisks denote dimensional variables)

Oscillatory instability not possible.

Case (ii) - Non-hydrostatic disturbances in neutrally stratified fluid:

$$\tau (\nabla^2)^3 \Psi = -\chi_{ii} \frac{\partial^2 \Psi}{\partial y \partial z} - \frac{\partial^2 \Psi}{\partial z^2} \qquad (10) \text{ and } (14)$$

$(y,z) \rightarrow (y,z)H$

Steady Overturning:

$$\tau = T;\ \chi_{ii} = + \frac{\overline{U_z}}{\overline{\eta}} (1+P)$$

Oscillatory:

$$\tau = T(1 + \frac{1}{P})^2;\ \chi_{ii} = \frac{\overline{U_z}}{\overline{\eta}} \frac{(3 + 1/P)}{2}$$

Boundary Conditions:

Free-slip: $\Psi,\ \frac{\partial^2 \Psi}{\partial z^2},\ \frac{\partial u}{\partial z},\ \frac{\partial p}{\partial z} = 0$ at boundaries

No-slip: $\Psi,\ \frac{\partial \Psi}{\partial z},\ u,\ \frac{\partial p}{\partial z} = 0$ at boundaries

CHAPTER 4

SOLUTION OF THE PERTURBATION EQUATIONS

The methods by which the equations developed within Chapter 3 are solved are described herein; the casual reader may proceed, without loss of continuity, to Chapter 5 in which the solutions are presented.

As a matter of general interest, certain aspects of the behavior of the solutions for vanishing and very large diffusivity are examined briefly, after which we describe a variational technique used to solve the equations for all values of the diffusion coefficients.

(a) Asymptotic Behavior for Vanishing Diffusion

If the coefficient of viscosity is vanishingly small (but P is finite), then the equations governing stationary and oscillatory instability may be solved forthwith. When T=0, these equations are reduced to second order and the boundary conditions are simply $\psi=0$ at $z=0,1$.

Equation (9) governing instability in a hydrostatic fluid (Case (i)) becomes:

$$\chi_i \frac{\partial^2\psi}{\partial y \partial z} + \chi_i \frac{\partial^2\psi}{\partial y^2} + \frac{\partial^2\psi}{\partial z^2} = 0$$

It should be remembered that Equation (9) exhibits multiple

boundary layers as $T \to 0$, so that the above provides an "outer" solution only. The equation governing the inner solution is obtained by noting that the boundary layer thickness is $O[(2\nu/f)^{1/2}]$; scaling y and z by this quantity gives

$$-4 \frac{\partial^6 \psi}{\partial z^6} = \chi_i \frac{\partial^2 \psi}{\partial y \partial z} + \chi_i \frac{\partial^2 \psi}{\partial y^2} + \frac{\partial^2 \psi}{\partial z^2}$$

(If z above is scaled by the boundary layer depth, the first order inner solution is obtainable analytically, but a match with the outer solution is impossible.) Since the inner solution is even more intractable than the complete solution, the boundary layer approach is not practical in this problem. As a review of the inviscid theory, we proceed to solve the outer equation, but the singularity of the fully viscous equation precludes the conclusion that as the diffusion becomes very small, the real solution approaches the inviscid result.

Applying the boundary conditions $\psi=0$ at $z=0,1$ the solution of the inviscid equation is

$$\psi = \sin \ell (y - \frac{\chi_i}{2} z) \sin n\pi z \qquad n=1,2,3$$

χ_i must satisfy the eigenvalue equation

$$\frac{\chi_i^2}{4} - \chi_i = \frac{n^2\pi^2}{\ell^2}$$

where ℓ is the horizontal wavenumber. The smallest value of χ_i is 4 and occurs as $\ell \to \infty$. From the definition of χ_i,

$$\frac{f}{\eta}\frac{1}{Ri}\frac{(1+P)^2}{P} = 4$$

The above is equivalent to the result of McIntyre (1969) for unbounded disturbances (see also Walton, 1975). The disturbances slope upward and to the left of the shear, corresponding to Stone's (1971) finding, with a dimensionless slope of 1/2 associated with $\chi_i = 4$. Dimensionally, the slope of the disturbances is:

$$\frac{\partial z}{\partial y} = \frac{f\overline{U_z}}{N^2}\left(\frac{1+P}{2P}\right)$$

This slope is greater than or less than that of the potential isotherms, depending on whether the Prandtl number is less than or greater than 1. The minimum possible slope is half that of the potential isotherms when $P \to \infty$; as the dimensional slope becomes large and approaches 1, the hydrostatic assumption will not be valid.

For Case (ii) (non-hydrostatic), the general form of

the inviscid equation is

$$\chi_{ii} \frac{\partial^2 \psi}{\partial y \partial z} + \frac{\partial^2 \psi}{\partial z^2} = 0$$

The solution corresponding to the boundary conditions $\psi=0$ at $z=0,1$ is:

$$\psi = \sin \pi z \cos \pi \left(\frac{2}{\chi_{ii}} y - z \right)$$

with $\chi_{ii} = 2\pi/\ell = L$, where L is the non-dimensional wavelength. The critical value of χ_{ii} is zero corresponding to a vanishing wavelength and a vertical disturbance orientation. For stationary overturning,

$$\chi_{ii} = \frac{\overline{U_z}}{\overline{\eta}} (1 + P)$$

and for oscillatory instability,

$$\chi_{ii} = \frac{\overline{U_z}}{\overline{\eta}} \frac{(3 + 1/P)}{2}$$

A comparison of these expressions indicates that as the fluid is destabilized, oscillatory instability will occur before stationary overturning in a neutrally stratified inviscid fluid whenever $P < 1$. It is also possible to show

that oscillatory instability can only occur when $P < 1$:

If the substitution $\psi = e^{i\sigma t}\Psi(y,z)$ is performed (σ and Ψ are both real), Equations (12a) and (12b) modified for the non-hydrostatic inviscid case may be written:

$$\sigma^2 \nabla^2 \Psi = 2 \frac{\overline{U_z}}{\overline{\eta}} \frac{\partial^2 \Psi}{\partial y \partial z} + \frac{\partial^2 \Psi}{\partial z^2}$$

$$\sigma^2 (1 + 2P) \nabla^2 \Psi = (1 + P) \frac{\overline{U_z}}{\overline{\eta}} \frac{\partial^2 \Psi}{\partial y \partial z} + \frac{\partial^2 \Psi}{\partial z^2}$$

where σ^2 has been non-dimensionalized by $f\overline{\eta}$. Eliminating the term $\partial^2\Psi/\partial y \partial z$ between the above, it is found that

$$\sigma^2 \nabla^2 \Psi [1 + 3P] = [1 - P] \frac{\partial^2 \Psi}{\partial z^2}$$

Multiplying through by Ψ and integrating between the boundaries in the vertical and across one wavelength in the horizontal, and employing integration by parts together with the boundary conditions $\Psi = 0$ at $z=0,1$ we arrive at:

$$\sigma^2 [1 + 3P] \int_0^1 \int_0^L [(\frac{\partial \Psi}{\partial z})^2 + (\frac{\partial \Psi}{\partial y})^2] dydz$$

$$= [1-P] \int_0^1 \int_0^L (\frac{\partial \Psi}{\partial z})^2 dydz$$

Clearly, σ will be real if and only if $P \leq 1$.

(b) Behavior of Eigenvalues Characterizing the Marginal State when the Diffusion is Very Large

Although general solutions by direct methods such as those employed in the last section are not attainable for large diffusion, certain aspects of the parameter relationships under these conditions become evident. As $T \to \infty$, we might expect that the equations governing hydrostatic and non-hydrostatic instability will take the respective forms:

$$\frac{T}{\chi_i} \frac{\partial^6 \psi}{\partial z^5} = - \frac{\partial^2 \psi}{\partial y \partial z} - \frac{\partial^2 \psi}{\partial y^2}$$

and

$$\frac{\tau}{\chi_{ii}} (\nabla^2)^3 \psi = - \frac{\partial^2 \psi}{\partial y \partial z}$$

where each equation has been divided through by χ. Since it must be true that $\chi \to \infty$ as $T \to \infty$, the term $\partial^2\psi/\partial z^2$ becomes subdominant in either case and may be neglected in the limit of large T.

As each of the preceding relations contains only one parameter, the solution of the eigenvalue problem must yield:

$$\frac{T}{\chi} \rightarrow \text{constant}$$

or

$$T \rightarrow \text{constant} \times \chi \text{ as } T \rightarrow \infty$$

Such linear asymptotic behavior will be evident in the complete solutions.

(c) A Variational Method for Obtaining Complete Solutions of the Characteristic Value Equations

A general technique for solving linear eigenvalue problems, first developed by Pellew and Southwell (1940) and used extensively by Chandrasekhar (1961), will be applied to solve the equations developed in Chapter 3. Although the method is based on entropy conservation within the fluid, the physical basis of its validity will not be apparent in the following derivations. The reader is referred to Chandrasekhar's text (ibid) for a discussion of the physical implications of the theorem.

(1) Free-Slip Boundaries

Equation (9), governing the onset of hydrostatic disturbances, is sixth order in z and hence requires three boundary conditions at both boundaries in order to be solved

uniquely. Two of these, ψ, $\partial^2\psi/\partial z^2 = 0$, follow directly from the statement of the boundary conditions. If Equation (2) is differentiated once with respect to z, it becomes evident that $\partial^4\psi/\partial z^4$ must also vanish at the boundaries. The conditions applied in the solution of Equation (9) will therefore be:

$$\psi, \frac{\partial^2\psi}{\partial z^2}, \frac{\partial^4\psi}{\partial z^4} = 0 \qquad \text{at } z=0,1 \tag{16}$$

Suppose that χ is specified in Equation (9). Then associated with a function ψ_j satisfying this equation will be a characteristic value T_j:

$$T_j \frac{\partial^6\psi_j}{\partial z^6} = -\chi \frac{\partial^2\psi_j}{\partial y\partial z} - \chi \frac{\partial^2\psi_j}{\partial y^2} - \frac{\partial^2\psi_j}{\partial z^2}$$

If the above is multiplied through by a different solution ψ_i (corresponding to the characteristic value T_i) and the resulting equation is integrated between the boundaries in z and across one wavelength in y, then

$$\int_0^1\int_0^L T_j\psi_i \frac{\partial^6\psi_j}{\partial z^6}\,dydz = -\chi \int_0^1\int_0^L \psi_i \frac{\partial^2\psi_j}{\partial y\partial z}\,dydz$$

$$- \chi \int_0^1\int_0^L \psi_i \frac{\partial^2\psi_j}{\partial y^2}\,dydz - \int_0^1\int_0^L \psi_i \frac{\partial^2\psi_j}{\partial z^2}\,dydz$$

(Henceforth, the domain of integration may be assumed to be in the y-z plane.) Applying the boundary conditions (16) and a sequence of integrations by parts, the above becomes

$$T_j \int_0^l\int_0^L \frac{\partial^3\psi_i}{\partial z^3}\frac{\partial^3\psi_j}{\partial z^3} = \chi \int_0^l\int_0^L \psi_i \frac{\partial^2\psi_j}{\partial y\partial z}$$

$$- \chi \int_0^l\int_0^L \frac{\partial\psi_i}{\partial y}\frac{\partial\psi_j}{\partial y} - \int_0^l\int_0^L \frac{\partial\psi_i}{\partial z}\frac{\partial\psi_j}{\partial z} \qquad (17)$$

It may also be shown, through integration by parts, that

$$\int_0^l\int_0^L \psi_i \frac{\partial^2\psi_j}{\partial y\partial z} = \int_0^l\int_0^L \psi_j \frac{\partial^2\psi_i}{\partial y\partial z}$$

From this symmetry, it is evident in Equation (17) that

$$\int_0^l\int_0^L \frac{\partial^3\psi_i}{\partial z^3}\frac{\partial^3\psi_j}{\partial z^3} = \delta_{ij}$$

so that the functions $\partial^3\psi_j/\partial z^3$ are orthogonal. Then, Equation (17) may be written in the form:

$$T = \frac{\chi \int_0^l\int_0^L \psi \frac{\partial^2\psi}{\partial y\partial z} - \chi \int_0^l\int_0^L \left(\frac{\partial\psi}{\partial y}\right)^2 - \int_0^l\int_0^L \left(\frac{\partial\psi}{\partial z}\right)^2}{\int_0^l\int_0^L \left(\frac{\partial^3\psi}{\partial z^3}\right)^2} \equiv \frac{I_1}{I_2} \qquad (18)$$

According to the variational theorem we will prove presently, that function ψ which satisfies the correct boundary conditions and maximizes the value of T given by Equation (18) satisfies the partial differential Equation (9). The proof is as follows:

If T is to be maximized in (18), a small variation in T satisfies

$$\delta T = \frac{1}{I_2} [\delta I_1 - \frac{I_1}{I_2} \delta I_2] = 0$$

or

$$\delta I_1 - T\delta I_2 = 0 \tag{19}$$

(I_1 and I_2 are the numerator and denominator of (18) respectively.) From Equation (18),

$$\delta I_1 = \chi \int_0^1 \int_0^L (\delta\psi \frac{\partial^2\psi}{\partial y \partial z} + \psi\delta \frac{\partial^2\psi}{\partial y \partial z})$$

$$- \chi \int_0^1 \int_0^L 2 \frac{\partial\psi}{\partial y} \delta \frac{\partial\psi}{\partial y} - \int_0^1 \int_0^L 2 \frac{\partial\psi}{\partial z} \delta \frac{\partial\psi}{\partial z}$$

A sequence of integrations by parts transforms the above to:

$$\delta I_1 = \chi \int_0^1\int_0^L \frac{\partial^2\psi}{\partial y\partial z}\,(2\delta\psi) + \chi \int_0^1\int_0^L \frac{\partial^2\psi}{\partial y^2}\,(2\delta\psi)$$

$$+ \int_0^1\int_0^L \frac{\partial^2\psi}{\partial z^2}\,(2\delta\psi)$$

Similarly, the increment δI_2 is:

$$\delta I_2 = - \int_0^1\int_0^L \frac{\partial^6\psi}{\partial z^6}\,(2\delta\psi)$$

Finally, the relation (19) becomes:

$$\int_0^1\int_0^L [\chi \frac{\partial^2\psi}{\partial y\partial z} + \chi \frac{\partial^2\psi}{\partial y^2} + \frac{\partial^2\psi}{\partial z^2} + T \frac{\partial^6\psi}{\partial z^6}]\,(2\delta\psi) = 0$$

For an arbitrary variation $\delta\psi$ that satisfies the boundary conditions (16) and which makes $\delta T=0$, the preceding relation is satisfied only if the expression in brackets vanishes. This expression is the original characteristic value Equation (9).

By parallel arguments, one may derive and prove a variational relation valid in the non-hydrostatic case (ii) for free-slip boundaries:

$$\tau = \frac{\chi_{ii} \int_0^1 \int_0^L \psi \frac{\partial^2 \psi}{\partial y \partial z} - \int_0^1 \int_0^L \left(\frac{\partial \psi}{\partial z}\right)^2}{\int_0^1 \int_0^L \left[\left(\frac{\partial^3 \psi}{\partial y^3}\right)^2 + 3\left(\frac{\partial^3 \psi}{\partial y^2 \partial z}\right)^2 + 3\left(\frac{\partial^3 \psi}{\partial y \partial z^2}\right)^2 + \left(\frac{\partial^3 \psi}{\partial z^3}\right)^2\right]} \quad (20)$$

In order to solve the characteristic value equations using the variational approach, it is necessary to find the form of the streamfunction ψ which satisfies the boundary conditions and maximizes T in Equation (18), for the hydrostatic case, and (20) in the neutral stratification case. One approach is to construct a Fourier series representation of ψ, each term of which satisfies the boundary conditions. For free-slip conditions (16), a series capable of completely describing an otherwise arbitrary structure within the boundaries is:

$$\psi = \sum_{n=1}^{\infty} \sin n\pi z \, (a_n \sin \ell y + b_n \cos \ell y) \quad (21)$$

where ℓ is the horizontal wavenumber. For a specified ℓ, we may treat the Fourier coefficients a_n and b_n as the variational parameters and proceed to find that set of coefficients which maximizes T in the relations (18) or (20). Enough terms of the Fourier series should be taken to assure a reasonably accurate approximation of the characteristic value T. The operation may be performed

for various wavenumbers ℓ in order to find which wavenumber first becomes unstable (i.e., we maximize T with respect to ℓ also). Following this procedure, we substitute the streamfunction form (21) into the integral relation (18) and require that

$$\frac{\partial I_1}{\partial a_n} - T \frac{\partial I_2}{\partial a_n} = 0$$

and for all n (22)

$$\frac{\partial I_2}{\partial b_n} - T \frac{\partial I_2}{\partial b_n} = 0$$

If the series (21) is truncated to N terms, these substitutions yield two sets of N equations for the Fourier coefficients:

$$-\chi_i \sum_{m=1}^{N} \frac{4nm\pi}{m^2-n^2}\left(\frac{1-(-1)^{n+m}}{2}\right) b_m + \left(\frac{1}{2} L\pi^2 n^2 + \frac{2\pi^2}{L} \chi_i + \frac{1}{2} L\pi^6 n^6 T\right) a_n = 0$$

and

$$\chi_i \sum_{m=1}^{N} \frac{4nm\pi}{m^2-n^2} \left(\frac{1-(-1)^{n+m}}{2}\right) a_m + \left(\frac{1}{2} L\pi^2 n^2 +\right.$$

$$+ \frac{2\pi^2}{L} \chi_i + \frac{1}{2} L\pi^6 n^6 T) b_n = 0$$

$$n = 1,2,3,\ldots,N$$

The first group in each equation is non-zero only when n+m is an odd integer. It follows that both of the above relations can be true if

$$b_n = a_n (-1)^{n+1}$$

Then, the preceding equations are identical; either constitutes a closed set of N linear equations for the N Fourier coefficients. Such a system will only have a solution for non-zero Fourier coefficients provided that the determinant of the coefficients vanishes. That is,

$$|A_{nm}| = 0 \qquad (23)$$

where the matrix elements of A are defined as follows:

$$\text{if } n=m,\ A_{nn} \equiv \frac{1}{2} L\pi^2 n^2 + \frac{2\pi^2}{L} \chi_i + \frac{1}{2} L\pi^6 n^6 T$$

$$\text{if } n+m = \text{odd integer},\ A_{nm} \equiv -\chi_i \frac{4nm\pi (-1)^{m+1}}{m^2-n^2}$$

if $n \neq m$ and $n+m =$ even integer, $A_{nm} = 0$

This may also be written in the form:

$$A_{nm} \equiv \left(\frac{1}{2} L\pi^2 n^2 + \frac{2\pi^2}{L} \chi_i + \frac{1}{2} L\pi^6 n^6 T\right) \delta_{nm}$$

$$+ \chi_i \frac{4nm\pi}{m^2-n^2} \left(\frac{(-1)^m - (-1)^n}{2}\right)$$

It may be seen that the parameter T only appears in the diagonal elements of the matrix A. If each row in A is divided through by $\frac{1}{2} L\pi^6 n^6$, then T will be a negative eigenvalue of the matrix A. In fact, A is symmetric so that all N eigenvalues are real. That eigenvalue corresponding to the largest positive value of T is taken to be the root of physical interest.

The method of solution of the determinant equation (23) is as follows: First, the solution obtained from the two term approximation of the Fourier Series (21) is computed by hand. (In this instance, one has only to solve a quadratic equation.) Then, a numerical solution of the eigenvalues of the matrix A is obtained on computer, using a commercial routine designed for the solution of such problems.* Initially, the calculations were performed for

* The routine used was obtained from the eigen analysis

values of N ranging from 2 to 10 in order that the convergence of the eigenvalues could be checked. The second order matrix result confirmed the hand analysis, and the eigenvalues were found to converge to 4 or 5 significant figures within four terms.* Thereafter, the program was run using five terms of the Fourier Series. The eigenvector of the matrix A corresponding to the eigenvalue T of interest is also found and normalized by the first Fourier coefficient a_1. The entire operation is repeated for different values of the horizontal wavelength L in order to find the most unstable wave.

An example of the values of the Fourier coefficients, corresponding to $T = 10^{-4}$, is presented in Table 1 for the hydrostatic case. The rapid decrease in the magnitude of the Fourier coefficients is found to occur in all the calculations presented here, the complete results of which will be presented in Chapter 5.

The parameter τ in Equation (20), for the non-hydrostatic disturbances, is maximized using the same streamfunction Fourier Series (21). The maximization of

---

section of the IMSL (International Mathematics and Statistics Libraries, Inc.) library as available in 1977. Double-Precision was used at all times; the program was run on an IBM 370 available at the MIT Computation Center.

---

* See Appendix 6

TABLE 1

Fourier Coefficients of the Series (21) Describing the Streamfunction of the Marginal State when the Disturbances are Hydrostatic, and $T = 10^{-4}$

($b_n = a_n(-1)^{n+1}$)

n	a_n
1	1.0000
2	-0.8572
3	-0.2445
4	0.0076
5	-0.0060

τ with respect to the two sets of Fourier coefficients a_n and b_n yields two sets of N linear equations:

$$4\pi\chi_{ii} \sum_{m=1}^{N} \left(\frac{nm}{m^2-n^2}\right) \varepsilon_{nm} b_m - \frac{1}{2}L[n^2\pi^2 + \tau(n^2\pi^2 + \ell^2)^3]a_n = 0$$

$$-4\pi\chi_{ii} \sum_{m=1}^{N} \left(\frac{nm}{m^2-n^2}\right) \varepsilon_{nm} a_m - \frac{1}{2}L[n^2\pi^2 + \tau(n^2\pi^2 + \ell^2)^3]b_n = 0$$

$$n = 1,2,3,\ldots,N$$

where

$$\varepsilon_{nm} \equiv \begin{cases} 1 \text{ if } n+m = \text{odd integer} \\ \\ 0 \text{ otherwise} \end{cases}$$

Again, it is evident that $b_n = a_n(-1)^{n+1}$. If the Fourier coefficients are non-zero, then the determinant of the matrix of these coefficients must yanish. The coefficient matrix A is defined from the preceding relations as follows:

$$A_{nm} = \frac{1}{2}L\,[n^2\pi^2 + \tau(n^2\pi^2 + \ell^2)^3]\,\delta_{nm}$$

$$+ 4\pi\chi_{ii} \frac{nm(-1)^{m+1}}{n^2-m^2}\,\varepsilon_{nm}$$

The eigenvectors τ (alternately χ_{ii}) may be obtained by solving the determinant equation. Since this particular problem has been solved exactly by Kuo (1954), we here solve the determinant equation to third order (N=3) analytically and compare this approximation with Kuo's results. The third order determinant equation may be written, in this case, as an explicit relationship between χ_{ii}^2 and the modified inverse Taylor number τ, together with the wavelength L ($= 2\pi/\ell$):

$$\chi_{ii}^2 = \left(\frac{5\pi L}{48}\right)^2 \left[\frac{(1+\pi^4\tau(1+4/L^2)^3)(4+\pi^4\tau(4+4/L^2)^3)(9+\pi^4\tau(9+4/L^2)^3)}{(1+\pi^4\tau(1+4/L^2)^3) + (5/9)^2(9+\pi^4\tau(9+4/L^2)^3)}\right] \quad \ldots(24)$$

Obviously, the positive root χ_{ii} is the one of physical interest in this case. The solutions of (24) are obtained and minimized with respect to L using an electronic calculator. The results will be presented graphically in Chapter 5; in Table 2, a few values obtained from (24) are compared with Kuo's (1954) results for selected values of τ. Kuo did not consider horizontal shear in the equilibrium flow, or the possibility of overstable oscillations; otherwise, his formulation of the problem

TABLE 2

Comparison of Kuo's (1954) Results
with Those Obtained Using a Variational Method
to Third Order, for Case (ii) (Non-Hydrostatic)

τ	χ_{ii} (Kuo)	χ_{ii} (Variational)	L (Kuo)	L (Variational)
10^{-6}	.603	.648	.51	.52
10^{-5}	1.007	1.065	.80	.79
10^{-4}	2.026	2.098	1.29	1.29
10^{-3}	6.100	6.146	2.07	2.07
10^{-2}	32.880	32.907	2.94	2.95

is the same. The relationship between his non-dimensional parameters, Q_o and T_o, and mine are as follows:

$$Q_o = \chi_{ii}/\tau$$

$$T_o = 1/\tau$$

$$a = \pi/L$$

Considering the complexity of the form of the stream-

function, the third order variational method yields surprisingly good results. The errors in χ_{ii} range from about 7.5% for $\tau = 10^{-6}$ to less than 0.1% when $\tau = 10^{-2}$. The largest errors occur for small τ, since the spatial variation of the streamfunction becomes increasingly great when τ decreases (the variation becomes infinitely rapid when τ=0), and exceeds the capacity of the truncated series (21) to adequately describe its structure. Note also that the approximate value of χ_{ii} is always greater than the exact result, as the degree to which χ_{ii} can be minimized depends on the precision of the streamfunction structure approximation.

(2) No-Slip Boundaries

The boundary conditions applicable when all velocity components as well as the temperature perturbation vanish at the boundaries are:

$$\psi, \frac{\partial \psi}{\partial z}, u, \frac{\partial p}{\partial z} = 0 \qquad \text{at boundaries}$$

It proves convenient, in this instance, to express both the latter two conditions in the form of constraints on the streamfunction ψ. In general, this is quite complicated; but for the special case of steady overturning under

hydrostatic conditions, the boundary conditions take a simple form.

If horizontal diffusion is neglected, the hydrostatic steady state forms of Equations (1)-(5) may be cross-differentiated to obtain expressions for the second derivatives in y of u and $\partial p/\partial z$. In dimensionless form, these are:

$$\frac{\partial^2 u}{\partial y^2} = (\chi_i - 2 - P)\frac{\partial \psi}{\partial y} - T\,\frac{\partial^5 \psi}{\partial y \partial z^4} + \left(1 - \frac{1+P}{\chi_i}\right)\left(\frac{\partial \psi}{\partial z} + T\,\frac{\partial^5 \psi}{\partial z^5}\right) \quad \ldots (25)$$

$$\frac{\partial^2}{\partial y^2}\,\frac{\partial p}{\partial z} = (\chi_i - 1 - P)\frac{\partial \psi}{\partial y} - T(1+P)\frac{\partial^5 \psi}{\partial y \partial z^4} + \frac{\partial \psi}{\partial z} + T\,\frac{\partial^5 \psi}{\partial z^5} \quad \ldots (26)$$

in which u and $\partial p/\partial z$ have been non-dimensionalized as follows:

$$u^* \rightarrow u\,\frac{\nu}{H\overline{\eta}}\,(1 + P)$$

$$\partial p^*/\partial z \rightarrow \frac{p}{z}\,\frac{\nu}{f U_z H^2}\,\chi_i \quad (27)$$

where the asterisks denote the dimensional variables. Two constants of integration involved in the derivation of these expressions have been set equal to zero to exclude the steady geostrophic solution

$$u = - \frac{\partial p}{\partial y}$$

$$\psi = 0$$

The requirement that u and $\partial p/\partial z$ vanish at the boundaries implies, in Equations (25) and (26), that

$$\frac{\partial^4 \psi}{\partial z^4} = \frac{\partial^5 \psi}{\partial z^5} = 0 \qquad \text{at boundaries} \qquad (28)$$

The uneven nature of these conditions increases the complexity of the problem, and in fact renders invalid the variational relations (18) and (20), since in deriving these expressions using integration by parts, either $\partial^2\psi/\partial z^2$ or $\partial^3\psi/\partial z^3$ must vanish at the boundaries. It is therefore necessary to construct a new variational method applicable to the no-slip boundary conditions. This method will involve two variables: ψ and a function F defined by

$$F \equiv - \frac{\partial^2 p}{\partial y \partial z}$$

We may then use the eight boundary conditions:

$$F,\ \psi,\ \frac{\partial \psi}{\partial z}\ ,\ \frac{\partial^4 \psi}{\partial z^4} = 0 \qquad \text{at } z=0,1 \tag{29}$$

For simplicity, the following derivation will be carried through with the Prandtl number set equal to unity. From the form of Equation (9) it is evident that the final characteristic value of the shear parameter will be equivalent to the general parameter if the former is multiplied by

$$\frac{(1+P)^2}{4P}$$

The dimensionless, hydrostatic forms of Equations (1), (2), and (4) may then be written:

$$\frac{\partial^2 u}{\partial z^2} = \frac{\partial \psi}{\partial z} + \frac{2f}{\overline{\eta}} \frac{1}{Ri} \frac{\partial \psi}{\partial y} \tag{30}$$

$$F = \frac{\partial u}{\partial z} + T \frac{\partial^4 \psi}{\partial z^4} \tag{31}$$

$$\frac{\partial^2 F}{\partial z^2} = - \frac{2f}{\overline{\eta}} \frac{1}{Ri} \frac{\partial^2 \psi}{\partial y \partial z} - \frac{4f}{\overline{\eta}} \frac{1}{Ri} \frac{\partial^2 \psi}{\partial y^2} \tag{32}$$

in which u has been normalized by $\nu/H\overline{\eta}$ and F by $\nu/f\overline{\eta}$. Equation (2) has been differentiated once with respect to

z in order to obtain (31), and Equation (4) has likewise been differentiated once in y to obtain (32). Equations (30) and (31) may be combined to yield:

$$\frac{\partial F}{\partial z} = \frac{\partial \psi}{\partial z} + \frac{2f}{\bar{\eta}} \frac{1}{Ri} \frac{\partial \psi}{\partial y} + T \frac{\partial^5 \psi}{\partial z^5} \tag{33}$$

If the above is multiplied through by F and integrated between the boundaries in z and across one wavelength in y, an integration by parts together with the boundary condition F = 0 at z=0,1 yields

$$\int_0^1 \int_0^L F \frac{\partial^2 F}{\partial z^2} = - \int_0^1 \int_0^L \frac{\partial F}{\partial z} \frac{\partial F}{\partial z}$$

$$= - \int_0^1 \int_0^L \frac{\partial F}{\partial z} \left(\frac{\partial \psi}{\partial z} + \frac{2f}{\bar{\eta}} \frac{1}{Ri} \frac{\partial \psi}{\partial y} + T \frac{\partial^5 \psi}{\partial z^5} \right)$$

The last equality follows from Equation (33), and is here separated into two parts:

$$\int_0^1 \int_0^L F \frac{\partial^2 F}{\partial z^2} = - \int_0^1 \int_0^L \frac{2f}{\bar{\eta}} \frac{1}{Ri} \frac{\partial \psi}{\partial y} \frac{\partial F}{\partial z} - \int_0^1 \int_0^L \left(\frac{\partial \psi}{\partial z} + T \frac{\partial^5 \psi}{\partial z^5} \right) \frac{\partial F}{\partial z}$$

(i) (ii)

Using Equation (33) for $\partial F/\partial z$, the first integral (i) becomes:

$$- \int_0^1 \int_0^L \frac{2f}{\bar{\eta}} \frac{1}{Ri} \frac{\partial \psi}{\partial y} \left(\frac{\partial \psi}{\partial z} + \frac{2f}{\bar{\eta}} \frac{1}{Ri} \frac{\partial \psi}{\partial y} + T \frac{\partial^5 \psi}{\partial z^5} \right) \qquad \text{(i)}$$

By an integration by parts, the second integral (ii) may be expressed:

$$\int_0^1 \int_0^L \left(\psi + T \frac{\partial^4 \psi}{\partial z^4} \right) \frac{\partial^2 F}{\partial z^2}$$

Using (32) for $\partial^2 F / \partial z^2$, the preceding becomes:

$$- \int_0^1 \int_0^L \left(\psi + T \frac{\partial^4 \psi}{\partial z^4} \right) \left(\frac{2f}{\bar{\eta}} \frac{1}{Ri} \frac{\partial^2 \psi}{\partial y \partial z} + \frac{4f}{\bar{\eta}} \frac{1}{Ri} \frac{\partial^2 \psi}{\partial y^2} \right) \qquad \text{(ii)}$$

The sum of (i) and (ii), after several integrations by parts, yields:

$$\int_0^1 \int_0^L F \frac{\partial^2 F}{\partial z^2} = \frac{4f}{\bar{\eta}} \frac{1}{Ri} \int_0^1 \int_0^L \left[\left(1 - \frac{f}{\bar{\eta}} \frac{1}{Ri} \right) \left(\frac{\partial \psi}{\partial y} \right)^2 + T \left(\frac{\partial^3 \psi}{\partial y \partial z^2} \right)^2 \right]$$

The variational principle may be written $\delta T = 0$ where

$$T = \frac{- \frac{\bar{\eta}}{f} \frac{Ri}{4} \int_0^1 \int_0^L \left(\frac{\partial F}{\partial z} \right)^2 + \int_0^1 \int_0^L \left(\frac{f}{\bar{\eta}} \frac{1}{Ri} - 1 \right) \left(\frac{\partial \psi}{\partial y} \right)^2}{\int_0^1 \int_0^L \left(\frac{\partial^3 \psi}{\partial y \partial z^2} \right)^2} \equiv \frac{I_1}{I_2} \qquad (34)$$

Admittedly, the motivation behind the preceding derivation is not apparent; however, the proof that the

maximization of T with respect to the function ψ yields the proper characteristic values is quite straightforward and may be found in Appendix 3.

In order to extract the proper eigenvalue T and the structure of the solutions ψ and F from the variational relation (34), we again construct Fourier Series representations of ψ and F, each term of which satisfies the boundary conditions. Since, by Equation (33), $\partial F/\partial z$ may be expressed explicitly in terms of ψ, however, we may alternatively write (34) in terms of ψ alone and use the eight boundary conditions on ψ:

$$\psi, \frac{\partial\psi}{\partial z}, \frac{\partial^4\psi}{\partial z^4}, \frac{\partial^5\psi}{\partial z^5} = 0 \qquad \text{at } z=0,1 \tag{35}$$

Since $F \equiv -\partial^2 p/\partial y\partial z$, the above conditions assure that F also vanishes at the boundaries.

In order to construct a Fourier Series representation of the streamfunction ψ, it is necessary to find orthogonal functions which satisfy, term by term, the boundary conditions (35) and are periodic in y. It proves convenient to shift the coordinate system so that the boundaries lie at $z = -1/2$ and $z = +1/2$. Then, as derived in Appendix 4, the functions S_m and C_m satisfy the conditions (35) in z,

and are also orthogonal:

$$S_m \equiv \frac{\sin\mu_m z}{\sin(\mu_m/2)} - \frac{\sinh\mu_m z}{\sinh(\mu_m/2)}$$

$$C_m \equiv \frac{\cos\lambda_m z}{\cos(\lambda_m/2)} - \frac{\cosh\lambda_m z}{\cosh(\lambda_m/2)} \qquad (36)$$

where the μ_m's and λ_m's are roots of the equations

$$\coth\frac{\mu}{2} - \cot\frac{\mu}{2} = 0$$

$$\tanh\frac{\lambda}{2} + \tan\frac{\lambda}{2} = 0$$

The functions (36) have been normalized so that

$$\int_{-1/2}^{1/2} S_m S_n = \int_{-1/2}^{1/2} C_m C_n = \delta_{mn}$$

Also, all functions S_m are orthogonal to all functions C_m:

$$\int_{-1/2}^{1/2} S_m(z) C_n(z) = 0$$

It is now possible to construct a complete Fourier Series describing a streamfunction ψ that is arbitrary except that it meets the boundary conditions (35) and is periodic in y:

$$\psi = \sum_{m=1}^{\infty} (a_m S_m \sin \ell y + B_m C_m \cos \ell y) \tag{37}$$

in which a_m and B_m are constant coefficients which will be treated as variational parameters.

The above is substituted into the integral relation (34) (using (33) for $\partial F/\partial z$), and T is maximized with respect to each of the coefficients a_m and B_m:

$$\begin{aligned} \frac{\partial I_1}{\partial a_m} - T \frac{\partial I_2}{\partial a_m} &= 0 \\ \frac{\partial I_1}{\partial B_m} - T \frac{\partial I_2}{\partial B_m} &= 0 \end{aligned} \tag{38}$$

$$m = 1,2,3,\ldots,M$$

When the Fourier Series (37) is truncated to M terms, the extremization of T with respect to each a_m and B_m results in two sets of M linear equations for the Fourier coefficients. Performing the integrals and the operations (38), these sets are:

$$a_n (1 + T\mu_n{}^4) \ell^2 \chi_i + \sum_{m=1}^{M} [a_m [\overline{S_n{}' S_m{}'}] (1 + T\mu_n{}^4)(1 + T\mu_m{}^4)$$

$$+ B_m \ell \chi_i [\overline{S_n C_m{}'}] (1 + \tfrac{1}{2} T(\mu_n{}^4 + \lambda_m{}^4))] = 0 \tag{39a}$$

$$B_n(1+T\lambda_n^4)\ell^2\chi_i + \sum_{m=1}^{M}[B_m[\overline{C_n'C_m'}](1+T\lambda_n^4)(1+T\lambda_m^4)$$

$$+ a_m[\overline{S_mC_n'}]\ell\chi_i(1+\frac{1}{2}T(\lambda_n^4+\mu_m^4))] = 0 \qquad (39b)$$

$n = 1,2,3,\ldots,M$

The Prandtl number dependence has been re-inserted and χ_i is defined in the usual way:

$$\chi_i \equiv \frac{f}{\eta}\frac{1}{Ri}\frac{(1+P)^2}{P}$$

The bracketed quantities denote the following:

$$[\overline{S_n'S_m'}] \equiv \int_{-1/2}^{1/2}\frac{\partial S_n}{\partial z}\frac{\partial S_m}{\partial z} = \begin{cases} \dfrac{8\mu_n^2\mu_m^2[\mu_n\cot\frac{\mu_n}{2} - \mu_m\cot\frac{\mu_m}{2}]}{\mu_m^4 - \mu_n^4} & n\neq m \\ \mu_m\cot\frac{\mu_m}{2}\,[\mu_m\cot\frac{\mu_m}{2} - 2] & n=m \end{cases}$$

$$\overline{[C_n' C_m']} \equiv \int_{-1/2}^{1/2} \frac{\partial C_n}{\partial z} \frac{\partial C_m}{\partial z} = \begin{cases} \dfrac{8\lambda_n^2\lambda_m^2[\lambda_m \tan\frac{\lambda_m}{2} - \lambda_n \tan\frac{\lambda_n}{2}]}{\lambda_m^4 - \lambda_n^4} & n \neq m \\ \lambda_n \tan\frac{\lambda_n}{2}\ [\lambda_n \tan\frac{\lambda_n}{2} + 2] & n = m \end{cases}$$

$$\overline{[S_n C_m']} \equiv \int_{-1/2}^{1/2} S_n \frac{\partial C_m}{\partial z} = \frac{-8\mu_n^2\lambda_m^2}{\mu_n^4 - \lambda_m^4}$$

The coefficients of the a_n's and B_n's in Equations (39) comprise a characteristic matrix for the value of χ_i, with T specified. The characteristic value problem may be phrased in terms of the eigenvalues of this matrix as follows:

First, define a new horizontal wavenumber ℓ':

$$\ell' \equiv \ell\chi_i$$

Then, divide through each of the M equations in sets (39a) and (39b) by $\ell'^2(1 + T\mu_n^4)$ and $\ell'^2(1 + T\lambda_n^4)$ respectively. The resulting sets are:

$$\frac{a_n}{\chi_i} + \sum_{m=1}^{M} \left[\frac{a_n}{\ell'^2} [\overline{S_n' S_m'}] (1 + T\mu_m^4) + \frac{B_m}{\ell'} [\overline{S_n C_m'}] \left(\frac{1 + \frac{1}{2}T(\mu_n^4 + \lambda_m^4)}{1 + T\mu_n^4} \right) \right] = 0$$

. . .(40a)

$$\frac{B_n}{\chi_i} + \sum_{m=1}^{M} \left[\frac{B_m}{\ell'^2} [\overline{C_n' C_m'}] (1 + T\lambda_m^4) + \frac{a_m}{\ell'} [\overline{S_m C_n'}] \left(\frac{1 + \frac{1}{2}T(\lambda_n^4 + \mu_m^4)}{1 + T\lambda_n^4} \right) \right] = 0$$

. . .(40b)

$n = 1,2,3,\ldots,M$

An order of the above set of linear equations is now constructed so that the quantity $1/\chi_i$ is an eigenvalue of the associated matrix of coefficients. The dimensions of the array will be 2M x 2M, as there are M equations for a_1, a_2, ..., a_n and M for B_1, B_2, ..., B_m. The first M rows of the array comprise the set of Equations (40a); the second M rows contain Equations (40b).

Also, the first M columns contain the coefficients of a_1-a_m, while the second M columns contain the B's:

$$
\begin{cases}
A_{11}a_1 + A_{12}a_2 + \cdots A_{1m}a_m + A_{1(1+m)}B_1 + A_{1(2+m)}B_2 + \cdots A_{1,(2M)}B_M = 0 \\
A_{21}a_2 + \cdots = 0 \\
\vdots \\
A_{(m+1),1}a_1 + A_{(m+1),2}a_2 + \cdots + A_{(M+1)2M}B_M = 0 \\
\vdots \\
A_{2M,1}a_1 + \cdots + A_{2m,2m}B_M = 0
\end{cases}
$$

By this construction, the quantity $-1/\chi_i$ is an eigenvalue of the matrix A, where A_{ij} is defined as follows:

(I) For $i \leq M$

(a) For $j \leq M$

$$A_{ij} \equiv \frac{[\overline{S_i' S_j'}]}{\ell'^2} [1 + T\mu_j^4]$$

(b) For $j > M$

$$A_{ij} \equiv \frac{[\overline{S_i C_{j-M}'}]}{\ell'} \frac{1 + \frac{1}{2}T(\mu_i^4 + \lambda_{j-M}^4)}{1 + T\mu_i^4}$$

(II) For $i > M$

(a) For $j \leq M$

$$A_{ij} \equiv \frac{[\overline{S_j C_{i-M}'}]}{\ell'} \quad \frac{1 + \frac{1}{2} T (\lambda_{i-M}^4 + \mu_j^4)}{1 + T \lambda_{i-M}^4}$$

(b) For $j > M$

$$A_{ij} \equiv \frac{[C_{i-M}' C_{j-M}']}{\ell'^2} [1 + T \lambda_{j-M}^4]$$

The largest positive eigenvalue $1/\chi_i$ is found from the matrix thus defined using the numerical methods described in Part I. The wavenumber ℓ' that minimizes χ_i is also obtained. In this instance, a manual calculation is only practical when M=1, but nevertheless provides a valuable check of the numerical scheme and computer program. Again, it is found that the eigenvalue converges to three or four significant figures as the number of terms in the Fourier Series (37) is increased to five, except for very small values of the parameter T ($< 10^{-6}$).* The results presented here are obtained using the five-term approximation of (37). Eigenvectors of the matrix A are also found, enabling one to compute the relative magnitudes of the Fourier coefficients and so construct an approximate

---

* See Appendix 6

streamfunction. The amplitude of these coefficients drops off rapidly with increasing order, as was found for the free-slip problem. In Table 3, examples of the Fourier coefficients associated with a diffusion parameter $T = 10^{-4}$ are listed. (All values have been normalized by a_1.)

A complete description of the marginal state for inertial instability in a hydrostatic fluid with no-slip boundaries will be found in the following chapter.

TABLE 3

Fourier Coefficients of the Series (37), Normalized by a_1, for No-Slip Boundaries and $T = 10^{-4}$

n	a_n	B_n
1	1.0000	1.0912
2	0.0105	-0.2785
3	0.0029	-0.0123
4	0.0006	-0.0016
5	0.0002	-0.0003

CHAPTER 5

RESULTS OF THE STABILITY ANALYSIS

The methods described in the preceding chapter have been used to solve the characteristic value equations derived within Chapter 3; the solutions are presented herein. Although these results are approximate, they may be made as accurate as one wishes, according to the degree of computation deemed practical. In most of the solutions discussed presently, the characteristic values of the stability parameters are correct to at least three significant figures. Any errors involved in the computation of the associated structure functions are completely masked by the inaccuracies of their graphing, with some exceptions as discussed below.

(a) Hydrostatic Disturbances

The critical values of the inertial stability parameter χ_i, as a function of T, are presented graphically in Figures 4a, b, and c for both sets of boundary conditions. (Each of the plots are presented as both linear and log-log curves in order to expose the details of the linear as well as exponential variation of the parameters.)

As one might expect, the critical value of the shear parameter χ_i increases monotonically with the diffusion

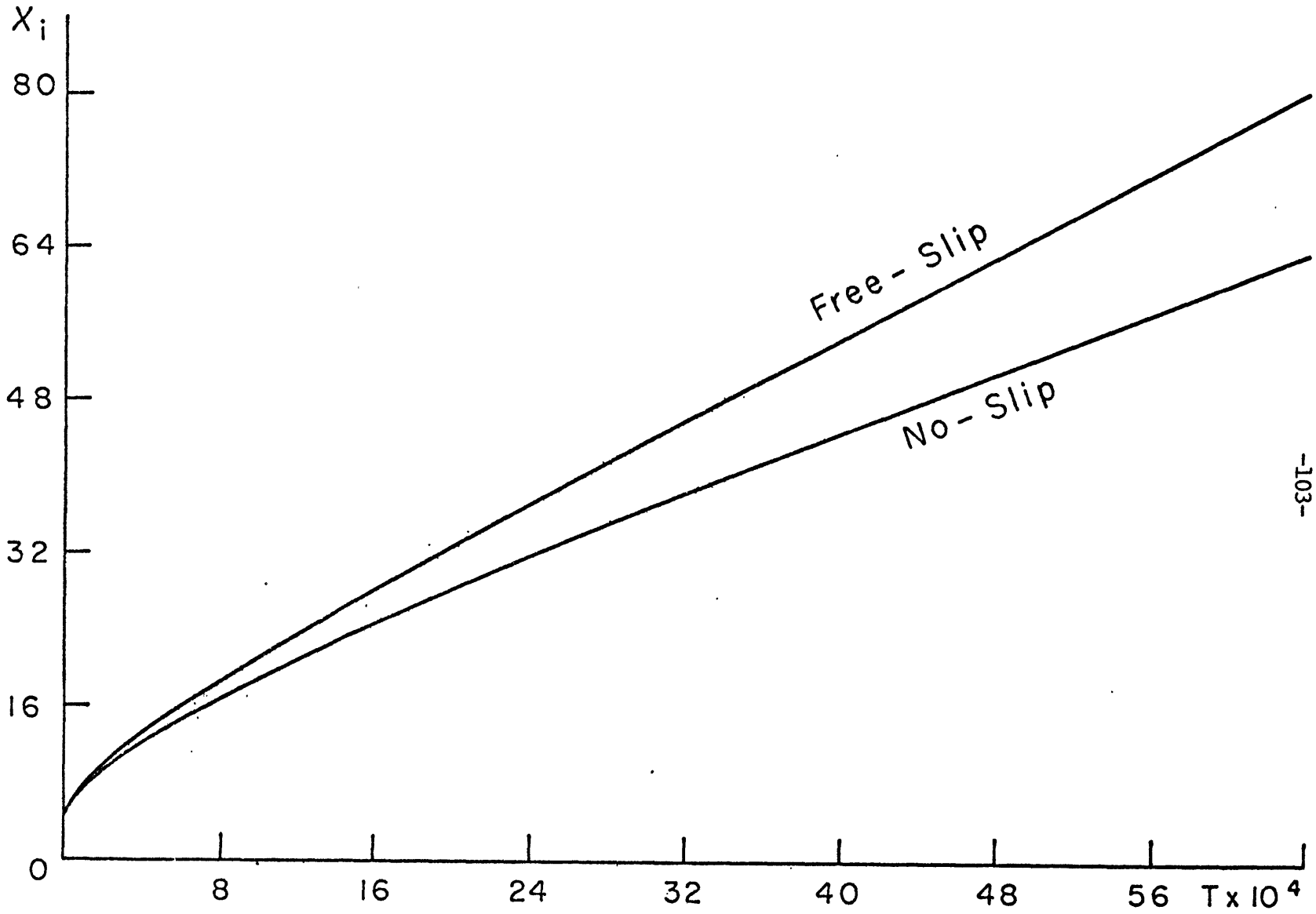

Figure 4a: The critical value of the inertial stability parameter X_i as a function of the diffusive parameter T, for hydrostatic disturbances in a stably stratified fluid.

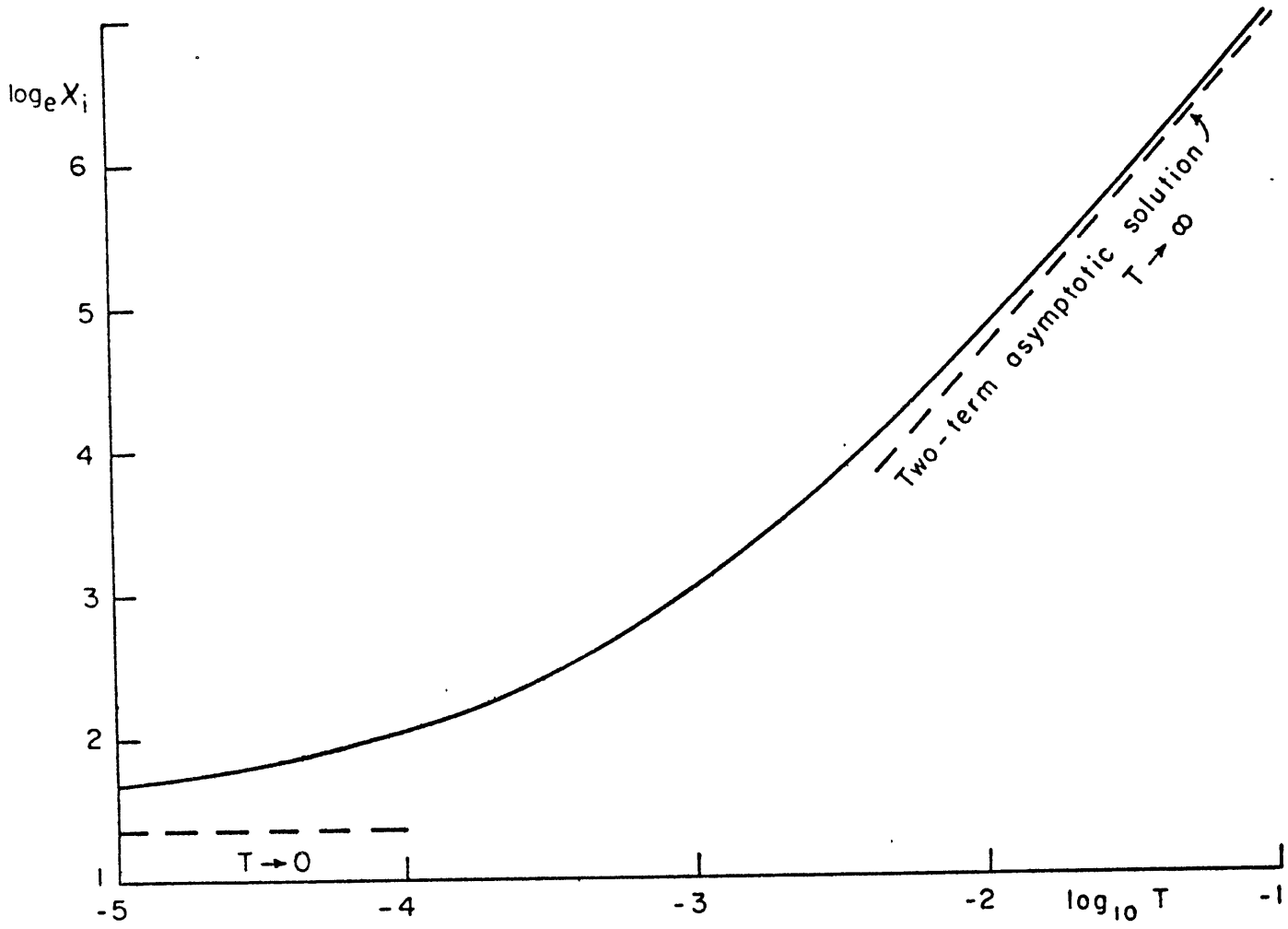

Figure 4b: Same as figure 4a, but for free-slip boundary conditions only. Asymptotic solution at T = 0 derived from inviscid theory; asymptotic curve as $T \to \infty$ deduced from second-order variational method.

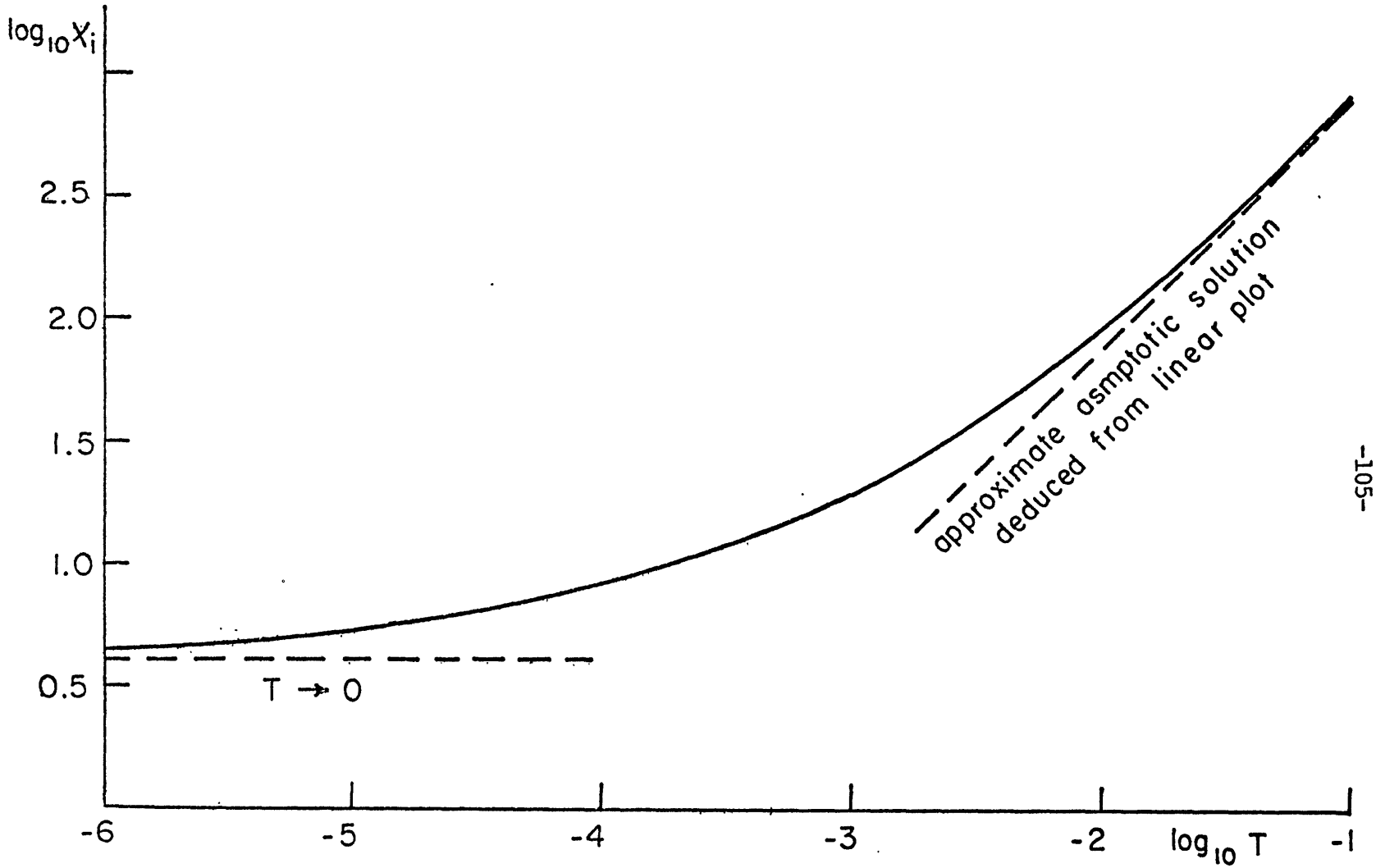

Figure 4c: Same as figure 4b, but for no-slip boundary conditions. Asymptotic curve as $T \to \infty$ deduced from linear dependence indicated in figure 4a.

parameter T and, compatible with the asymptotic results of Chapter 4, becomes a linear function of T when the latter is greater than about 2×10^{-3}. A linear regression through selected values associated with large values of T gives an asymptotic dependence of approximately

$$\chi_i \simeq 10920\ T + 11.05 \qquad T \to \infty$$

for the free-slip case, and

$$\chi_i \simeq 7800\ T + 13.30 \qquad T \to \infty$$

when the horizontal velocity components are constrained to vanish at the boundaries. These results have been obtained using a fifth-order variational method. When the two-term approximation to the Fourier Series used to represent the streamfunction is employed instead, one may procure an analytic approximation to the χ_i-T curve as $T \to \infty$. For free-slip boundaries, this is:

$$\chi_i \to 10950T$$

as $T \to \infty$

$$L \to 7.5$$

This is quite close to the fifth-order asymptotic dependence.

When the diffusion is small ($T \lesssim 10^{-4}$), the type of boundary condition present has little effect on the criterion of instability, but as viscous dissipation increases, it is apparent that the instability sets in sooner when the boundaries are no-slip. This discrepancy occurs despite the larger shears generated near the no-slip boundaries. The explanation of this phenomenon may be found in a comparison of the structures of the tangential perturbation velocity components in the free-slip and no-slip cases, as will be discussed presently.

The non-dimensional horizontal wavelength L at which the flow first becomes unstable is presented as a function of T in Figure 5. The dimension of the disturbance increases rapidly with the diffusion when the latter is small, but this dependency is much smaller when T exceeds about 10^{-4}. When the boundaries are no-slip, the most unstable wavelength rapidly reaches an asymptotic value of about 3 for increasing diffusion, whereas the disturbance wavelength increases more slowly and approaches a value of 7.5 if the boundaries are free-slip. The greater dissipation at the no-slip boundaries apparently discourages large wavelengths even when the diffusion is large.

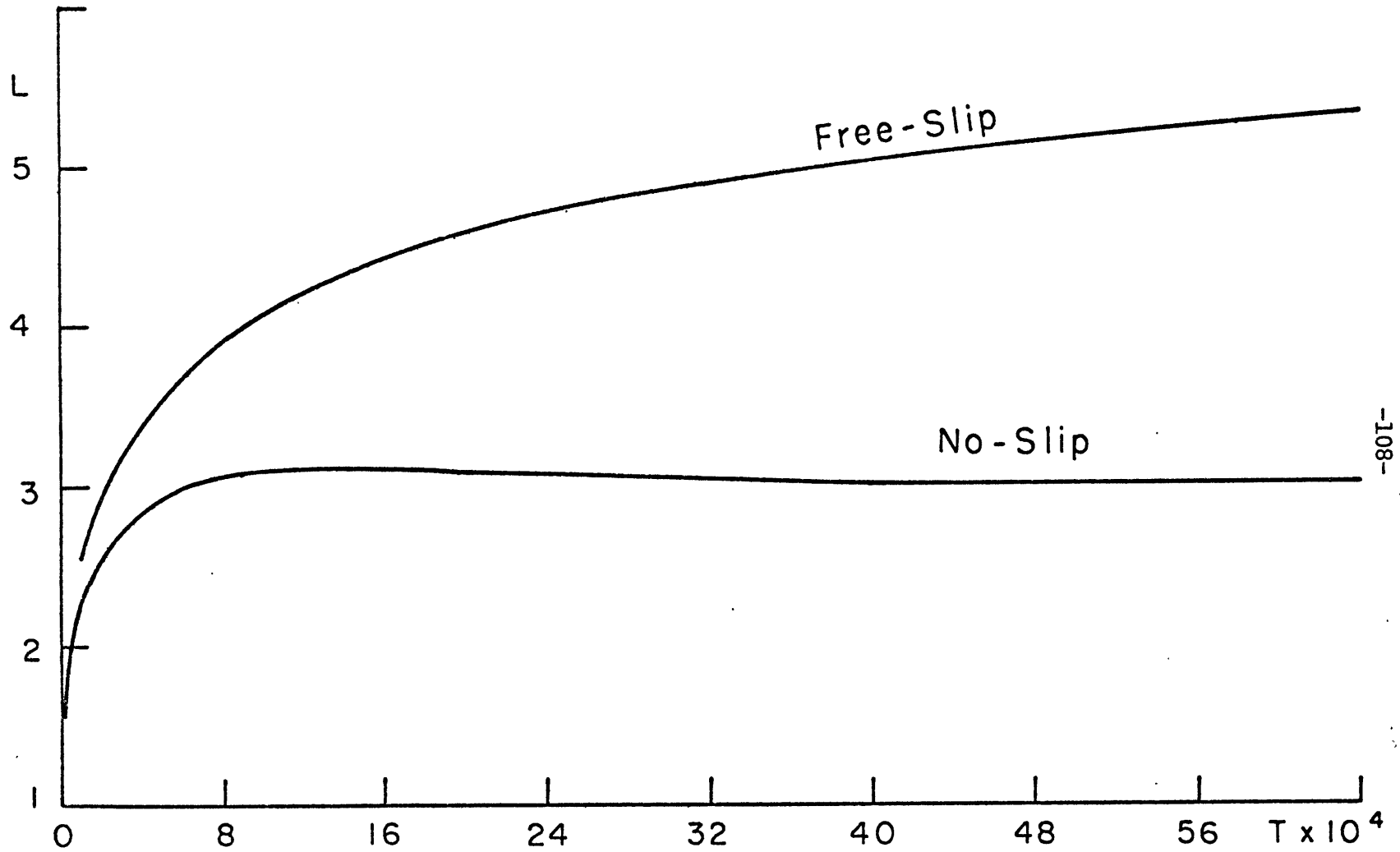

Figure 5a: Most unstable non-dimensional horizontal wavelength L associated with the critical value of χ_1 , as a function of the diffusion parameter T.

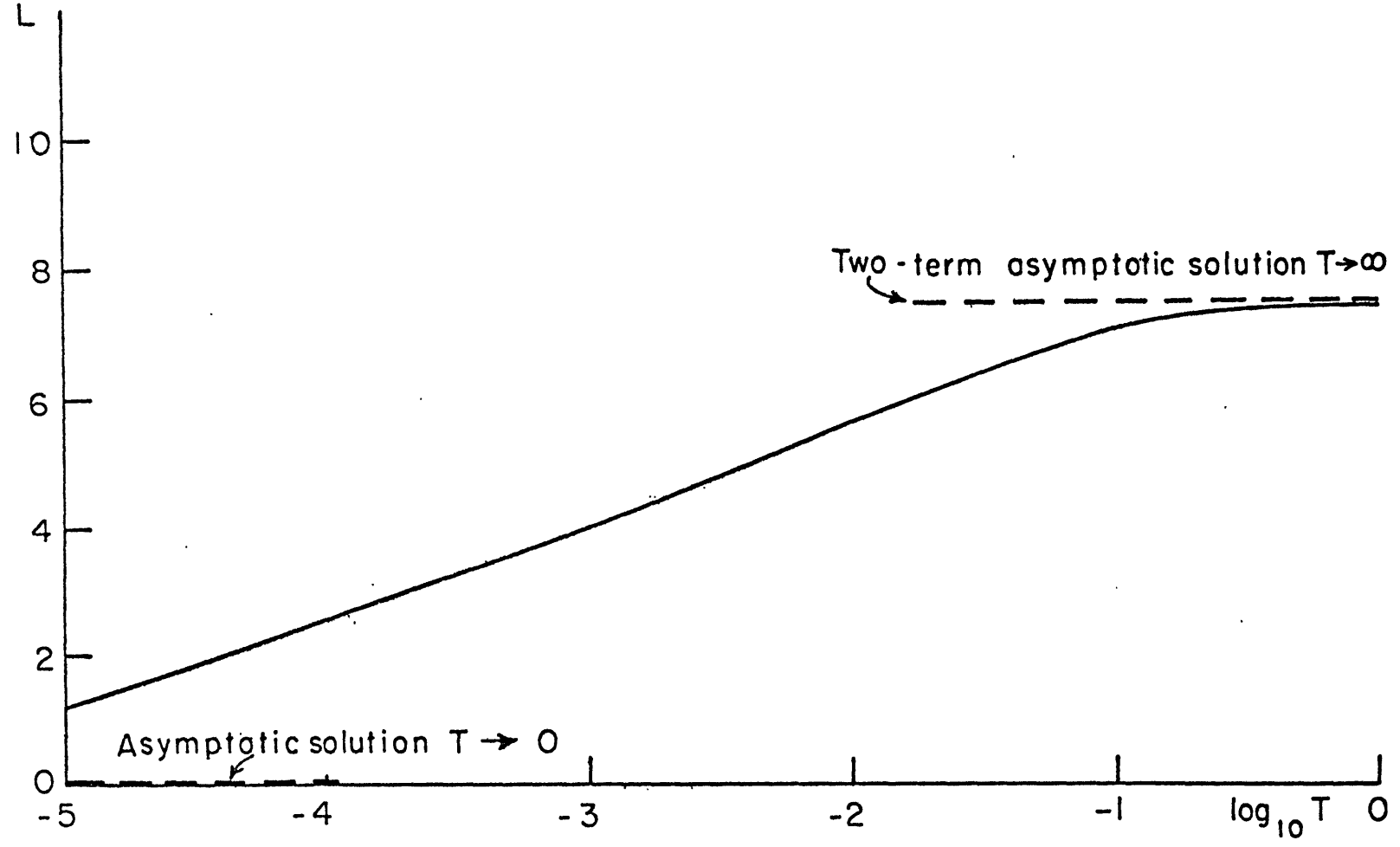

Figure 5b: Same as figure 5a, but for free-slip boundaries only. Solution at T = 0 derived from inviscid theory; asymptotic curve as T → ∞ deduced from second-order variational method.

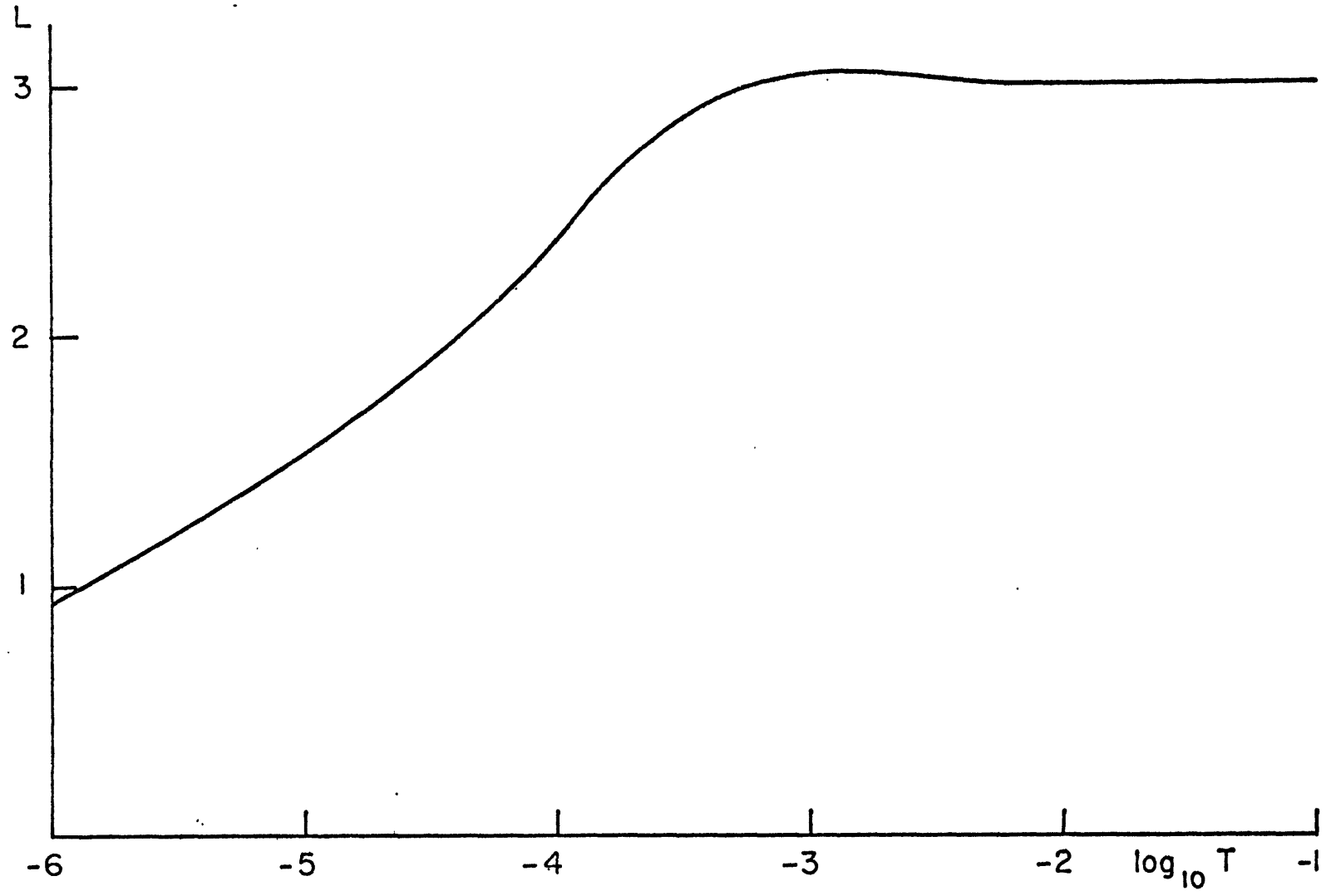

Figure 5c: Same as figure 5b, but for no-slip boundaries.

Streamfunctions associated with the onset of unstable motion are presented in Figures 6a-d for free-slip and no-slip boundaries, each for two values of the parameter T. These have been constructed using five terms of the Fourier Series (21) for free-slip and (37) for no-slip boundaries; the horizontal wavenumber in each instance represents that of the disturbance which first becomes unstable. The dashed line indicates the orientation of the potential isotherms, and the Ekman depth δ defined by

$$\delta = \left(\frac{2\nu}{f}\right)^{1/2} = \sqrt{2}\ H\ \left(\frac{\bar{\eta}}{f}\ T\right)^{1/4}$$

is depicted in the lower left portion of the diagrams.

The instability is clearly manifest as a series of sloped roll vortices oriented more or less along the potential isotherms. As one would expect, large horizontal velocities occur near the free-slip boundaries, but the circulations withdraw outside the boundary layer in the no-slip case. The motions take the form of highly elongated bands when dissipation is small, but become more circular as the viscous forces become more important. As may be surmised from the form of Equation (9), the conditions determining the marginal state are dependent on the Prandtl number, but the streamfunctions in the marginal

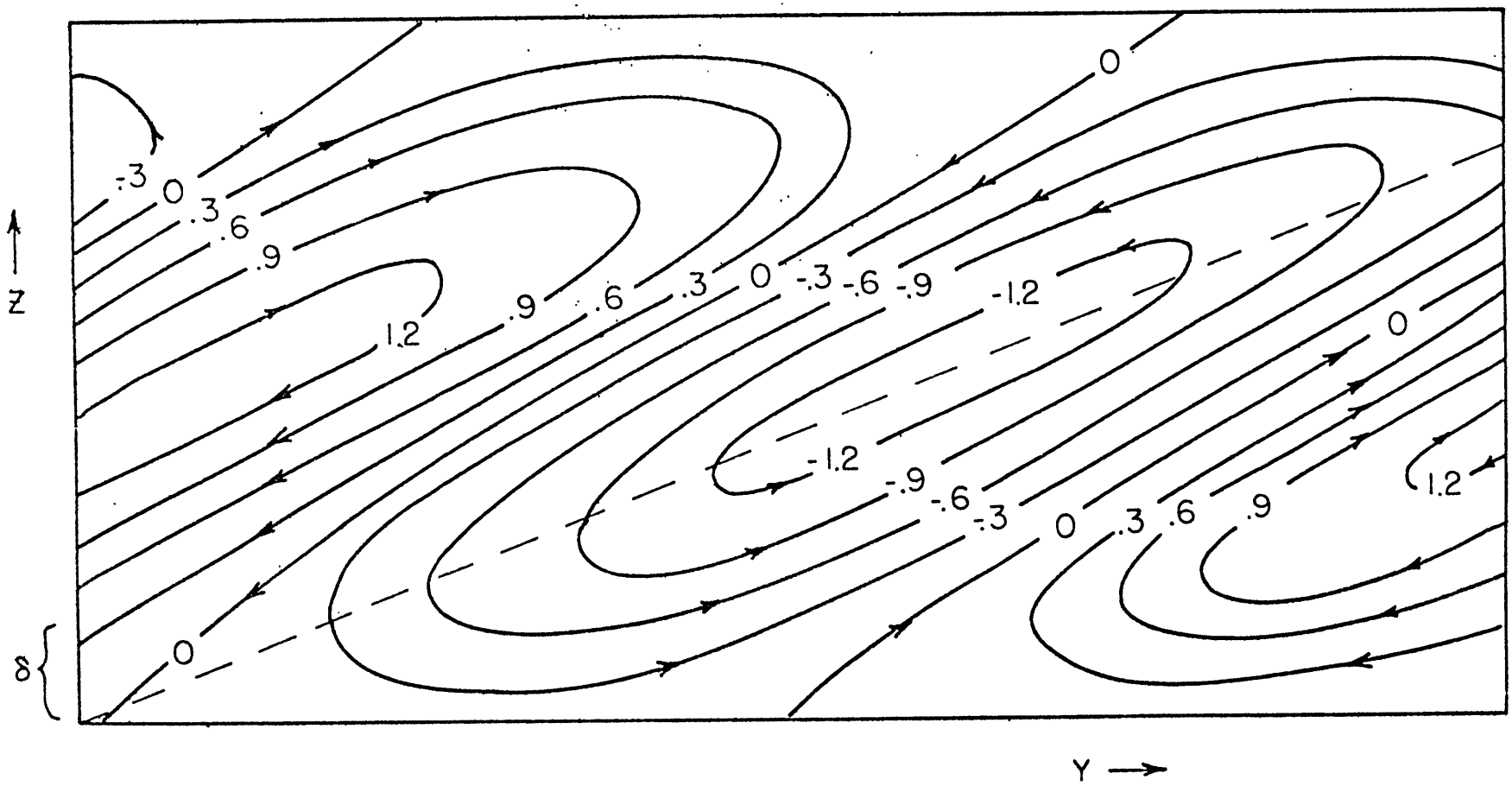

Figure 6a: Streamfunctions at the onset of instability when the boundaries are free-slip and $T = 10^{-4}$. Dashed line indicates relative orientation of potential temperature surfaces at Prandtl Number = 1, and nominal boundary layer depth δ is indicated in lower left.

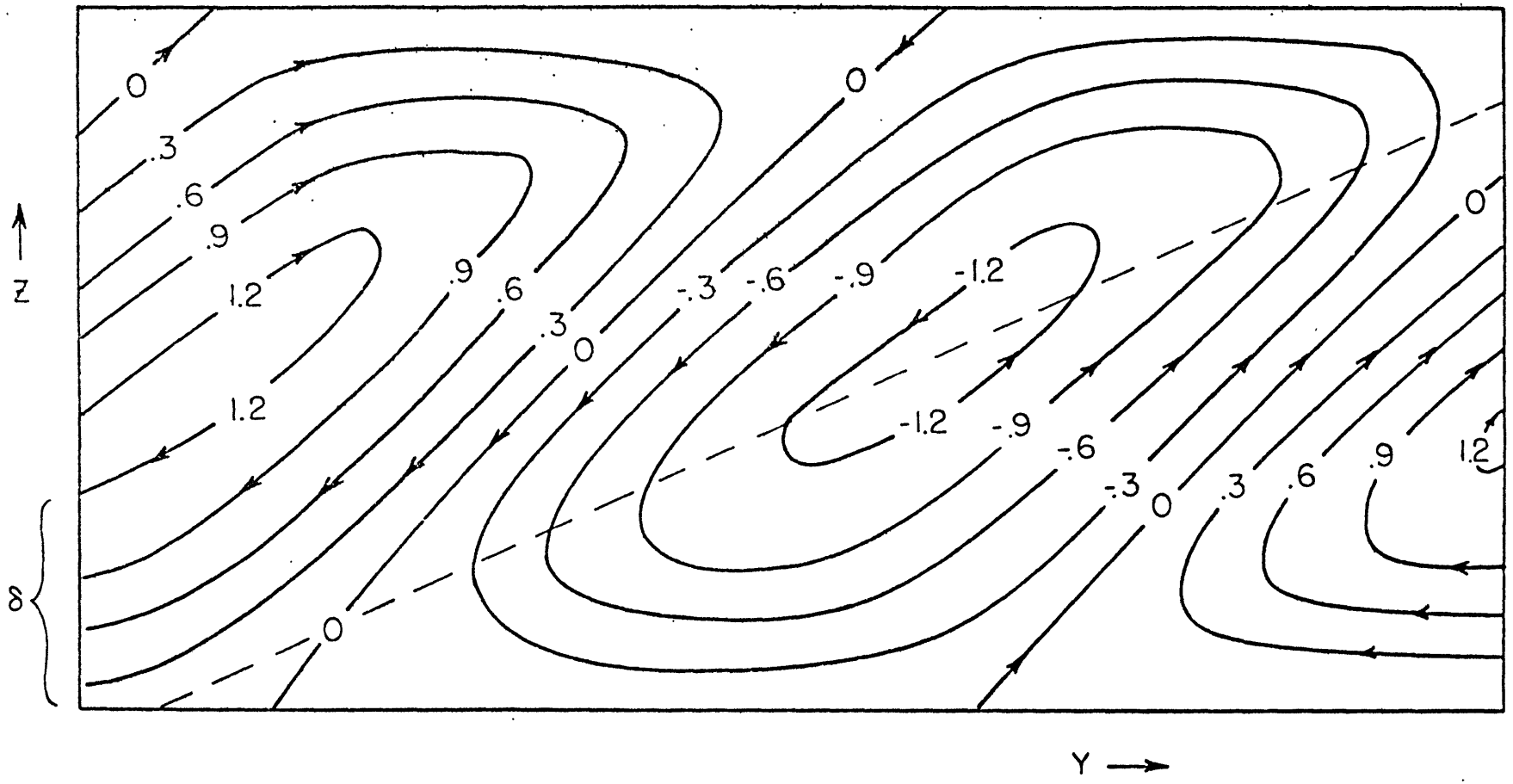

Figure 6b: Same as figure 6a, but with $T = 1.6 \times 10^{-3}$.

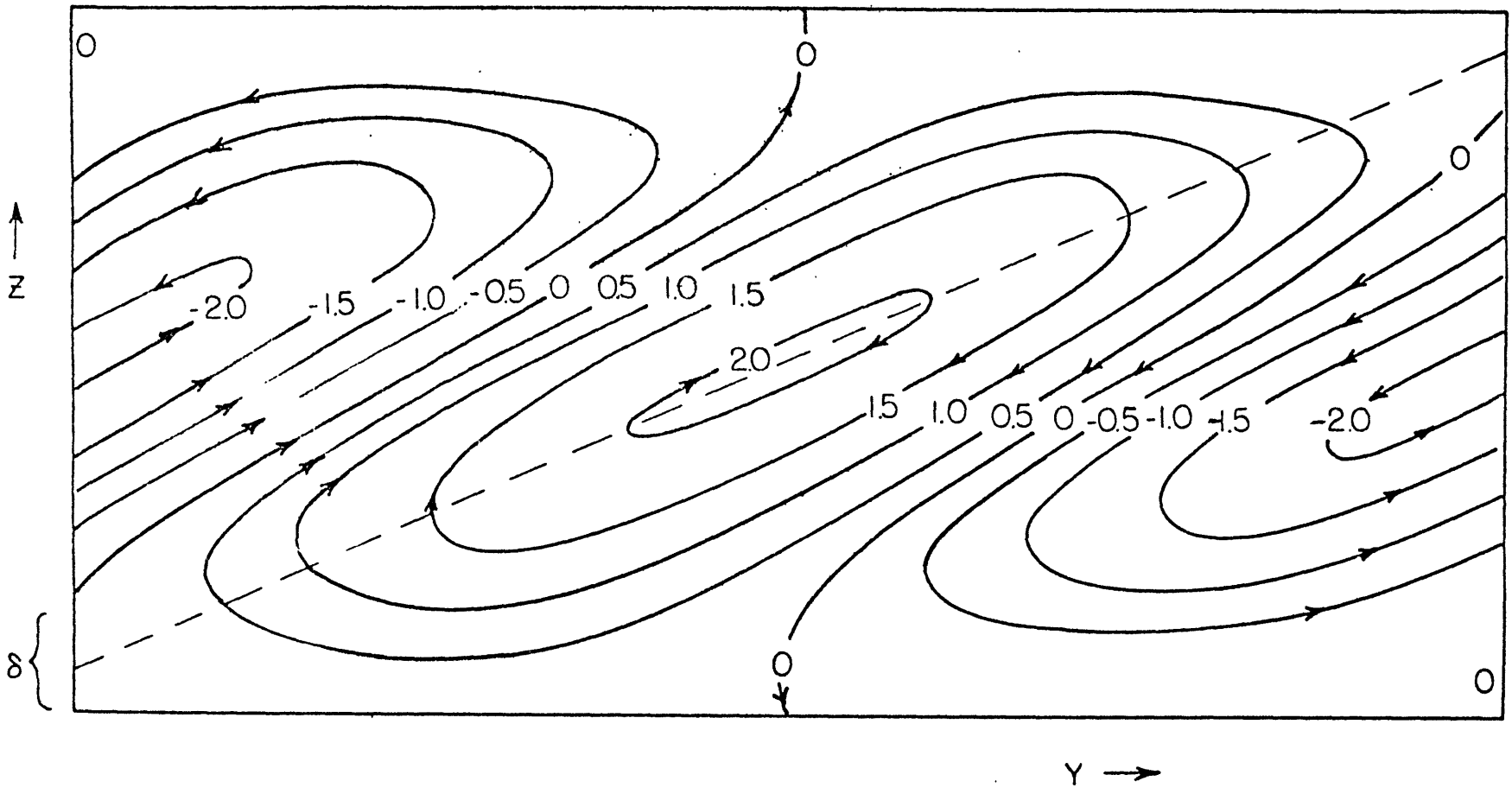

Figure 6c: Same as figure 6a but with no-slip boundary conditions. $T = 10^{-4}$.

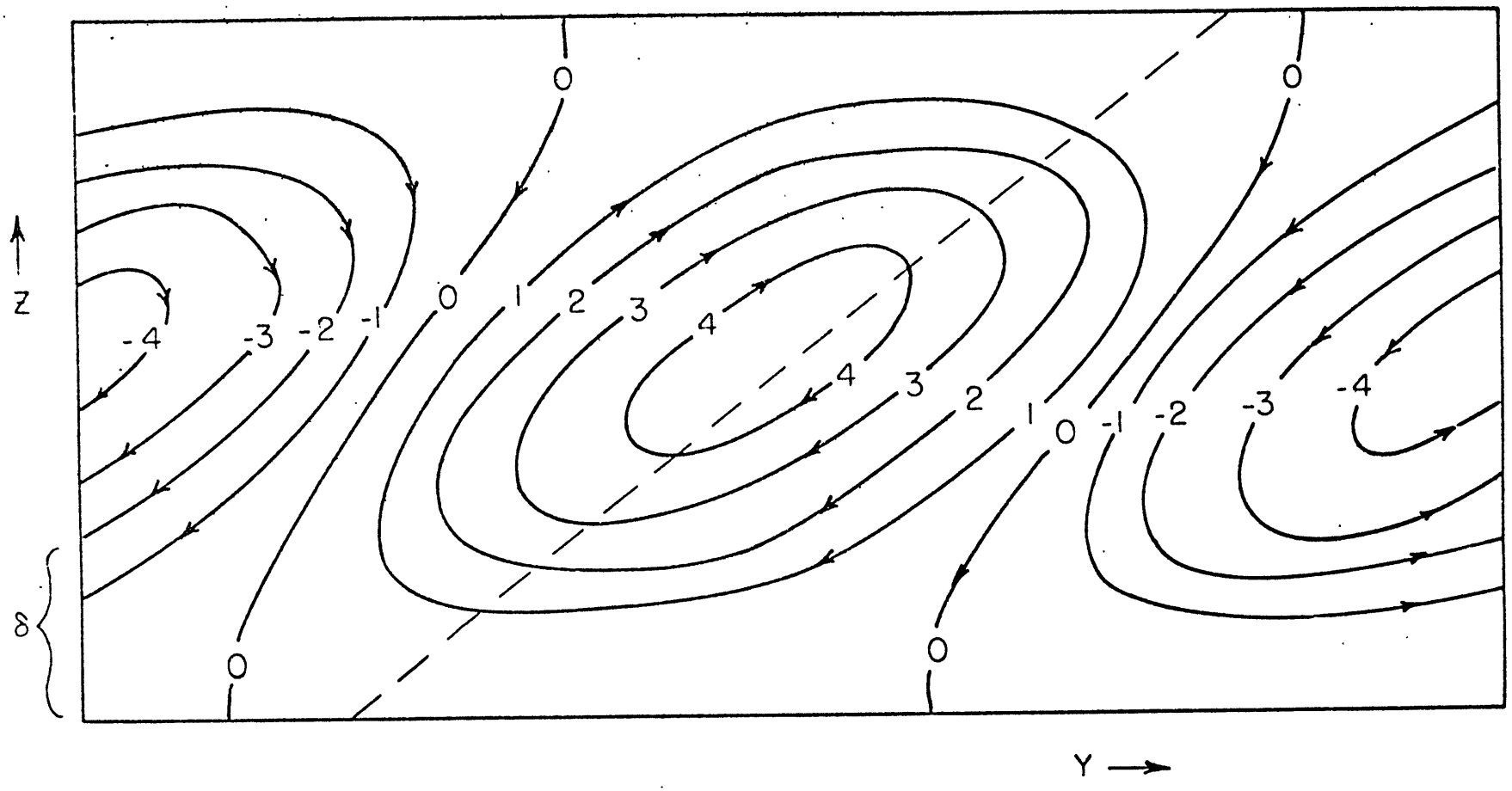

Figure 6d: Same as figure 6a but with no-slip boundary conditions and $T = 10^{-3}$.

state are not.

The tangential (zonal) velocity component as well as the perturbation pressure gradient may be obtained directly from Equations (1) and (4) together with the known streamfunction and the boundary conditions. As the Fourier Series (21) and (37) are only approximations to the real streamfunctions, however, mathematical difficulties arise when one attempts to construct solutions for u and p in this manner. These problems occur because the accuracy of the truncated series used to describe the streamfunction is not guaranteed for all values of its derivatives. In fact, the series need only provide an accurate description of the function itself and its first three derivatives in z in order to correctly derive the characteristic values of the stability parameters (see Chapter 4). In order to insure rapid convergence of the solutions for u and p, it proves necessary to construct elliptic diagnostic equations for these variables from the basic Equations (1) - (4). When the motions may be considered hydrostatic, and horizontal diffusion is unimportant, these equations are particularly simple, and may be written in scaled form:

$$(1+\frac{1}{P})\ \frac{\partial^3 u}{\partial z^3} = \frac{\partial^2 \psi}{\partial z^2} - \frac{\chi_i}{P}\ \frac{\partial^2 \psi}{\partial y^2} - \frac{T}{P}\ \frac{\partial^6 \psi}{\partial z^6} \qquad (41)$$

$$\frac{\partial^4 p}{\partial y \partial z^3} = \chi_i \frac{\partial^2 \psi}{\partial y^2} - P \frac{\partial^2 \psi}{\partial z^2} - PT \frac{\partial^6 \psi}{\partial z^6} \qquad (42)$$

Here, u and p have been scaled by $\nu/H\bar{\eta}$ and $(\nu/\bar{\eta}H^2)(\chi_i/\overline{U_z})$ respectively. Either the above set or (25) and (26) may be solved for u and p.

Figures 7a-d illustrate the distributions of tangential velocity corresponding to the streamfunctions presented in the preceding figures. The structures are obtained using the five-term Fourier Series representation of the stream-functions in Equation (41) for free-slip boundaries, and (25) for no-slip boundaries. The Prandtl number, here, is unity.

The contrasting structures of the tangential velocity components for the two sets of boundary conditions are striking. In the free-slip case, the maximum velocities are found at the boundaries at the point of intersection of the "stagnation" streamline, whereas the no-slip boundaries favor maximum velocities in the center of the domain. The build-up of large vorticities at the free-slip boundaries undoubtedly inhibits the vertical motions, as the resulting mass adjustments tend to oppose the vertical accelerations. This may explain the tendency of instabilities of this kind to favor no-slip boundaries. The same phenomenon occurs in the rotating Rayleigh convection

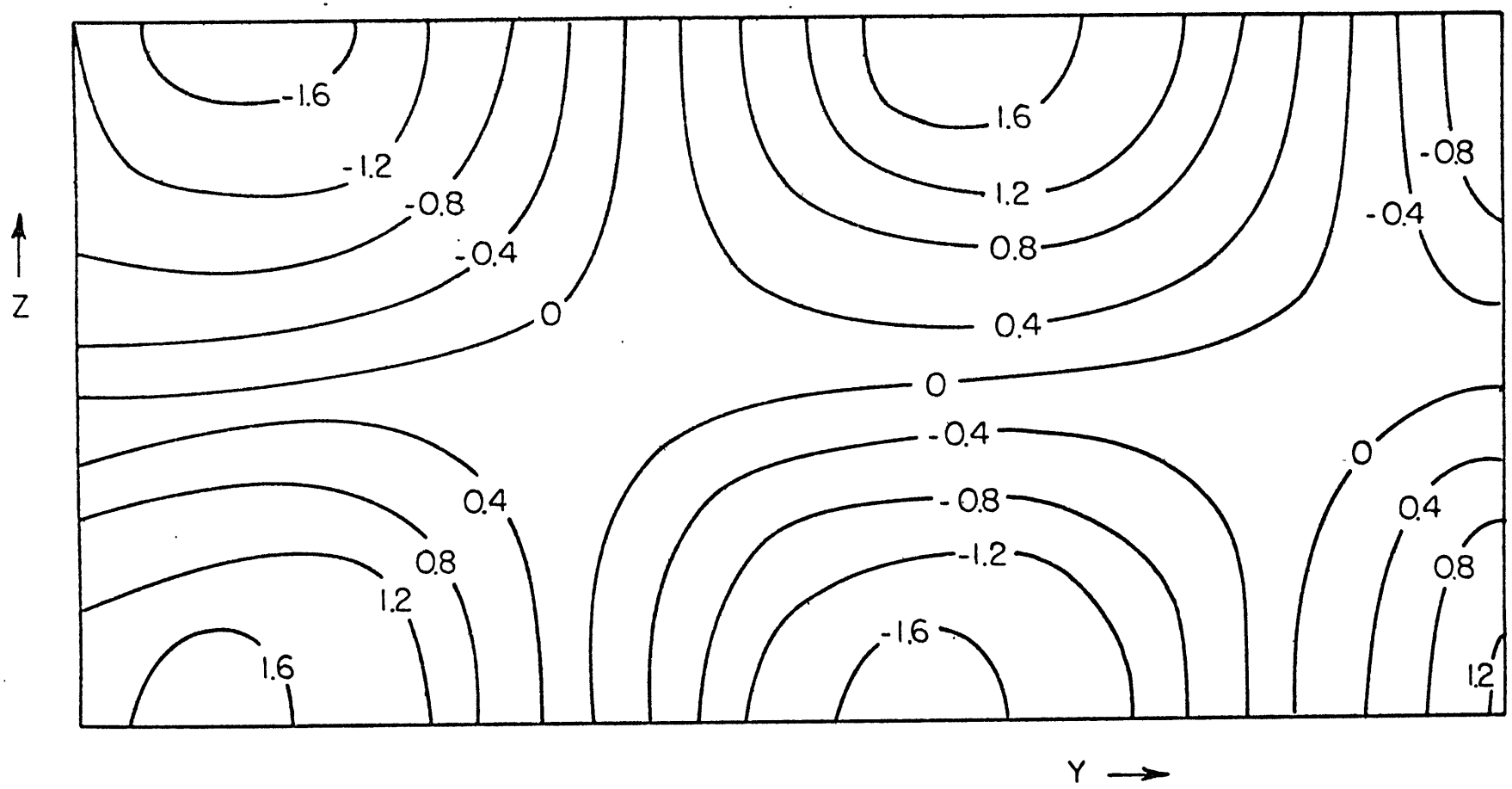

Figure 7a: Normalized perturbation tangential velocity associated with the streamfunctions of figure 6a. Positive values denote flow out of the page. Free-slip boundaries, $T = 10^{-4}$, $P = 1$.

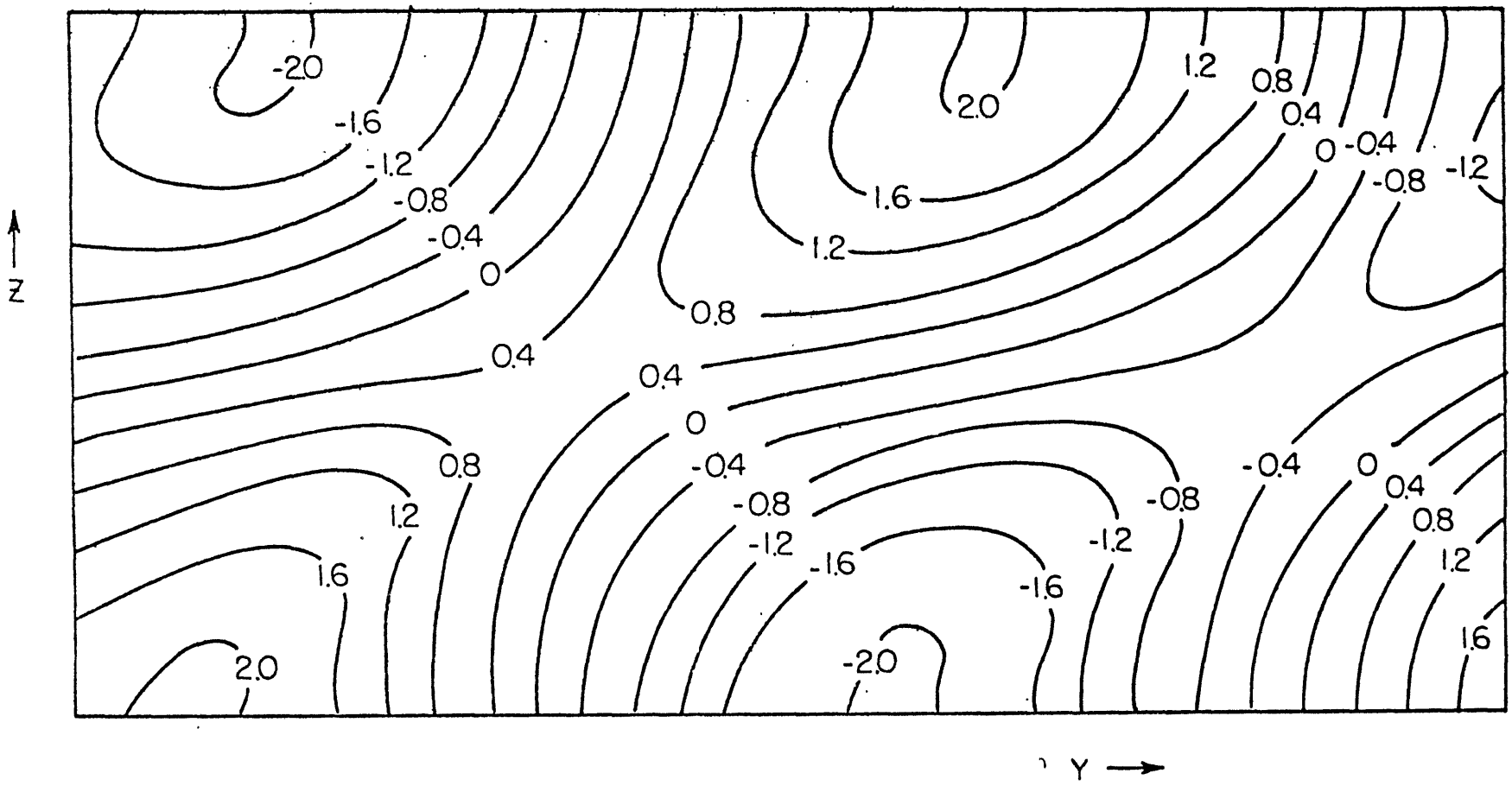

Figure 7b: Tangential velocity associated with streamfunctions of figure 6b. Free-slip boundaries, $T = 1.6 \times 10^{-3}$, $P = 1$.

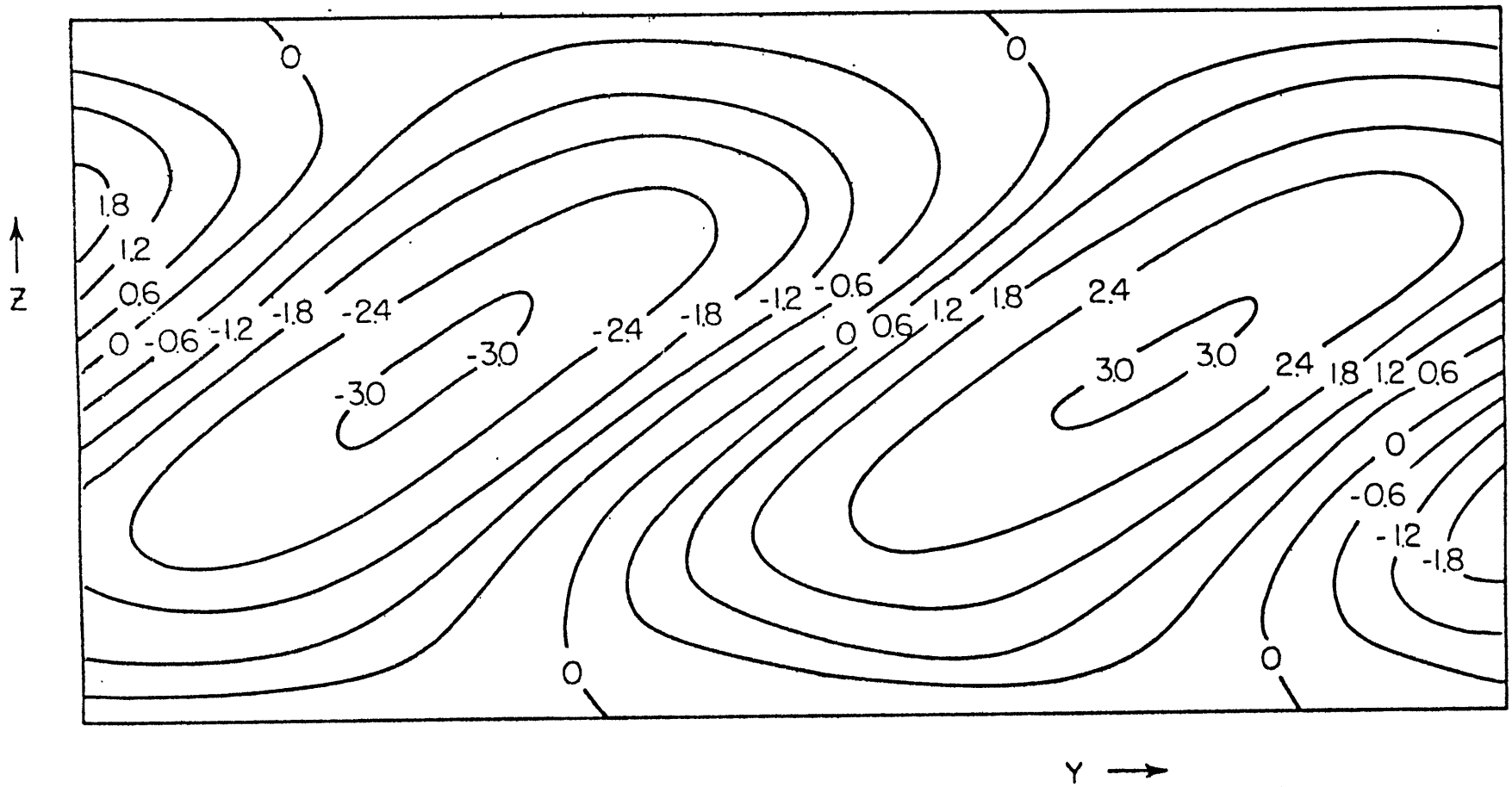

Figure 7c: Tangential velocity associated with the streamfunctions of figure 6c. No-slip boundaries, $T = 10^{-4}$, $P = 1$.

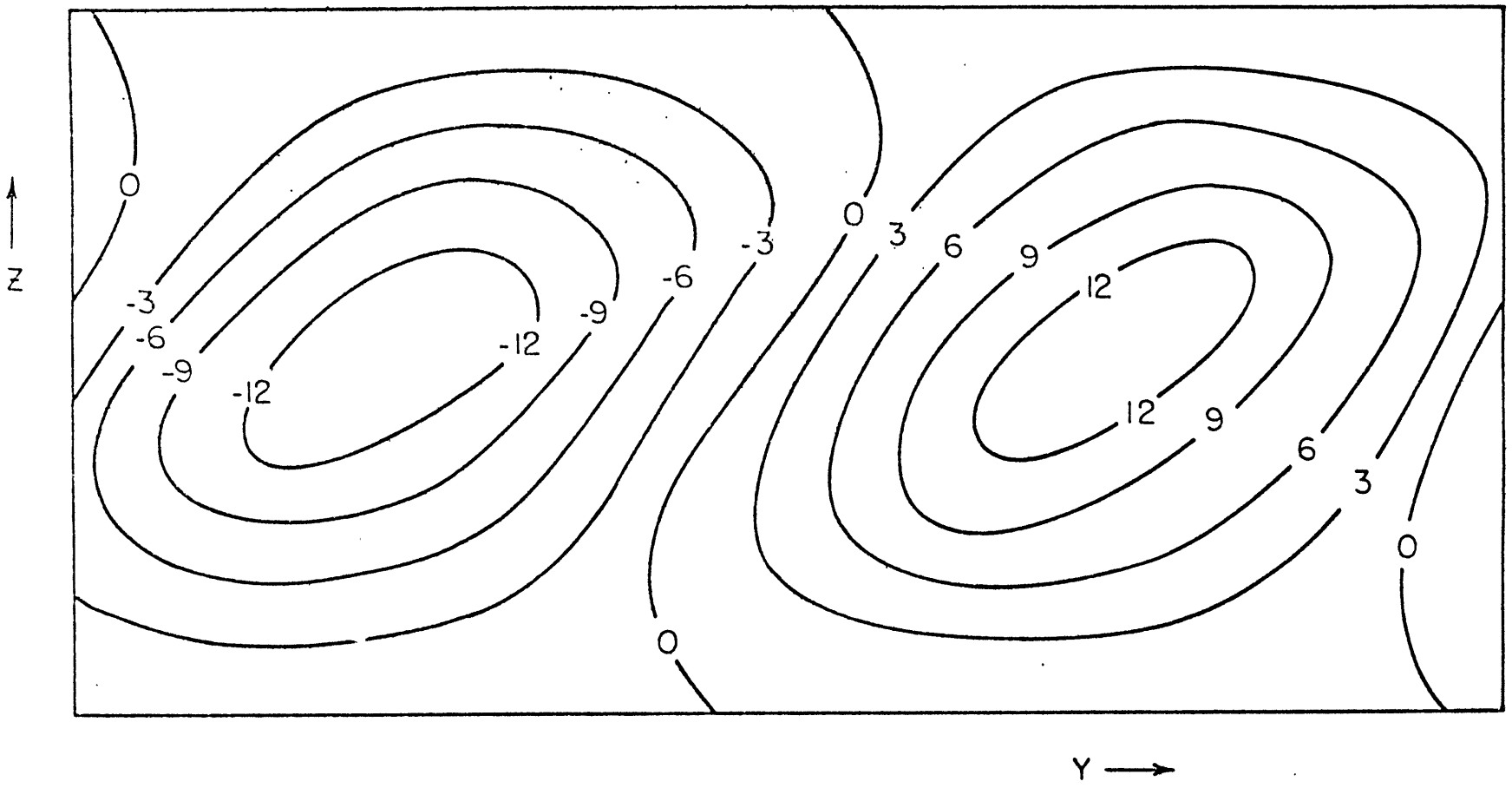

Figure 7d: Tangential velocity associated with the streamfunctions of figure 6d. No-slip boundaries, $T = 10^{-3}$, $P = 1$.

problem for certain values of the Taylor number (see Chandrasekhar, 1961).

Under both types of boundary conditions, a strong negative correlation of u and w is evident and the pattern also suggests a similar association of u and v. When no-slip boundaries are present, the generation of tangential velocity perturbations is evidently accomplished, for the most part, by vertical advection.

The structures of the temperature perturbations, $\partial p/\partial z$, are depicted in Figures 8a-d for free-slip and no-slip boundaries, and for a Prandtl number of unity. In either case, the temperature perturbations reflect the distortion of the equilibrium state potential isotherm field by the flow, especially when the latter is topologically forced to cross potential isotherms. The temperature perturbations are confined to the interior of the domain due to the boundary condition $\partial p/\partial z = 0$. The eddy transport of potential temperature appears to be countergradient, i.e., $\overline{w'\theta'} < 0$, $\overline{v'\theta'} < 0$, where θ is the potential temperature. The total flux of temperature, however, involves a transport of the mean temperature field by the eddies; such a transport is not accounted for here. We may state, however, that if a second-order expansion of the perturbation streamfunction does not contain a term

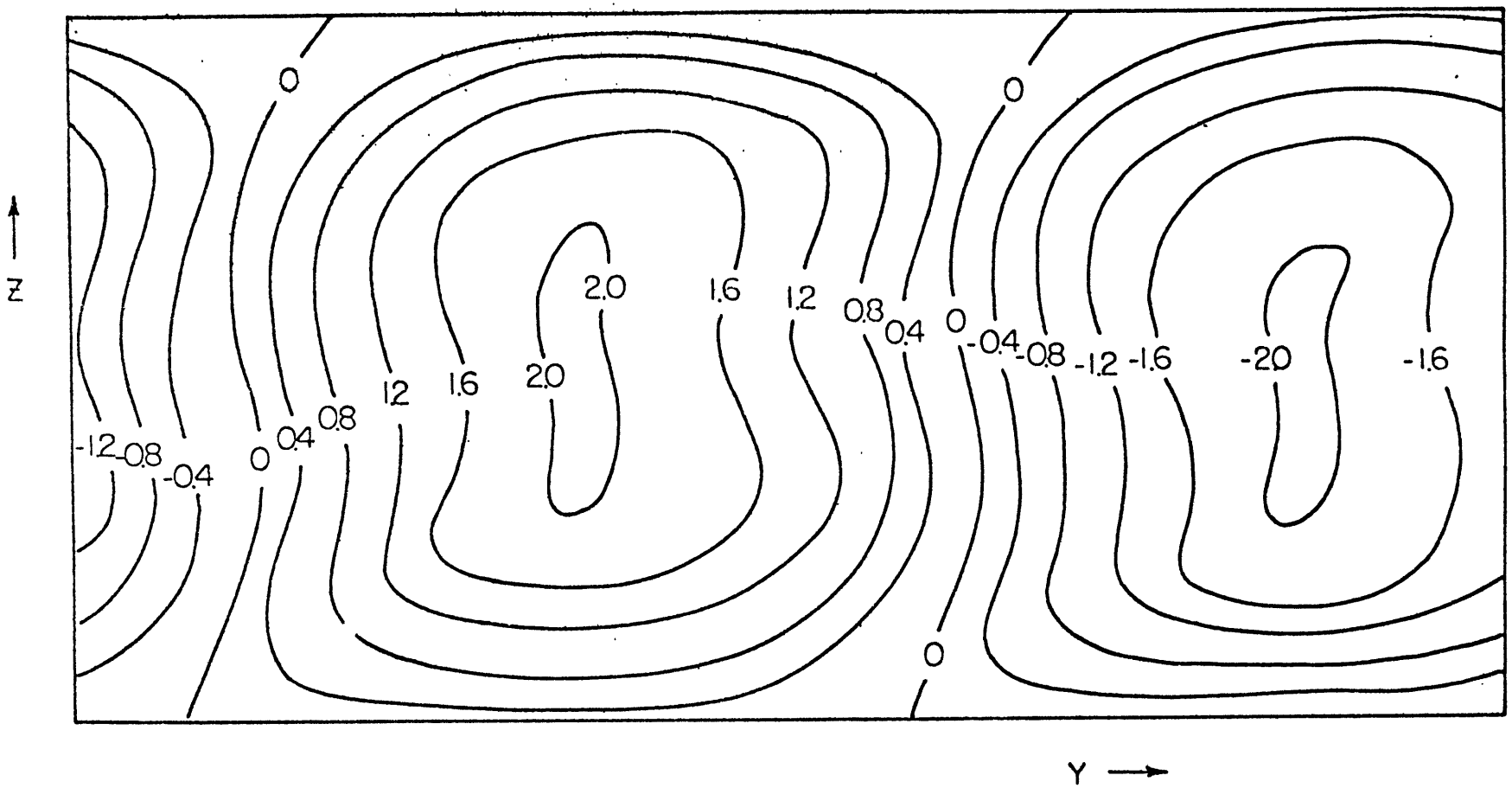

Figure 8a: Normalized temperature perturbation ($\delta p/\delta z$) associated with the streamfunctions of figure 6a, with the Prandtl Number equal to 1. Pressure distribution may be inferred from symmetry, with high pressure below and low pressure above negative (cold) perturbations, etc. Free-slip boundaries, $T = 10^{-4}$.

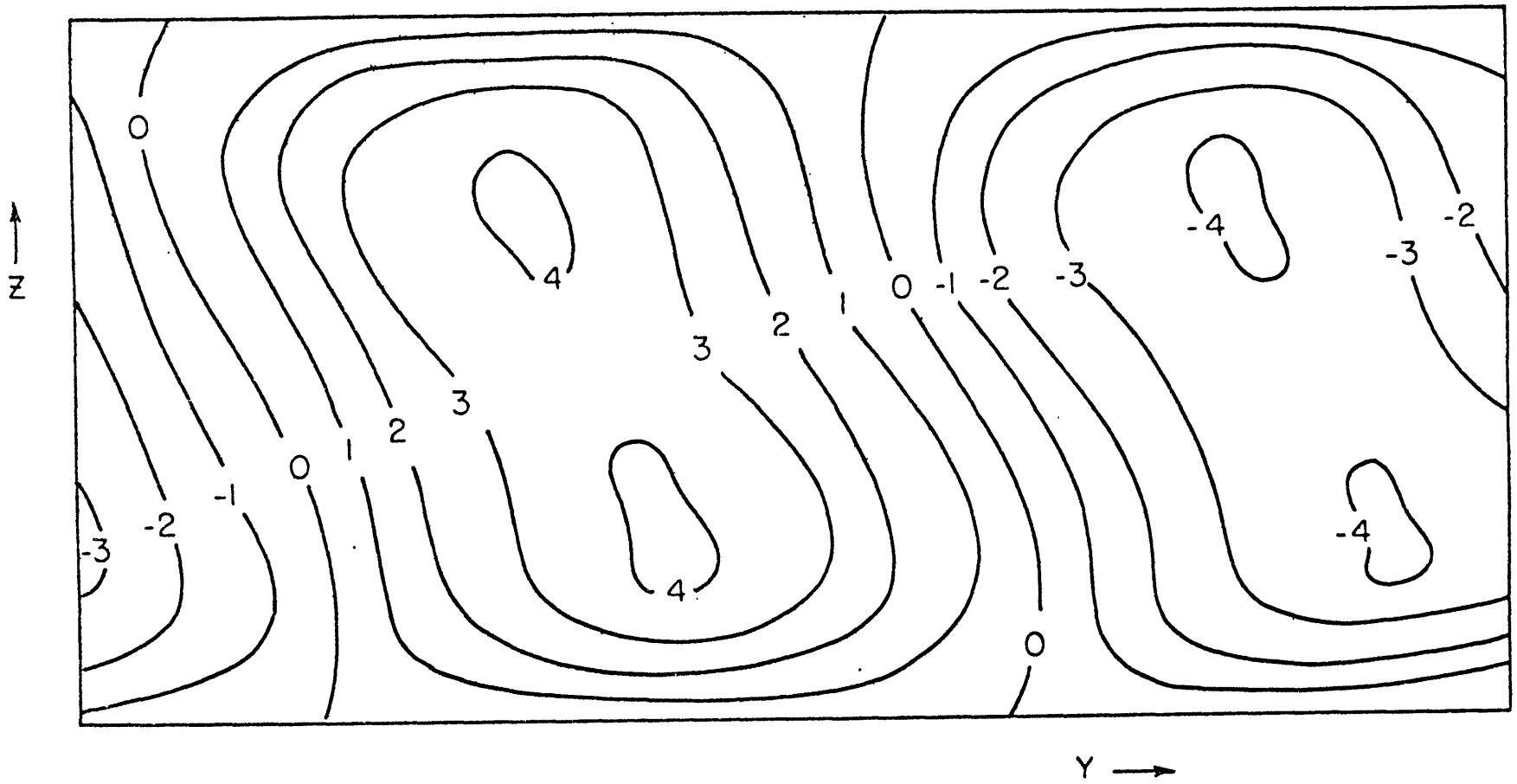

Figure 8b: Temperature perturbation associated with the streamfunctions of figure 6b. Free-slip boundaries, $T = 1.6 \times 10^{-3}$, $P = 1$.

Mis-type: PG. 125 does not exist

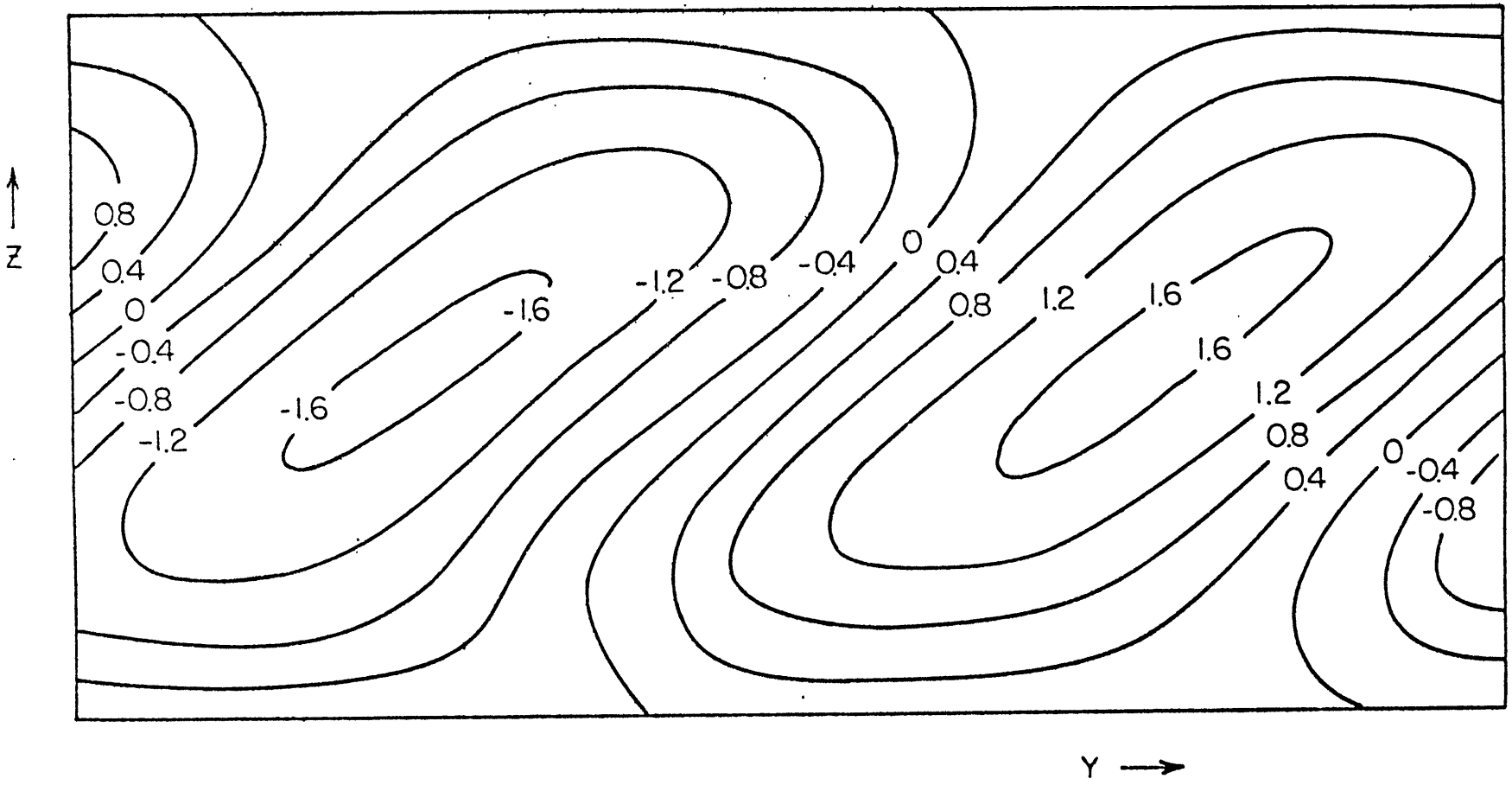

Figure 8c: Temperature perturbation associated with the streamfunctions of figure 6c. No-slip boundaries, $T = 10^{-4}$, $P = 1$.

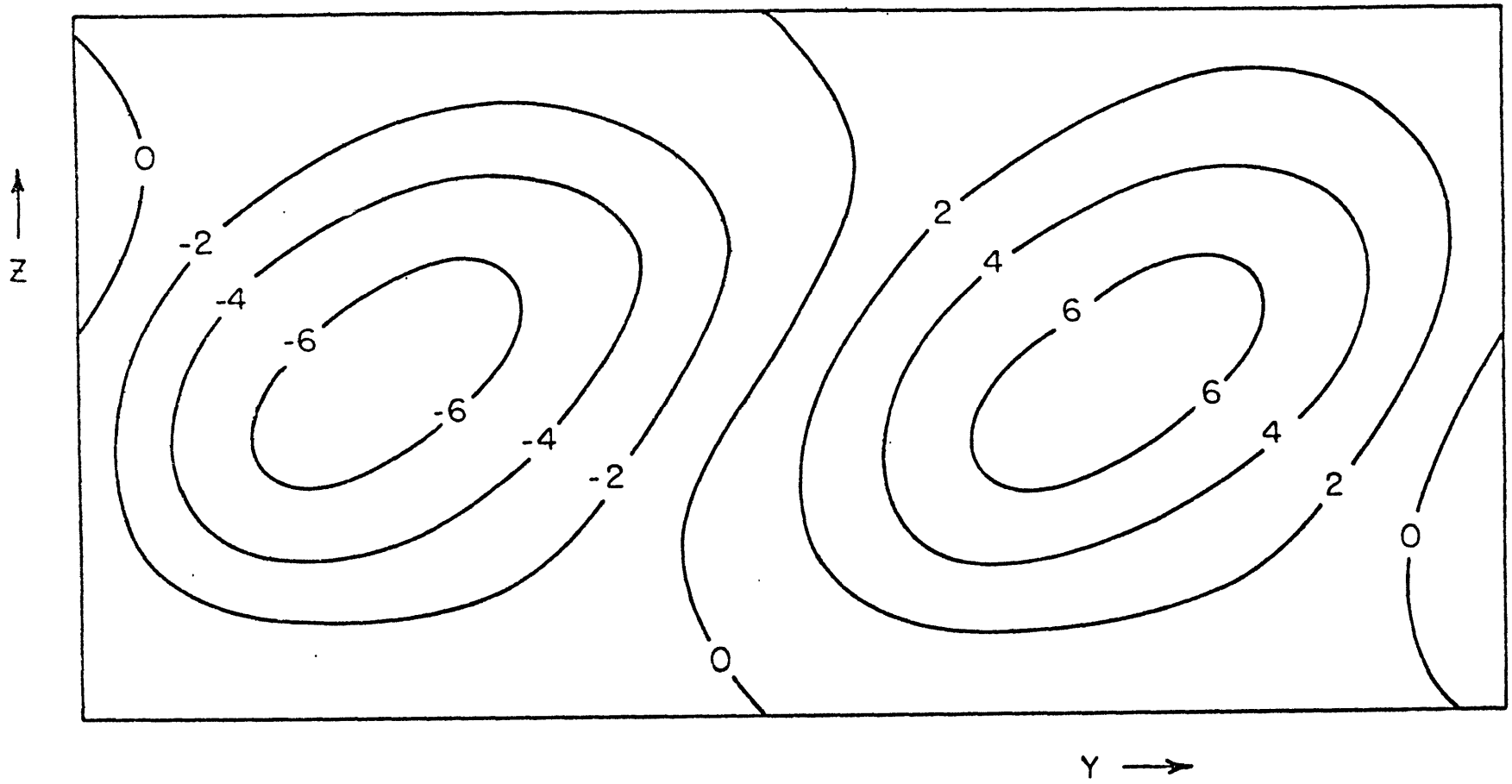

Figure 8d: Temperature perturbations associated with the streamfunctions of figure 6d. No-slip boundaries, $T = 10^{-3}$, $P = 1$.

independent of the horizontal dimension, then the total horizontal transport, to second order, will involve only the eddy flux of potential temperature. This conclusion is reached as follows:

If each of the variables u, ψ, p, and ρ are expanded to second order in a small amplitude parameter ε:

$$u = u_o + \varepsilon u_1 + \varepsilon^2 u_2 + \ldots$$

$$\psi = \psi_o + \varepsilon \psi_1 + \varepsilon^2 \psi_2 + \ldots$$

etc., then the total horizontal flux of potential temperature to second order in ε is:

$$\overline{v' \ln\theta'} = - \overline{\frac{\partial \psi'}{\partial z} \ln\theta'} = - \frac{1}{L} \int_0^1 \int_0^L \left(\frac{\partial \psi_1}{\partial z} \ln\theta_1 + \frac{\partial \psi_2}{\partial z} \ln\theta_0 \right) dy dz$$

By an integration by parts together with the boundary condition on ψ_2, the second term in the integral becomes:

$$- \frac{1}{L} \int_0^L [\psi_2 \ln\theta_0] \Big|_0^1 dy + \frac{1}{L} \int_0^1 \int_0^L \psi_2 \frac{\partial \ln\theta_0}{\partial z} dy dz$$

Since in this theory $\partial \ln\theta_0 / \partial z$ is constant, and as $\overline{\psi_2} \equiv 0$, the second term above vanishes. The boundary condition $w_2 \equiv \partial \psi_2 / \partial y = 0$ indicates that the first term will also

vanish unless ψ_2 is a function of z alone at the boundaries. Stone (1972) has shown that ψ_2 is, in the inviscid theory, a function of the vertical coordinate only, so that the possibility of a contribution by the advection of the mean temperature field by the eddies cannot be discounted. The same arguments apply, incidentally, to the second-order horizontal flux of tangential (zonal) momentum. It may be shown, however, that the second-order <u>vertical</u> fluxes of these quantities are identical to the eddy fluxes alone, for example:

$$\overline{w'\ln\theta'} = \frac{1}{L}\int_0^1\int_0^L \left(\frac{\partial\psi_1}{\partial y}\ln\theta_1 + \frac{\partial\psi_2}{\partial y}\ln\theta_0\right)dydz$$

the second term of which reduces to

$$\frac{1}{L}\int_0^1 [\psi_2 \ln\theta_0]\Big|_0^L dz - \frac{1}{L}\int_0^1\int_0^L \psi_2 \frac{\partial \ln\theta_0}{\partial y}\, dydz$$

Since $\partial\ln\theta_0/\partial y$ is constant and $\overline{\psi}_2 \equiv 0$, the second term above vanishes; the first term also vanishes due to the imposed periodicity in y. The total second-order flux in the vertical reduces to

$$\overline{w'\ln\theta'} = \frac{1}{L}\int_0^1\int_0^L \frac{\partial\psi_1}{\partial y}\ln\theta_1 dydz$$

Similarly, the vertical flux of tangential (zonal) momentum is

$$\overline{w'u'} = \frac{1}{L} \int_0^1 \int_0^L \frac{\partial \psi_1}{\partial y} u_1 \, dydz$$

Inspection of the streamfunctions, tangential velocity fields, and temperature distributions illustrated in the preceding figures reveals that the vertical eddy fluxes of potential temperature ($\partial p/\partial z$) and tangential momentum are downward; the former is destabilizing while the latter is stabilizing.

The distribution of pressure, especially near the boundaries, may be inferred from Figures 8a-d together with the imposed symmetries. The perturbation pressure appears to vanish at the intersection of the stagnation streamline with the boundaries. High pressure is centered under the core of the upward motion, and low pressure occurs under the descending (warm) branch of the circulation.

It is of interest to compare the relative amplitudes of u and v and also those of the temperature and velocity perturbations for various Taylor numbers and boundary conditions.

In general, it is found that the ratio u_m/v_m is somewhat larger than unity for all T less than about 10^{-2}.

(The subscript m denotes the maximum value of the dimensional quantity within the domain.) For example, when $T = 10^{-4}$, $u_m/v_m \approx 27$ for free-slip boundaries and 19 when the boundaries are no-slip. As dissipation increases, the ratio becomes smaller: when $T = 10^{-3}$, for instance, $u_m/v_m \approx 15.5$ (free-slip) and 13.7 (no-slip). Similarly, the relative amplitude of the pressure perturbation (measured against the intensity of the streamfunction) decreases with increasing dissipation. The magnitudes of both tangential velocity and temperature perturbations are greater when the boundaries are free-slip.

In summary, the onset of hydrostatic inertial disturbances in a bounded fluid is characterized by roll vortices more or less parallel to the potential isotherms, with a horizontal wavelength on the order of the ratio of the fluid depth and the slope of the potential isotherms. The region of upward motion is characterized by low temperature and negative perturbation tangential velocity; the converse is true in the region of descent. The highest surface pressure occurs somewhat toward the colder air from the position of the updraft near the surface.

(b) Non-Hydrostatic Disturbances in a Fluid with Neutral Stratification

The onset of unstable motions in a viscous fluid with constant shear and neutral stratification is described by Equation (10), when the instability begins as steady overturning, and (14) if the disturbances appear as oscillations. The general form of both these equations is:

$$\tau(\nabla^2)^3\psi = -\chi_{ii}\frac{\partial^2\psi}{\partial y\partial z} - \frac{\partial^2\psi}{\partial z^2} \qquad (43)$$

The parameters τ and χ_{ii} have different interpretations depending on whether the disturbances begin as steady overturning or oscillatory motion:

Steady overturning:

$$\begin{cases} \tau = T = \dfrac{\nu^2}{f\overline{\eta}H^4} \\ \chi_{ii} = \dfrac{\overline{U_z}}{\overline{\eta}}\,(1+P) \end{cases}$$

Oscillations:

$$\begin{cases} \tau = T\left(1 + \dfrac{1}{P}\right)^2 \\ \chi_{ii} = \dfrac{\overline{U_z}}{\overline{\eta}}\,\dfrac{\left(3 + \frac{1}{P}\right)}{2} \end{cases}$$

The reader is reminded that in order that standing oscillations be possible at all, not only must Equation (43)

be satisfied, but the oscillation frequency as given by (12a) or (12b) (as modified for the non-hydrostatic neutral stratification case) must be real. Applying arguments parallel to those used to exclude the possiblity of standing oscillations in the hydrostatic case (see Chapter 3), one may show that instability may only set in as oscillations in the parameter range in which the stationary solution decays with time. The domain of Prandtl and Taylor numbers in which oscillatory instability is possible is bounded by the locus of points in the T-P plane for which the marginal states of each form are identical. This domain is found by varying the Prandtl and Taylor numbers and finding, from the relationship of χ_{ii} and τ given by Equation (43) and the boundary conditions, which form of instability arises first.

Since the solutions of the neutral stratification problem have already been discussed by Kuo (1954), we present this section in order to:

(a) Compare a "third-order" approximate solution obtained using the methods described in Chapter 4 with Kuo's exact solutions;

(b) Find the parameter ranges in which over-stability occurs.

A discussion of the comparison between Kuo's results and those obtained using a variational method to third-order may be found in Chapter 4. The relationship between χ_{ii} and τ characterizing the marginal state is illustrated in Figure 9, and the wavelength at which instability first occurs is presented in Figure 10. Both Kuo's results and those obtained using the approximate method are illustrated; the two curves describing the most unstable wavelength are indistinguishable.

The range of T and P in which overstability occurs at the onset of instability is illustrated in Figure 11. It is noted that overstability cannot occur if T is greater than 10^{-5} or P greater than 1. Overstable oscillations are only likely for very small diffusion when the Prandtl number is less than unity. If oscillatory instability does occur, the period of oscillation is on the order of 1/f; a wave of 100 km length, for example, might be expected to propagate at a few meters per second.

In Chapter 4, an explicit formula for the variation of the critical value of χ_{ii} with τ and L was derived from the third-order variational method (Equation 24). We have found that the results obtained by this technique compare favorably with the exact results of Kuo (1954), and that the accuracy of the results is better for larger τ. From

Mis-type: PG. 135 does not exist

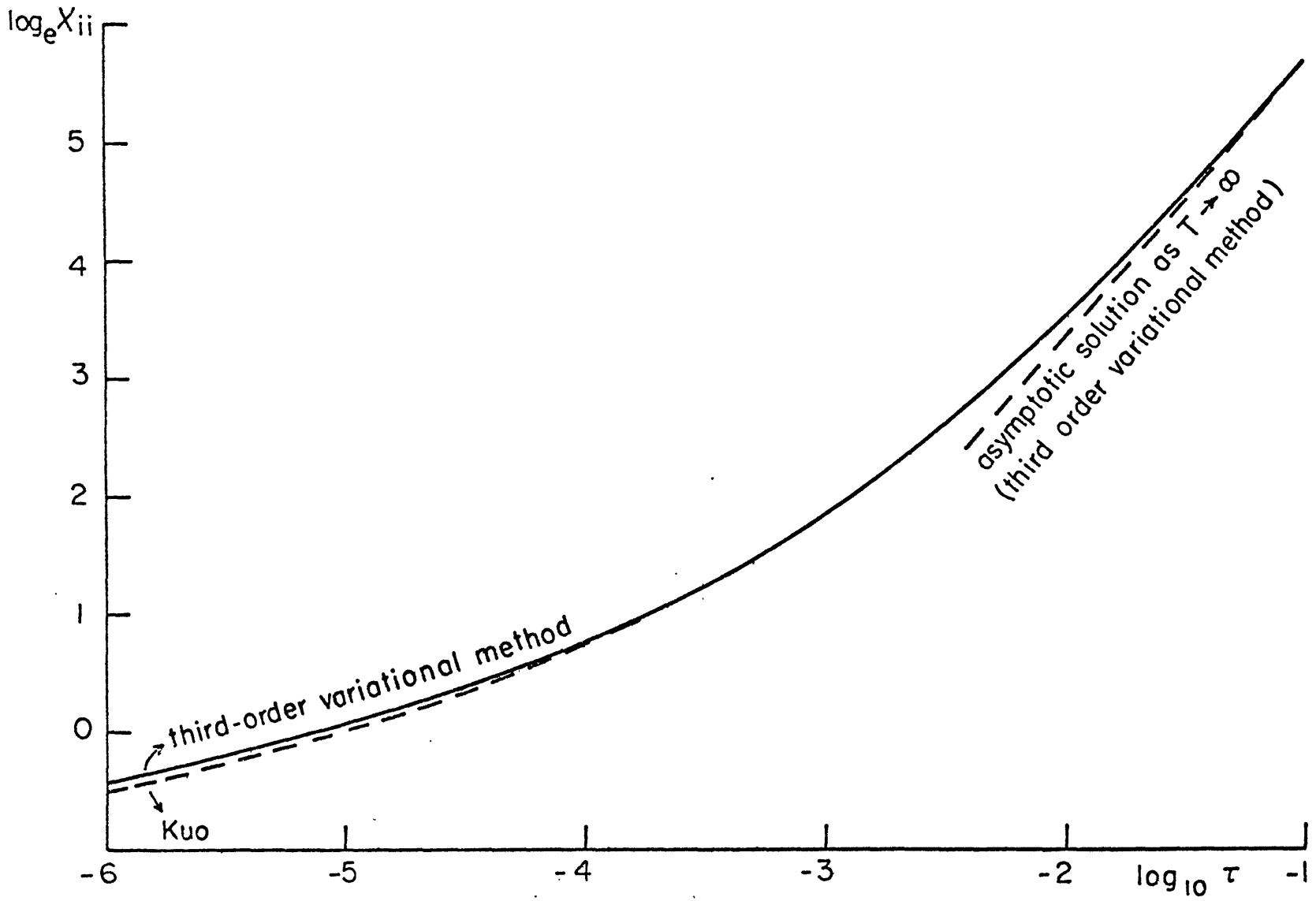

Figure 9: Critical values of the stability parameter χ_{ii} as a function of the diffusion parameter τ, for inertial instability in a neutrally stratified fluid. The parameters χ_{ii} and τ are defined differently for steady and overstable motion (see text). Solid χ_{ii} curve indicates values obtained by the third-order variational method; dashed curve follows the results of Kuo (1954). Asymptotic solution as $T \to \infty$ derived from third-order variational method.

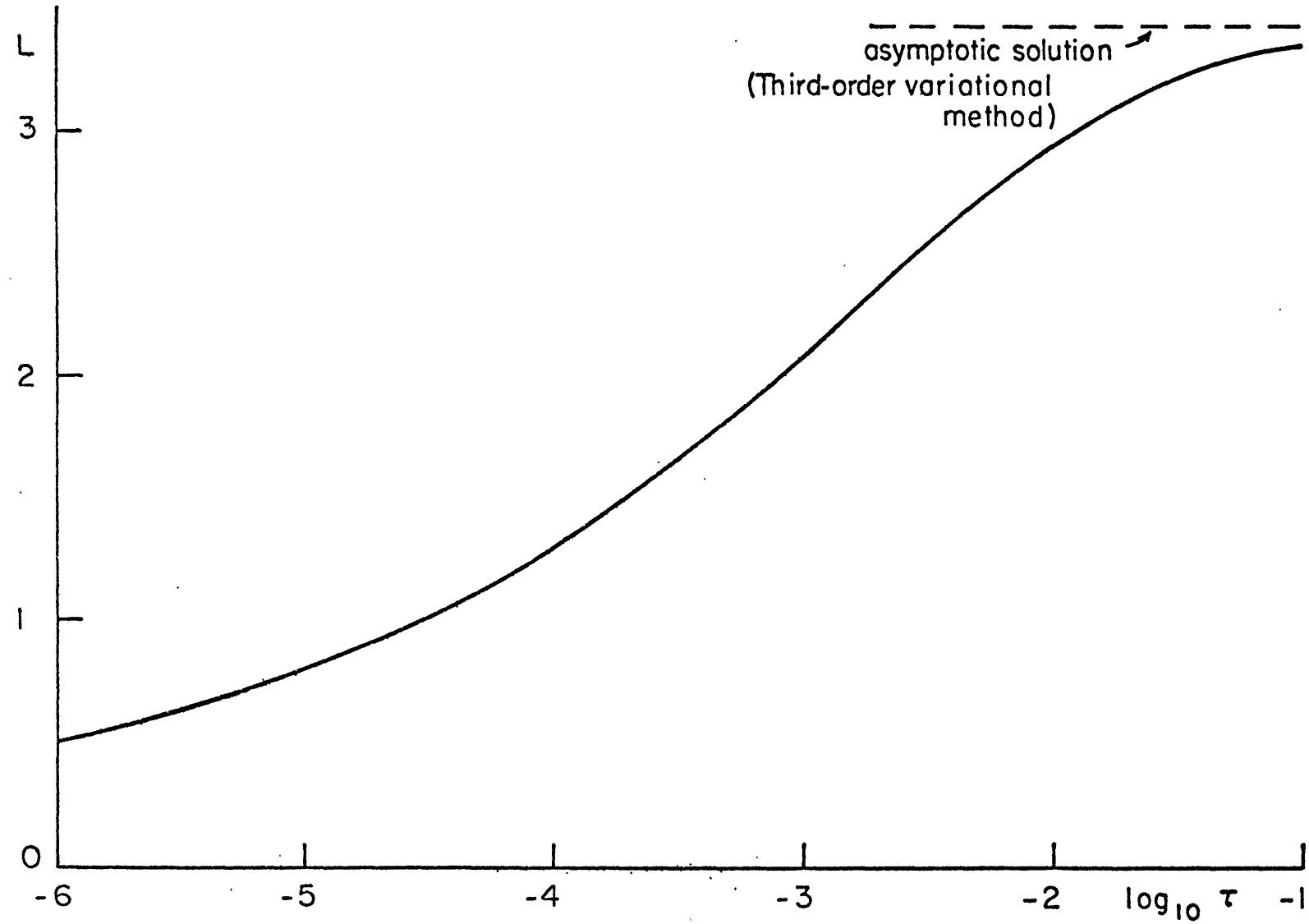

Figure 10: Non-dimensional wavelength L at which instability first appears, as a function of τ, for inertial instability in a neutrally stratified fluid. The results of Kuo (1954) are indistinguishable. Asymptotic as well as complete solution obtained by third-order variational method.

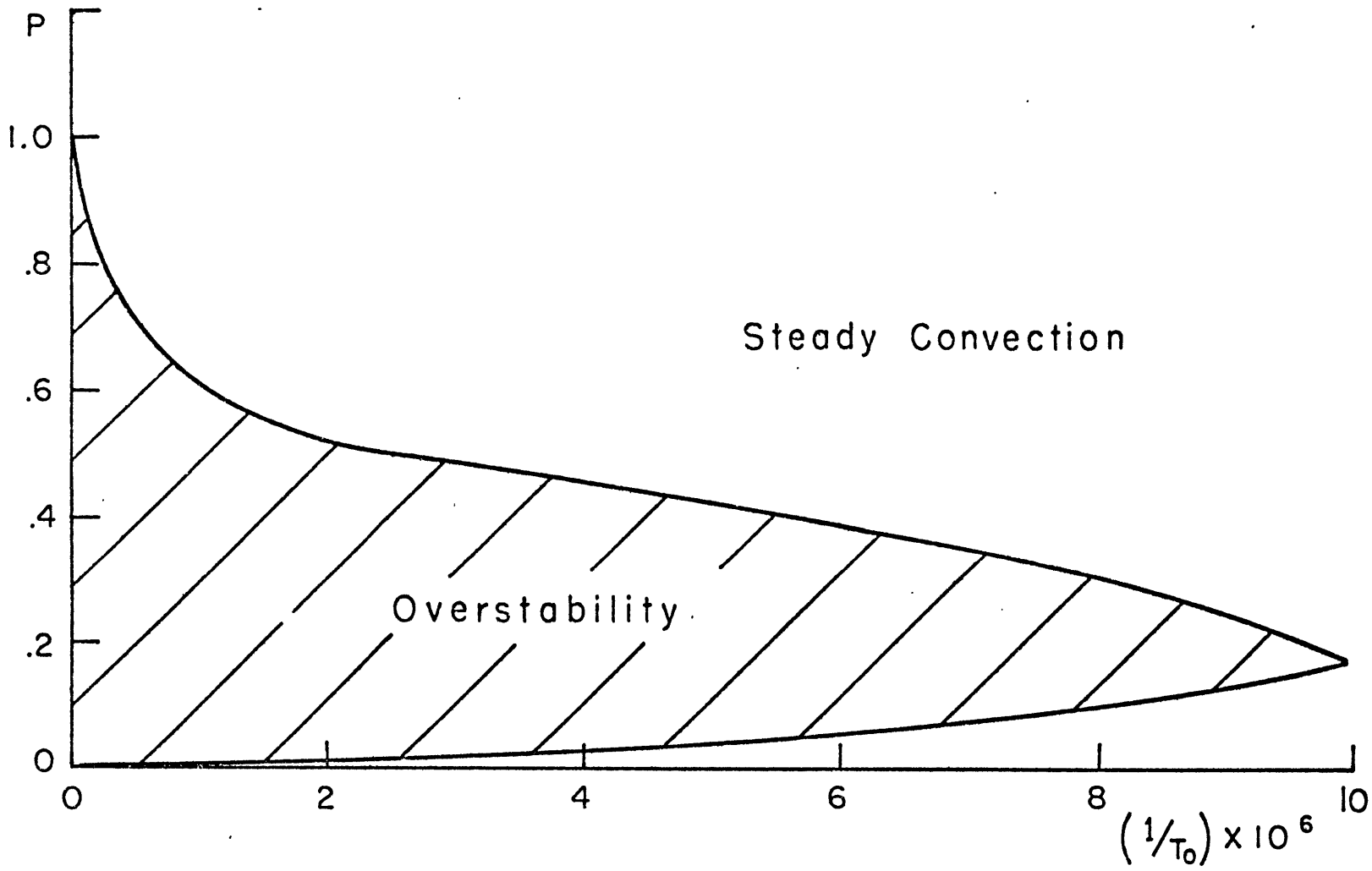

Figure 11: Domain of Prandtl and Taylor Numbers in which instability begins as oscillations in a neutrally stratified fluid.

Equation (24), we may derive an asymptotic relation for large T ($\pi^4 T >> 1$):

$$\chi_{ii} \rightarrow 2747\tau$$

$$\text{as } \tau \rightarrow \infty$$

$$L \rightarrow 3.41$$

Corresponding to the first relation, the asymptotic curve

$$\ln\chi_{ii} = 7.918 + 2.3026 \log_{10}\tau$$

is also depicted in Figure 9.

The structures of the streamfunctions, tangential velocity, and temperature perturbations associated with inertial motions in a neutrally stratified shear flow are similar to those occurring in connection with unstable motions in a stratified, hydrostatic flow. Although the potential temperature surfaces are vertically oriented in the former instance, the disturbances slope upward toward the cold air and transport momentum downward. The maximum negative tangential velocity at the surface occurs considerably north (toward the colder air) of the region of upward motion near the surface, instead of coinciding with the latter as occurs in the hydrostatic case. The reader

is referred to Kuo's 1954 paper for a complete discussion of the structures of the velocity and temperature perturbations.

CHAPTER 6

INERTIAL STABILITY AND MESOSCALE CONVECTIVE CIRCULATIONS

The stability analyses of shear flow in rotating diffusive fluids indicate that circulations may develop in lines parallel to the shear when the Richardson number is sufficiently low. The important characteristics of inertial motion deduced from the stability analyses are:

(a) The instability favors regions of low Richardson number and anticyclonic shear ($\frac{f}{\eta}\frac{1}{Ri}$ large).

(b) The circulations occur as roll vortices sloped along potential temperature surfaces, with wavelengths on the order of the ratio of the depth of the unstable region and the slope of the potential isotherms. In the atmosphere, this quantity is on the order of 100 km; the instability may therefore be regarded as a mesoscale phenomenon.

(c) The circulations exhibit strong convergence in the boundary layer and may thereby support cumulus convection when the distributions of moisture and temperature are favorable.

(d) The mesoscale updraft is cold and has less horizontal (zonal) momentum than the mean environmental flow. The density distributions favor high surface pressure under the mesoscale updraft and low pressure below the regions of descent.

(e) The disturbances, unless they are growing rapidly, have a greater effect on the component of flow parallel to the shear than on the normal component.

(f) In the absence of asymmetries, the inertial circulations show little tendency to propagate - their motion relative to the ground is determined by the component of flow normal to the shear.

(g) Unequal diffusions of heat and momentum appear to enhance inertial instability.

Many of these deduced characteristics of inertial circulations are similar to those observed in connection with mesoscale convective lines; one is therefore led to inquire whether the conditions favorable to inertial circulations are actually found in the vicinity of convective lines, and if so, what processes operating within the atmosphere

act to destabilize the flow. In this chapter, we investigate atmospheric processes that act to destroy inertial stability, and explore observational evidence of the operation of such processes in connection with various mesoscale line phenomena.

(a) Destruction of Inertial Stability in the Atmosphere

In order to examine the types of processes within the atmosphere that may cause inertial instability, it is convenient to relate the hydrostatic linear inertial growth rate σ for Prandtl number 1

$$\frac{\sigma^2}{f^2} = \frac{1}{Ri} - \frac{\eta}{f}$$

to the potential vorticity of the flow. The latter may be defined

$$q \equiv (\nabla_3 \times \underset{\sim}{V} + \hat{k}f) \cdot \nabla \ln\theta$$

where θ is the potential temperature. If the flow is zonal and in geostrophic balance, then

$$\frac{\partial \ln\theta}{\partial z} = \frac{N^2}{g} \qquad\qquad \frac{\partial \ln\theta}{\partial y} = -f\,\frac{U_z}{g}$$

where N is the Brunt-Väisälä frequency, g is the acceleration of gravity, and U_z is the vertical shear of the zonal velocity. From these relations,

$$q = \eta\frac{N^2}{g} - f\frac{U_z^2}{g}$$

from which one may obtain an expression relating the inertial growth rate to the potential vorticity:

$$\frac{\sigma^2}{f^2} = \frac{1}{Ri} - \frac{\eta}{f} = -\frac{g}{fN^2}q \qquad (44)$$

Inertial stability is small when the potential vorticity is small. If the effective Prandtl number is unity, the potential vorticity must be negative for instability; otherwise, circulations may develop for small positive values of q.

Equation (44) is particularly significant in that it allows one to relate changes in the inertial stability to corresponding variations in the potential vorticity of the flow, which can only be brought about by dissipative and diabatic processes. Inertial instability may occur due to:

(a) Diabatic heating that acts to increase the thermal wind and/or reduce the static stability.

(b) Dissipative processes that increase the

vertical shear (or decrease the vertical component of the vorticity).

(c) Adiabatic and non-dissipative processes that decrease the static stability (see Equation (44)).

Low values of potential vorticity are found beneath the anticyclonic shearing side of jet streams, where the absolute vorticity is small and the vertical shear large. Further reduction of inertial stability by diabatic and dissipative processes would be expected to occur near the surface, especially when there is strong solar heating and the surface wind is large and in the same direction as the shear. Adiabatic and non-dissipative processes that act to decrease the static stability include vertical motion and differential temperature advection accomplished by ageostrophic motion. The latter process might be expected to be of some importance, for example, beneath the right-front quadrant of an advancing isotach maximum associated with a jet stream. In this region, the decelerating parcels move to the right of the geostrophic wind and advect colder temperatures at middle or upper levels in the troposphere, thereby destabilizing the lower troposphere. In general, the area near, to the right of, and ahead of

the core of jet streams would appear to be a favored region for the development of inertial instability, especially when diabatic and dissipative processes also cooperate to reduce the stability.

(b) Inertial Stability and Observations of Intense Convection

Having ascertained, in Chapter 1, that convective lines in mid-latitudes are generally associated with strong vertical shear of the horizontal wind, we must now inquire as to whether the flow observed in the environment of such convective lines is specifically characterized by low inertial stability. Measurements needed to compute the inertial stability index, $\frac{g}{fN^2}q$, may be obtained directly from a set of standard rawinsonde observations, but calculations of the Richardson number are rarely found in the literature on organized convection. Nevertheless, certain observations of flow patterns typically associated with intense convection reveal aspects of the inertial stability of the flow.

Ludlam (1963) notes that intense thunderstorms in Europe are usually found in the right-front quadrant of surface-to-500 mb wind shear isotach maxima. His illustration of several examples of the location of severe convection with respect to wind shear isotachs is

reproduced in Figure 12. Similarly, Endlich and Mancuso (1968) find that the negative magnitude of the relative vorticity of the wind shear vector between the low and middle troposphere is a good indicator of severe convection. Numerous studies of severe line squalls mention the presence of strong anticyclonic shear near squall lines. A line studied by Breiland (1958) coincided with the "marked right-hand edge" of a belt of strong winds at 700 mb. Similarly, the upper level flow associated with an intense squall line examined by Eisen (1972) shows strong anticyclonic shear vorticity of about -5×10^{-5} sec^{-1} (-60% of f) near the line (Figure 13). The component of low level flow parallel to the line reaches a minimum at the location of the line (Figure 14) suggesting that $\overline{u'w'} < 0$ in this region. Strong anticyclonic shear and negative absolute vorticity near a squall line is reported by McLean (1961) on the basis of aircraft measurements. Paine and Kaplan (1976) find that severe convection is common on the anticyclonic shearing side of a large scale jet stream as it advances into a geopotential field that is strongly diffluent (indicating ageostrophic motion to the right of the geostrophic wind). They also find very good correlation between the location of developing squall lines and regions in which the local time rate of change of

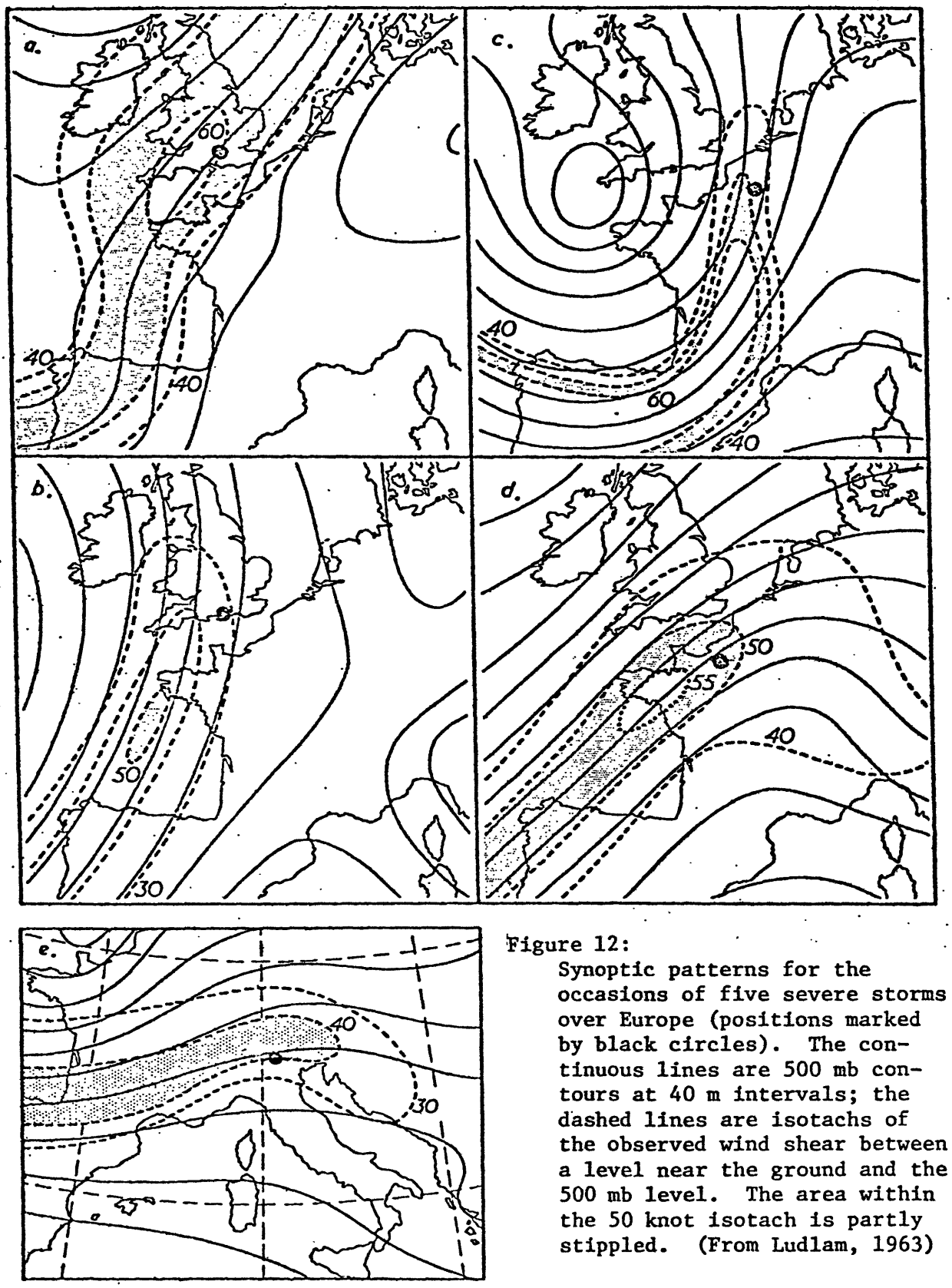

Figure 12:
Synoptic patterns for the occasions of five severe storms over Europe (positions marked by black circles). The continuous lines are 500 mb contours at 40 m intervals; the dashed lines are isotachs of the observed wind shear between a level near the ground and the 500 mb level. The area within the 50 knot isotach is partly stippled. (From Ludlam, 1963)

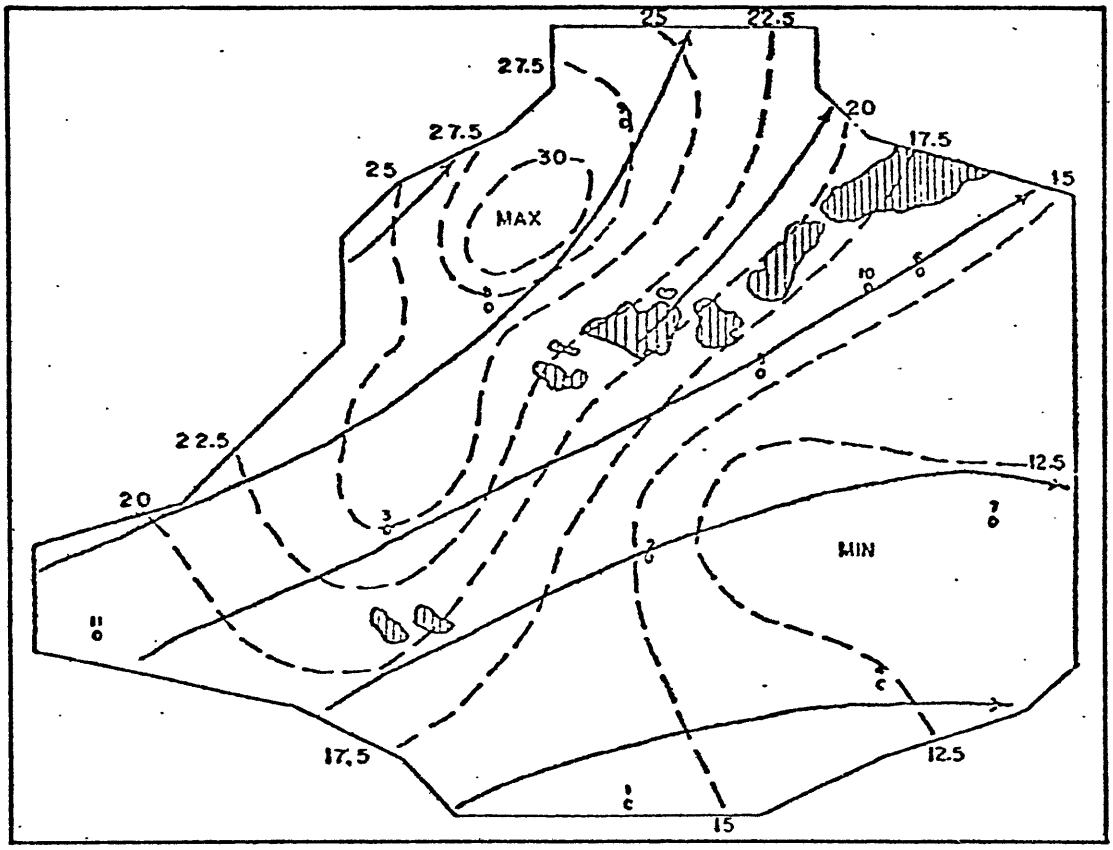

Figure 13: Streamlines (solid) and isotachs (m sec^{-1}) (dashed) at the 200 mb level at 0200Z on 9 June, 1966. Radar echoes are shaded. (From Eisen, 1972)

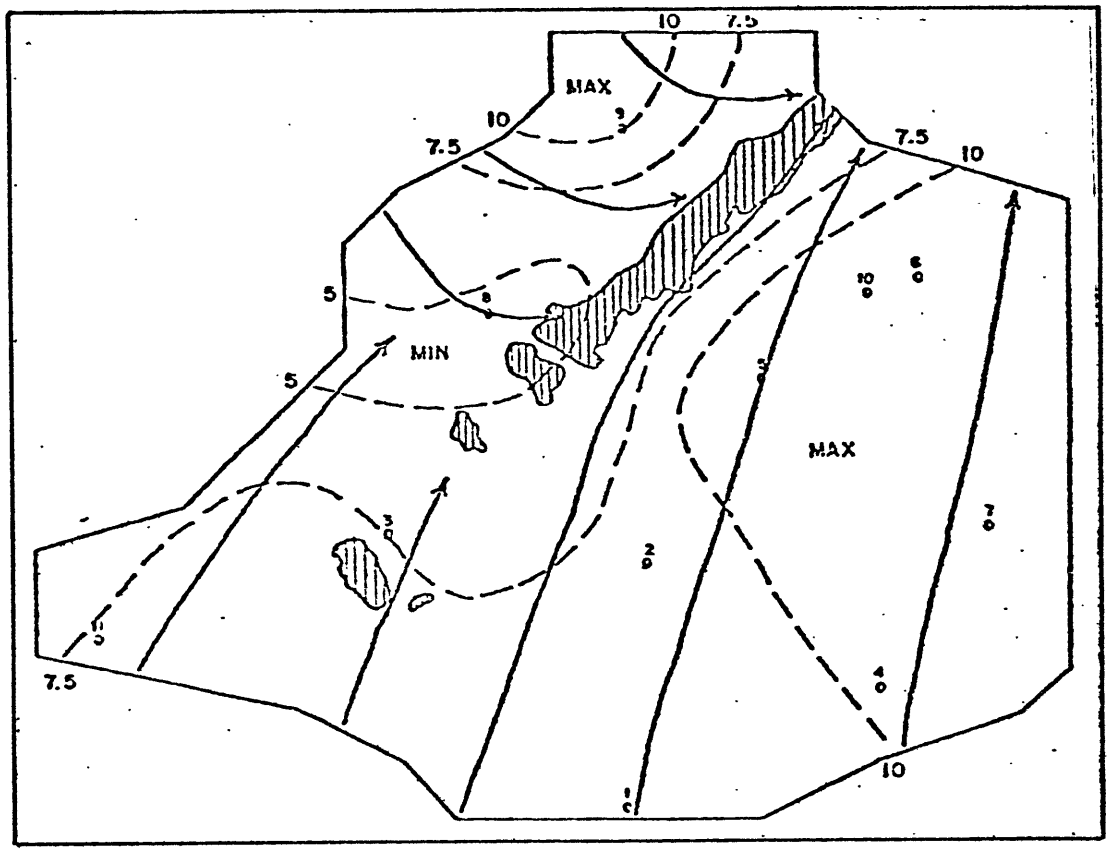

Figure 14: Streamlines (solid) and isotachs (m sec^{-1}) (dashed) at the 950 mb level at 0300Z on 9 June, 1966. Radar echoes are shaded. (From Eisen, 1972)

equivalent potential vorticity (defined in the same way as potential vorticity but using the equivalent potential temperature) is negative. Severe convection was found by Porter, et.al. (1955) to prefer a region 200 to 300 miles to the right of a mid-troposphere jet core, in flow which is either straight or shows slight anticyclonic curvature. Finally, Sasaki (1973) studied a squall line that occurred in a region of strong moisture convergence, which preceded the line development by several hours. This area of moisture convergence was found in a region in which the gradient of the bulk Richardson number (computed between the surface and 700 mb) was strong and indicative of anticyclonic shear aloft. (The squall line occurred along an isopleth of Richardson number 2, with lower values to the left of the shear.) Sasaki also concludes that strong downward momentum transport is intimately associated with the squall line.

While these observational studies seem to show that severe convection occurs within large scale flow patterns indicative of low inertial stability, a direct measure of the inertial stability parameters is needed in order to ascertain the degree of stability. As a preliminary attempt at such an analysis, the author computed the stability parameter $\frac{\eta}{f}$ Ri along a vertical cross-section

through one of the severe squall lines that occurred in the central United States on 3-4 April 1974. This cross-section represents a composite of four standard rawinsonde measurements, the locations of which are illustrated, together with the isotachs of the wind component normal to the cross-section and potential temperature, in Figure 15. The Richardson number, which involves only vertical derivatives, may be computed at different levels from each sounding individually; the horizontal shear vorticity must be estimated from the composite wind field. This case was selected partially because the horizontal synoptic scale flow in the vicinity of the lines showed very little curvature or directional variation with height. The computed field of $(\eta/f)Ri$ is also illustrated in Figure 15.

A vigorous, tornado-producing squall line is located just west of Huntington, West Virginia, in a region of very low inertial stability. A second, weaker line occurs somewhat to the west in an area of marginal stability. The region of low stability does not appear to penetrate above 700 mb in this case.

The effects of moisture are not, of course, accounted for in computing the stability parameter. If a part of the mesoscale area is saturated, then the inertial stability will be less than the indicated values in this region since

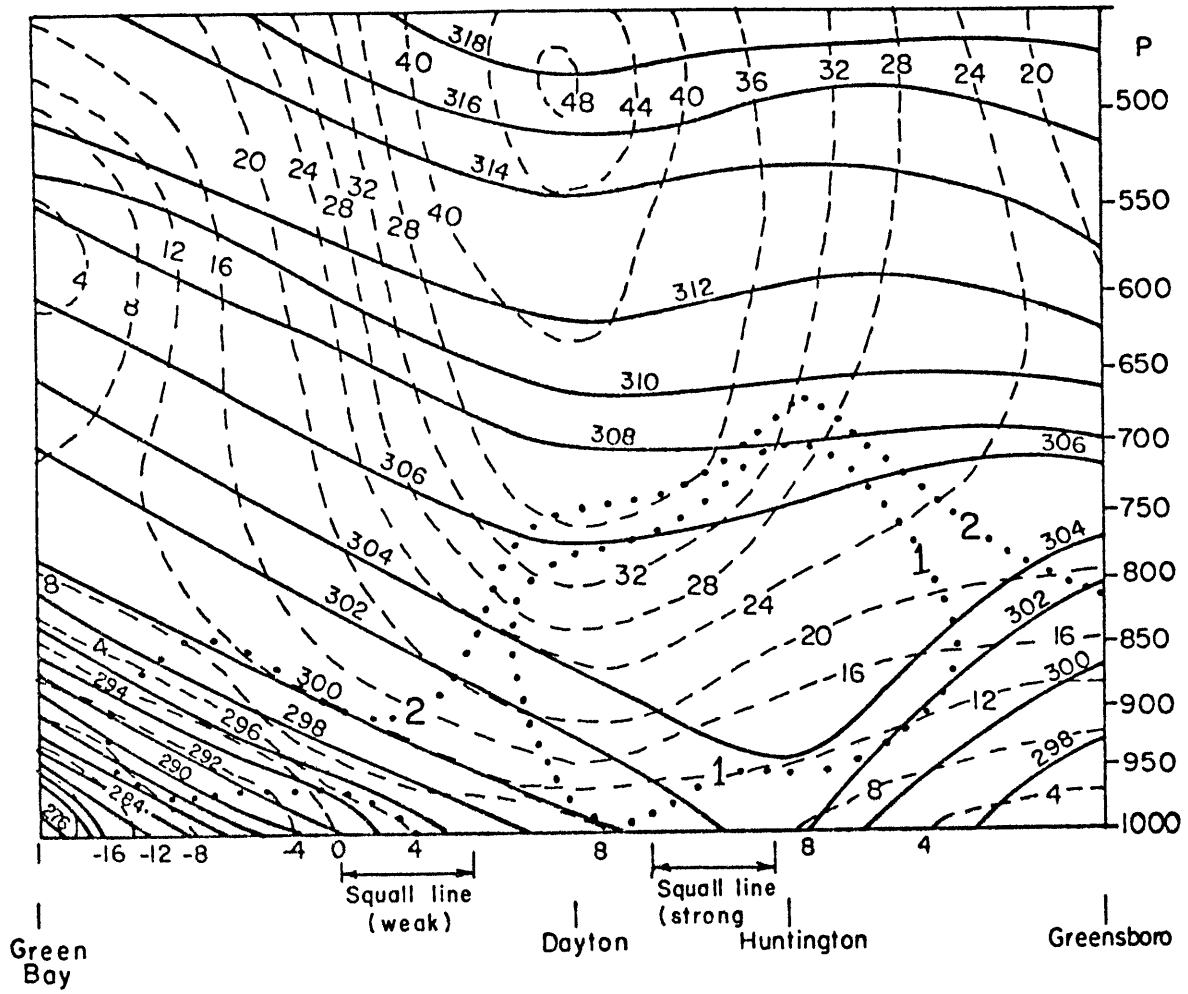

Figure 15: Vertical cross-section from Green Bay, Wisconsin to Greensboro, North Carolina at 00Z on 4 April, 1974. Isotherms of potential temperature (°K) are denoted by solid lines; dashed lines indicate the component of velocity (m sec^{-1}) normal to the cross-section, with positive values into the page. Dotted lines are contours of the inertial stability index $(\eta/f)Ri$. Positions of squall lines are indicated at bottom.

the effective static stability is also less. Sanders and Paine (1975) found that a mesoscale circulation associated with a vigorous frontal thunderstorm line contained a saturated region of ascent, suggesting that inertial stability may be lowered by latent heating on the mesoscale.

The observations reviewed here strongly support the premise that vigorous organized convection is related to the inertial stability of the large scale flow, although further observational evidence is clearly needed to substantiate this hypothesis.

(c) Effect of Cumulus Convection on Inertial Circulations

It is not possible to incorporate cumulus heating into the linear theory of inertial instability without complicating the problem enormously; however, certain aspects of the modification of inertially induced motion by latent heat release may be inferred from the general theory of cumulus convection.

Once an inertial circulation is established, the development of cumuli will favor regions of low static stability and moisture convergence, both of which occur in connection with the upward branch of the mesoscale circulation. As the inertial circulation is sloped upward and to the left of the shear, the individual cumulus elements

will tend to move, relative to the mesoscale pattern, across the isotherms toward colder air. To have the appearance of a quasi-steady mesoscale convective line, new cells must form, intensify to maturity, then decay while moving through the mesoscale pattern from right to left with respect to the thermal wind. In a north-south oriented line imbedded in a thermal wind directed toward the north, for example, new cells form on the east flank of the line reach maximum intensity near the center, and decay while moving off the western flank. Such discrete behavior is frequently observed on radar in connection with convective lines (see, for example, Sanders and Emanuel, 1977; Houze, 1977; Zipser, 1977), and also characterizes some numerical models of frontal thunderstorm lines (Gordon, 1978).

Once established, the cumuli affect the mesoscale fields through latent heating and vertical transport of heat, moisture, liquid water, and momentum. The net effect of precipitating cumuli is certainly to heat the mesoscale updraft, forcing the upward branch of the circulation to flow across potential isotherms. The cumuli act most efficiently when the fractional area covered by the updraft is much smaller than that of the downdraft; the mesoscale circulation is likely affected accordingly. The idealized dry inertial circulations indicated by linear stability

theory show that adiabatic warming and low surface pressures occur in conjunction with the mesoscale downdraft, while high surface pressures and adiabatic cooling are associated with updrafts. The cumuli act to counter this adiabatic cooling, except near the surface within the region of evaporating cloud and precipitation. The evaporative cooling and liquid water loading undoubtedly act to reinforce the mesoscale surface high pressure in the region of active convection (Fujita, 1955). Evaporation of liquid water within the mesoscale downdraft acts to mitigate the otherwise adiabatic warming that occurs there; the perturbation surface pressure response in view of this effect is ambiguous. A "wake low" is sometimes, but not always, observed behind pre-cold frontal squall lines.

A speculative depiction of an inertio-convective circulation, that ties together the effects of the processes enumerated above, is illustrated in Figure 16. The updraft is concentrated and more erect than the downdraft, which is nearly parallel to the potential temperature surfaces except where evaporation occurs. Cumulus scale downdrafts and a "gust front" are indicated. The pressure field, illustrated near the bottom of the figure, is fashioned after the results of the linear stability analysis (e.g., see Figures 8), with modifications according to the

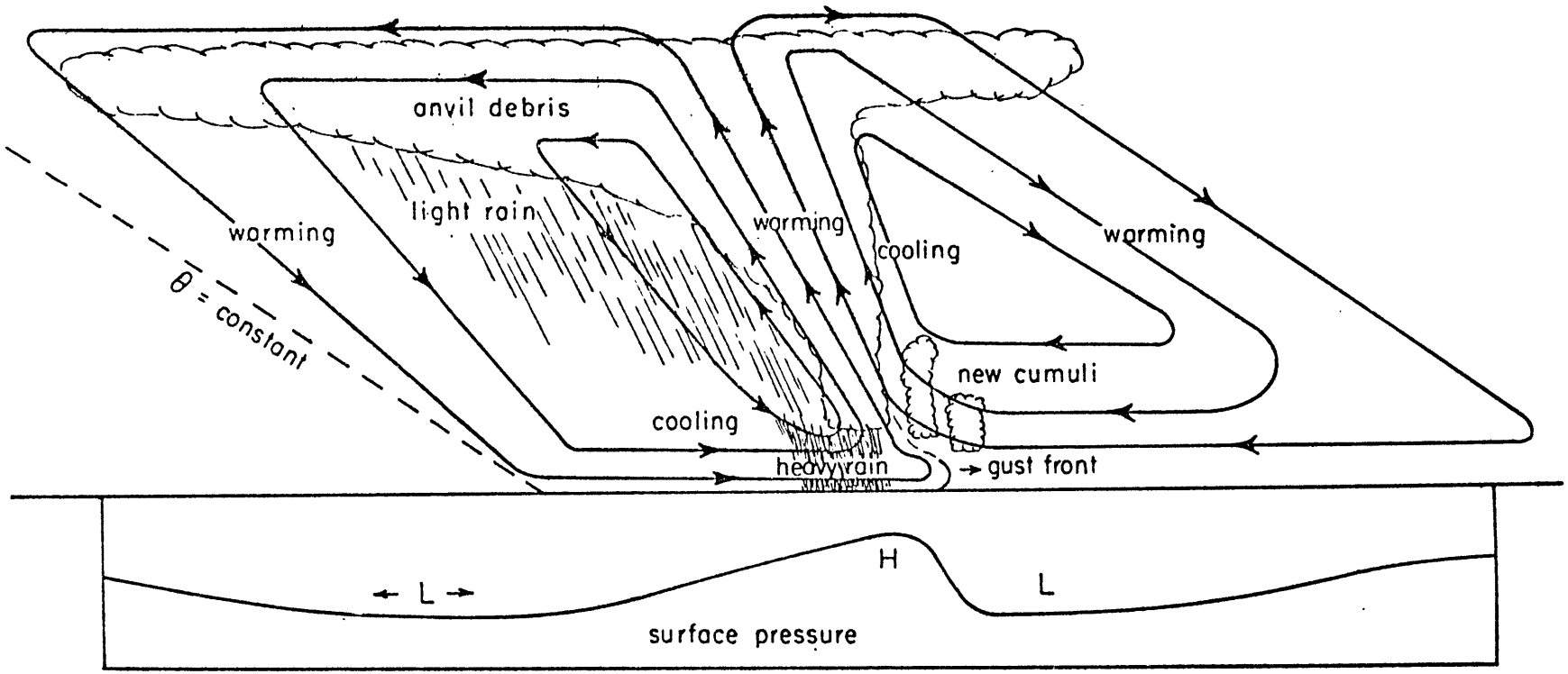

Figure 16; Schematic of mesoscale circulation associated with a squall line. Streamlines are denoted by solid curves; dashed line indicates orientation of potential temperature surfaces. Cloud outlines are scalloped and shading denotes precipitation. Relative surface pressure profile depicted at bottom.

hydrostatic effects of evaporative cooling and liquid water loading.

The asymmetries induced by the convection may also force the system to propagate. If, for example, the cumuli develop most vigorously where the mesoscale vertical motion near the top of the boundary layer is strongest, then the mid-troposphere vertical motion within the cumuli would be most intense in the atmosphere above this region, which is somewhat removed from the mesoscale ascent maximum in the middle troposphere. Perhaps, the mesoscale circulation responds by adjusting the vertical velocity field toward the cumulus scale maximum. Such an effect would be manifest as a propagation to the right of the shear. A far more complete treatment of cumulus-mesoscale interaction is necessary in order to resolve the possibility of such behavior.

One further aspect of the character of some severe squall lines deserves comment here; that is, the tendency to develop waves and eventually mesocyclones along the line. Observations of tornado outbreaks within the National Severe Storms Laboratory mesonetwork reveal that the development of LEWPS (Line Echo Wave Patterns) often precedes the generation of tornadic mesocyclones. As illustrated in

Chapter 5, inertial instabilities are capable of inducing large horizontal shears of tangential velocity in the region of maximum vertical motion, through the twisting of the large scale shear vorticity. We speculate that the waves sometimes observed within squall lines are manifestations of inflectional instability of the mesoscale horizontal shear induced by the twisting effect. Cyclonic vortices would be found, under these circumstances, to the right of the region of maximum vertical motion. As this is also the region in which individual cumulus cells intensify, the cyclonic instabilities would tend to develop in preference to anticyclonic vortices, which occur where the cumulus cells decay.

(d) Other Forms of Banded Overturning Motion in the Atmosphere

The occurrence of banded structures aligned with the local vertical wind shear is common in the atmosphere. Perhaps the most familiar examples of phenomena of this nature are long cirrus streaks often observed in the vicinity of jet streams. A study of such bands, conducted by Schaefer and Hubert (1955) reveals that the streaks are often more than 1000 km long and are generally found in regions of strong anticyclonic shear south of and under the core of upper level jet streams. McLean (1961) finds

evidence that the magnitude of the anticyclonic vorticity may exceed the Coriolis parameter by as much as 50% in small regions to the south of a strong jet.

Cloud streets are another familiar form of banded overturning motion in the atmosphere. Kuettner (1971) notes that the cloud streets observed during the BOMEX occur in a layer with strong vertical shear but small variation in wind direction with height. These roll vortices had width-to-depth ratios of from 2 to 4 and were aligned with the wind. Since cloud streets often occur in unstable boundary layer flow and have been observed directly at the equator (where f vanishes), they are most likely an example of Rayleigh convection in shear, rather than an inertial instability.

Numerous investigations of the neutrally stratified Ekman layer have, however, revealed the existence of two forms of motion: a slow moving type oriented about 15° counterclockwise from the direction of the geostrophic wind above the Ekman layer, and a rapidly moving instability which is closely aligned with the geostrophic flow. Lilly (1966) shows that this second form, which he calls parallel instability, occurs at lower Reynolds numbers than the first, and depends directly on the presence of rotation; whereas the low speed bands are essentially a form of Rayleigh instability occuring in conjunction with an

inflection point in the Ekman flow profile. Experiments by Tatro and Mollo-Christensen (1967) confirm the theoretical predictions of Lilly (1966), and also reveal that the finite amplitude parallel instabilities excite inertial waves in the neutrally stratified geostrophic flow above the Ekman layer. This observation, together with the apparent direct dependence of the parallel instability on rotation, suggests that these motions are a form of inertial instability. In order to test this hypothesis, we develop a linear stability analysis of incompressible Ekman flow, applying the following crude assumptions:

(a) The instabilities are two-dimensional and aligned with the geostrophic flow in the interior.

(b) The shear along the line is approximated by a constant value representing the mean shear in the layer in which the instabilities occur.

(c) The component of flow normal to the geostrophic wind is approximately constant in the layer of instability.

(d) The motion is confined above and below by rigid, free-slip boundaries.

The last assumption is the most vulnerable, since the tank experiments and the Ekman layer flow itself depend on the presence of a lower, no-slip boundary. The analysis performed in Chapter 4 and discussed in Chapter 5 indicates, however, that there is little difference in the critical values of the stability parameters for differing boundary conditions when the effects of diffusion are small; otherwise, the no-slip boundaries appear to be more conducive to the onset of instability. Assumption (c) is supported by the very small mean shear of the normal component of flow within the Ekman layer. The ill effects of Assumption (b) are somewhat mitigated if we require that the total kinetic energy available to the instabilities from the approximated shear flow be equal to that from the actual Ekman flow. The total kinetic energy of the shear flow in a layer of depth H is proportional to

$$\frac{1}{H}\int_0^H U^2 dz \equiv \overline{U^2}$$

If turbulence acts to completely mix the momentum, then the

velocity of the final state will be the same everywhere and equal to the initial mean momentum. The total energy of this final state will then be proportional to

$$\left[\frac{1}{H}\int_0^H U dz\right]^2 = \bar{U}^2$$

The kinetic energy available to the disturbances is then the difference between the kinetic energies of the initial and final states:

$$AKE \equiv \overline{U^2} - \bar{U}^2$$

The mean value of the parallel component of shear that we will use in the stability analysis is simply

$$\frac{1}{H}\int_0^H \frac{\partial u}{\partial z}\, dz = \frac{U(H)}{H}$$

We choose the height H so that the available kinetic energy computed assuming this constant shear profile is identical to that calculated using the actual Ekman flow component parallel to the line.

The stability problem is solved using the same techniques employed previously; details may be found in Appendix 5. The Reynolds number is defined in the

conventional manner for such problems:

$$Re \equiv \frac{U_g \delta}{\nu}$$

in which U_g is the geostrophic wind, ν is the coefficient of viscosity, and δ is the Ekman layer depth:

$$\delta \equiv \left(\frac{\nu}{\Omega}\right)^{1/2}$$

where Ω is the rotation rate of the fluid.

The analysis carried through in Appendix 5 yields a critical Reynolds number of 54.5 associated with instabilities of horizontal wavelength 2.19H (= 8.07δ) moving with the mean normal component of flow, through the depth H, of 14% U_g. The critical Reynolds number deduced from a complete eigenanalysis of the Ekman layer instability problem performed by Lilly (1966) was 55; nearly identical to the value obtained through experiment by Tatro and Mollo-Christensen (1967). The latter observed the parallel instabilities to drift to the left of the geostrophic flow at 16% U_g.

The very good agreement of these experimental and theoretical results with those obtained from the simplified theory presented here suggests that the parallel instability

observed within Ekman layers is a form of inertial instability, since this is the only form of instability permitted by this treatment. (The constant shear prohibits Rayleigh instability.) In the present case, the inertial motion occurs as a consequence of an unstable distribution of Coriolis, pressure, and viscous forces within the fluid. As the inertial instability sets in before the inflectional type (characterized by a critical Reynolds number of 125) and is observed in tank experiments to reach finite amplitude before the latter begins (Tatro and Mollo-Christensen, 1967), one might expect to observe them in geophysical boundary layers. Numerous observations within the planetary boundary layer reveal the existence of periodic fluctuations of temperature, moisture, and velocity, but more detailed measurements are needed before the origin of such disturbances is understood.

CONCLUSIONS

Persistent, organized convection depends not only on the availability of buoyant energy, as reflected in the vertical stratification of moisture and temperature, but also on the presence of circulations much larger than those associated with the cumulus cloud; circulations which provide the moisture convergence necessary to the maintenance of the convection. Observations of convection in middle latitudes reveal that cumuli often occur in lines parallel to the shear of the flow in which they are imbedded, suggesting that the larger scale supportive circulations are roughly two-dimensional. The stability analysis performed here indicates that the origin of such circulations, or else the facility with which they are driven by the cumulus convection, depends on the inertial stability of the large scale flow. In addition, the analyses reveal that inertial circulations generally take the form of elongated roll vortices sloped upward and to the left of the shear, with dimensions typical of the mesoscale in the atmosphere. Properties of these vortices, such as the velocity, temperature, and pressure distributions, are similar to those found in connection with squall lines, and an examination of the flow patterns associated with observed intense convective lines suggests

that the latter form in regions of low and decreasing inertial stability. It is also demonstrated that other forms of banded overturning motion in the atmosphere, such as certain forms of boundary layer rolls, may be associated with a down-gradient transport of momentum accomplished through the action of Coriolis and pressure forces.

Although a relationship between inertial circulations and cumulus bands in the atmosphere is strongly implied by observations of convection in the atmosphere, together with inferences concerning the characteristics of inertial motion drawn from linear stability theory, a clarification of the role of inertial stability in geophysical fluids is needed. The effects of variable shear and static stability on inertial motions, as well as the interaction of the latter with cumulus convection and the large scale flow, are the next important steps to be taken in this direction. A complete investigation of the dynamics of the mesoscale link between convective processes and those operative on the synoptic scale will lead to an important new understanding of organized convection in the atmosphere.

APPENDIX 1

Derivation of the Perturbation Equation for the Streamfunction

Equation (6) is derived from the five perturbation equations for the three velocity components, pressure, and density as follows:

Equations (1)-(4) may be re-written using a streamfunction constructed from Equation (5):

$$\left(\frac{\partial}{\partial t} - \nu\nabla^2\right)u = -\overline{\eta}\,\frac{\partial \psi}{\partial z} - \overline{U_z}\,\frac{\partial \psi}{\partial y} \tag{1}$$

$$\left(\frac{\partial}{\partial t} - \nu\nabla^2\right)\frac{\partial \psi}{\partial z} = \frac{1}{\rho_o}\,\frac{\partial p}{\partial y} + fu \tag{2}$$

$$\alpha\left(\frac{\partial}{\partial t} - \nu\nabla^2\right)\frac{\partial \psi}{\partial y} = -\frac{1}{\rho_o}\,\frac{\partial p}{\partial z} - \frac{\rho}{\rho_o}g \tag{3}$$

$$\left(\frac{\partial}{\partial t} - \kappa\nabla^2\right)\frac{\rho}{\rho_o} = \frac{f\overline{U_z}}{g}\,\frac{\partial \psi}{\partial z} + \frac{N^2}{g}\,\frac{\partial \psi}{\partial y} \tag{4}$$

The primes denoting perturbation quantities have been dropped, and by definition

$$v \equiv -\frac{\partial \psi}{\partial z} \qquad\qquad w \equiv \frac{\partial \psi}{\partial y}$$

If the perturbation density is eliminated between (3) and (4), the result is:

$$-\left(\frac{\partial}{\partial t} - \kappa\nabla^2\right)\frac{1}{\rho_o}\frac{\partial p}{\partial z} = \alpha\left(\frac{\partial}{\partial t} - \kappa\nabla^2\right)\left(\frac{\partial}{\partial t} - \nu\nabla^2\right)\frac{\partial \psi}{\partial y}$$

$$+ f\overline{U}_z \frac{\partial \psi}{\partial z} + N^2 \frac{\partial \psi}{\partial y}$$

The perturbation pressure may now be eliminated between the above and Equation (2):

$$\alpha\left(\frac{\partial}{\partial t} - \kappa\nabla^2\right)\left(\frac{\partial}{\partial t} - \nu\nabla^2\right)\frac{\partial^2 \psi}{\partial y^2} + f\overline{U}_z \frac{\partial^2 \psi}{\partial y \partial z} + N^2 \frac{\partial^2 \psi}{\partial y^2}$$

$$= f\left(\frac{\partial}{\partial t} - \kappa\nabla^2\right)\frac{\partial u}{\partial z} - \left(\frac{\partial}{\partial t} - \nu\nabla^2\right)\left(\frac{\partial}{\partial t} - \kappa\nabla^2\right)\frac{\partial^2 \psi}{\partial y^2}$$

Finally, the perturbation tangential velocity u is eliminated between the preceding and Equation (1), resulting in the perturbation Equation (6) for the streamfunction:

$$\left(\frac{\partial}{\partial t} - \kappa\nabla^2\right)\left(\frac{\partial}{\partial t} - \nu\nabla^2\right)^2 \left(\alpha \frac{\partial^2}{\partial y^2} + \frac{\partial^2}{\partial z^2}\right)\psi$$

$$= \left(\frac{\partial}{\partial t} - \nu\nabla^2\right)\left(f\overline{U}_z \frac{\partial^2 \psi}{\partial y \partial z} + N^2 \frac{\partial^2 \psi}{\partial y^2}\right)$$

$$- \left(\frac{\partial}{\partial t} - \kappa\nabla^2\right)\left(f\overline{U}_z \frac{\partial^2 \psi}{\partial y \partial z} + f\overline{\eta} \frac{\partial^2 \psi}{\partial z^2}\right)$$

If the time dependence is zero (i.e., $\partial/\partial t = 0$), the above may be integrated twice to yield

$$\kappa\nu^2(\nabla^2)^3\psi = -(\nu+\kappa)f\overline{U_z}\frac{\partial^2\psi}{\partial y\partial z} - \nu N^2\frac{\partial^2\psi}{\partial y^2}$$

$$- \kappa f\bar{\eta}\frac{\partial^2\psi}{\partial z^2} + \phi \qquad (1\text{-}1)$$

where ϕ is a function whose Laplacian vanishes. Through the boundary conditions, this function may be shown to be zero as follows: For free-slip boundary conditions,

$$\psi = \frac{\partial^2\psi}{\partial z^2} = \frac{\partial u}{\partial z} = \frac{\partial p}{\partial z} = 0 \quad \text{at } z=0,H \qquad (1\text{-}2)$$

Equation (1) is differentiated once in z, Equation (2) is differentiated three times in z, and the equation for $\partial p/\partial z$ is differentiated once in y to yield:

$$(\frac{\partial}{\partial t} - \nu\nabla^2)\frac{\partial u}{\partial z} = -\bar{\eta}\frac{\partial^2\psi}{\partial z^2} - \overline{U_z}\frac{\partial^2\psi}{\partial y\partial z} \qquad (1\text{-}3)$$

$$(\frac{\partial}{\partial t} - \nu\nabla^2)\frac{\partial^4\psi}{\partial z^4} = \frac{\partial^3 p}{\partial y\partial z^3} + f\frac{\partial^3 u}{\partial z^3} \qquad (1\text{-}4)$$

$$\frac{1}{\rho_o}(\frac{\partial}{\partial t} - \kappa\nabla^2)\frac{\partial^2 p}{\partial y\partial z} = -f\overline{U_z}\frac{\partial^2\psi}{\partial y\partial z} - N^2\frac{\partial^2\psi}{\partial y^2}$$

$$- (\frac{\partial}{\partial t} - \kappa\nabla^2)(\frac{\partial}{\partial t} - \nu\nabla^2)\frac{\partial^2\psi}{\partial y^2} \qquad (1\text{-}5)$$

Also, if (2) is differentiated once in z, it is evident that $\partial^4\psi/\partial z^4 = 0$ on the free-slip boundaries. Then, the

preceding three equations become, on the boundaries,

$$-\nu \frac{\partial^6 \psi}{\partial z^6} = \frac{\partial^4 p}{\partial y \partial z^3} + f \frac{\partial^3 u}{\partial z^3}$$

$$\nu \frac{\partial^3 u}{\partial z^3} = \overline{U_z} \frac{\partial^2 \psi}{\partial y \partial z} \qquad \text{(on boundaries)}$$

$$\kappa \frac{\partial^4 p}{\partial y \partial z^3} = f\overline{U_z} \frac{\partial^2 \psi}{\partial y \partial z}$$

Combining the above, we obtain

$$-\nu^2 \kappa \frac{\partial^6 \psi}{\partial z^6} = f\overline{U_z} (\nu + \kappa) \frac{\partial^2 \psi}{\partial y \partial z} \qquad \text{(on boundaries)}$$

Examination of Equation (1-1) shows that the function ϕ must also vanish at the boundaries. Since $\nabla^2 \phi = 0$, the only function ϕ which satisfies the boundary conditions (and is not exponential in y) is $\phi = 0$.* This argument is unaffected by setting α equal to zero or letting $\nabla^2 = \partial^2/\partial z^2$.

When the boundaries are no-slip,

$$\psi = \frac{\partial \psi}{\partial z} = u = \frac{\partial p}{\partial z} = 0 \qquad \text{(on boundaries)}$$

---

* I am indebted to David Andrews of the MIT Department of Meteorology for deriving the proof that $\phi = 0$.

If Equation (1) is differentiated once in z, the equation for $\partial p/\partial z$ is differentiated once in y, and the operator $(\partial/\partial t - \nu\nabla^2)\partial/\partial z$ is applied to (2), we obtain:

$$(\frac{\partial}{\partial t} - \nu\nabla^2)\frac{\partial u}{\partial z} = -\overline{\eta}\,\frac{\partial^2\psi}{\partial z^2} - \overline{U}_z\,\frac{\partial^2\psi}{\partial y\partial z}$$

$$(\frac{\partial}{\partial t} - \kappa\nabla^2)\frac{\partial^2 p}{\partial y\partial z} = \alpha(\frac{\partial}{\partial t} - \kappa\nabla^2)(\frac{\partial}{\partial t} - \nu\nabla^2)\frac{\partial^2\psi}{\partial y^2}$$

$$+ f\overline{U}_z\,\frac{\partial^2\psi}{\partial y\partial z} + N^2\,\frac{\partial^2\psi}{\partial y^2}$$

$$f(\frac{\partial}{\partial t} - \nu\nabla^2)\frac{\partial u}{\partial z} = -(\frac{\partial}{\partial t} - \nu\nabla^2)\frac{\partial^2 p}{\partial y\partial z} + (\frac{\partial}{\partial t} - \nu\nabla^2)\frac{\partial^2\psi}{\partial z^2}$$

On the no-slip boundaries, the above become

$$(\frac{\partial}{\partial t} - \nu\nabla^2)\frac{\partial u}{\partial z} = -\overline{\eta}\,\frac{\partial^2\psi}{\partial z^2}$$

$$-\kappa\,\frac{\partial^4 p}{\partial y\partial z^3} = \alpha(\frac{\partial}{\partial t} - \kappa\nabla^2)(\frac{\partial}{\partial t} - \nu\nabla^2)\frac{\partial^2\psi}{\partial y^2} \qquad \text{(on boundaries)}$$

$$f(\frac{\partial}{\partial t} - \nu\nabla^2)\frac{\partial u}{\partial z} = \nu\,\frac{\partial^4 p}{\partial y\partial z^3} + (\frac{\partial}{\partial t} - \nu\nabla^2)\frac{\partial^2\psi}{\partial z^2}$$

Eliminating u and p from the above, we arrive at:

$$(\frac{\partial}{\partial t} - \nu\nabla^2)\frac{\partial^2\psi}{\partial z^2} = \alpha\,\frac{\nu}{\kappa}\,(\frac{\partial}{\partial t} - \kappa\nabla^2)(\frac{\partial}{\partial t} - \nu\nabla^2)\frac{\partial^2\psi}{\partial y^2}$$

$$- \bar{\eta} f \frac{\partial^2 \psi}{\partial z^2} \qquad \text{(on boundaries)}$$

If $\partial/\partial t = 0$, the above becomes (with $\alpha=1$):

$$\nu^2 \kappa (\nabla^2)^3 \psi = -\bar{\eta} f \kappa \frac{\partial^2 \psi}{\partial z^2} \qquad \text{(on boundaries)}$$

Comparison with Equation (1-1) shows that again, $\phi = 0$ on the boundaries, so that ϕ itself must vanish in the entire domain.

APPENDIX 2

Hydrostatic Oscillatory Instability when the Prandtl Number is Unity

When the slope of the potential isotherms is small ($f\overline{U_z}/N^2 << 1$), then horizontal diffusion and the momentum of the vertical motions may be neglected, and Equation (6) is instead:

$$\left(\frac{\partial}{\partial t} - \nu\frac{\partial^2}{\partial z^2}\right)^2\frac{\partial^2\psi}{\partial z^2} = -2f\overline{U_z}\,\frac{\partial^2\psi}{\partial y\partial z} - N^2\,\frac{\partial^2\psi}{\partial y^2}$$

$$- f\overline{\eta}\,\frac{\partial^2\psi}{\partial z^2} \qquad (2\text{-}1)$$

Since (2-1) is linear with constant coefficients, the time dependence may be separated as follows:

$$\psi = e^{\sigma t}\Psi(y,z)$$

in which both σ and Ψ may be complex. If this form of the streamfunction is substituted into Equation (2-1) and the entire equation is then multiplied through by the complex conjugate of Ψ and integrated between the boundaries in the vertical and across one wavelength in the horizontal, the result is:

$$\sigma^2 \int_0^H\int_0^L \Psi^* \frac{\partial^2\Psi}{\partial z^2} - 2\sigma\nu \int_0^H\int_0^L \Psi^* \frac{\partial^4\Psi}{\partial z^4} + \nu^2 \int_0^H\int_0^L \Psi^* \frac{\partial^6\Psi}{\partial z^6}$$

$$= -2f\overline{U_z} \int_0^H\int_0^L \Psi^* \frac{\partial^2\Psi}{\partial y\partial z} - N^2 \int_0^H\int_0^L \Psi^* \frac{\partial^2\Psi}{\partial y^2}$$

$$- f\overline{\eta} \int_0^H\int_0^L \Psi^* \frac{\partial^2\Psi}{\partial z^2}$$

where Ψ^* is the complex conjugate of Ψ. If one applies the free-slip boundary conditions

$$\Psi = \frac{\partial^2\Psi}{\partial z^2} = \frac{\partial^4\Psi}{\partial z^4} = 0 \qquad \text{at } z=0,H$$

the preceding equation may be transformed, through integration by parts, to:

$$-\sigma^2 \int_0^H\int_0^L \left|\frac{\partial\Psi}{\partial z}\right|^2 - 2\sigma\nu \int_0^H\int_0^L \left|\frac{\partial^2\Psi}{\partial z^2}\right|^2 - \nu^2 \int_0^H\int_0^L \left|\frac{\partial^3\Psi}{\partial z^3}\right|^2$$

$$= 2f\overline{U_z} \int_0^H\int_0^L \left(\frac{\partial\Psi_r}{\partial z}\frac{\partial\Psi_r}{\partial y} + \frac{\partial\Psi_i}{\partial z}\frac{\partial\Psi_i}{\partial y}\right)$$

$$+ N^2 \int_0^H\int_0^L \left|\frac{\partial\Psi}{\partial y}\right|^2 + f\overline{\eta} \int_0^H\int_0^L \left|\frac{\partial\Psi}{\partial z}\right|^2$$

in which Ψ_r and Ψ_i are the real and imaginary parts of Ψ (i.e., $\Psi = \Psi_r + i\Psi_i$) and the vertical bars denote absolute values of the functions. All the integrals of the above equation are real, as are all the coefficients except σ. If σ is expanded into real and imaginary parts;

$$\sigma = \sigma_r + i\sigma_i$$

and the imaginary parts of the preceding equation are equated, the result is:

$$\sigma_i\sigma_r \int_0^H\int_0^L \left|\frac{\partial\Psi}{\partial z}\right|^2 = -\nu\sigma_i \int_0^H\int_0^L \left|\frac{\partial^2\Psi}{\partial z^2}\right|^2 \qquad (2\text{-}2)$$

Both the integrands in this expression are real and positive. It is therefore evident that if the growth rate σ_r is either zero or positive, then the only solution of the above is

$$\sigma_i = 0$$

We conclude that oscillations are not possible under hydrostatic conditions when the Prandtl Number is 1 unless the disturbances are decaying.

In fact, the preceding conclusion applies as well to

the non-hydrostatic case when P=1. If the slope of the potential isotherms is not small, Equation (2-2) becomes instead:

$$\sigma_i\sigma_r \int_0^H\int_0^L \left(\left|\frac{\partial\Psi}{\partial z}\right|^2 + \left|\frac{\partial\Psi}{\partial y}\right|^2\right) = -\nu\sigma_i \int_0^H\int_0^L \left(\left|\frac{\partial^2\Psi}{\partial z^2}\right|^2 + 2\left|\frac{\partial^2\Psi}{\partial y\partial z}\right|^2 + \left|\frac{\partial^2\Psi}{\partial y^2}\right|^2\right)$$

Since the integrands are, again, both real and positive, the same arguments apply as in the previous discussion. It is always true that when P=1,

If $\sigma_r \geq 0$, then $\sigma_i = 0$.

APPENDIX 3

Proof of the Variational Theorem for No-Slip Boundaries

If the parameter T, as expressed by Equation (33),

$$T = \frac{-\frac{1}{4\chi_i}\int_0^1\int_0^L \left(\frac{\partial F}{\partial z}\right)^2 + \int_0^1\int_0^L (\chi_i - 1)\left(\frac{\partial \psi}{\partial y}\right)^2}{\int_0^1\int_0^L \left(\frac{\partial^3 \psi}{\partial y \partial z^2}\right)^2} = \frac{I_1}{I_2}$$

is maximized with respect to F and ψ, each of which satisfy the boundary conditions (28) and the relations (31) and (32), then it may be shown that F and ψ satisfy the original perturbation equations. The condition that T be a maximum is

$$\delta T = \frac{1}{I_2}(\delta I_1 - T\delta I_2) = 0 \qquad (3\text{-}1)$$

From Equation (33),

$$\delta I_1 = -\frac{1}{2\chi_i}\int_0^1\int_0^L \frac{\partial F}{\partial z}\,\delta\frac{\partial F}{\partial z} + 2(\chi_i - 1)\int_0^1\int_0^L \frac{\partial \psi}{\partial y}\,\delta\frac{\partial \psi}{\partial y}$$

$$= \frac{1}{2\chi_i}\int_0^1\int_0^L F\delta\frac{\partial^2 F}{\partial z^2} + 2(\chi_i - 1)\int_0^1\int_0^L \frac{\partial \psi}{\partial y}\,\delta\frac{\partial \psi}{\partial y}$$

By Equation (31),

$$\frac{\partial^2 F}{\partial z^2} = -2\chi_i \frac{\partial^2 \psi}{\partial y \partial z} - 4\chi_i \frac{\partial^2 \psi}{\partial y^2}$$

so that

$$\delta I_1 = -\int_0^l \int_0^L F\left(\frac{\partial^2 \psi}{\partial y \partial z} + 2\frac{\partial^2 \psi}{\partial y^2}\right) + 2(\chi_i - 1)\int_0^l \int_0^L \frac{\partial \psi}{\partial y}\delta\frac{\partial \psi}{\partial y}$$

Using integration by parts and the boundary conditions,

$$\delta I_1 = -\int_0^l \int_0^L \left[\frac{\partial^2 F}{\partial y \partial z} + 2\frac{\partial^2 F}{\partial y^2} + 2(\chi_i - 1)\frac{\partial^2 \psi}{\partial y^2}\right]\delta\psi$$

and also,

$$\delta I_2 = \int_0^l \int_0^L 2\frac{\partial^3 \psi}{\partial y \partial z^2}\delta\frac{\partial^3 \psi}{\partial y \partial z^2} = -2\int_0^l \int_0^L \frac{\partial^6 \psi}{\partial y^2 \partial z^4}\delta\psi$$

Therefore, by Equation (3-1),

$$\delta I_1 - T\delta I_2 = \int_0^l \int_0^L \left[\frac{\partial F}{\partial z} + 2\frac{\partial F}{\partial y} + 2(\chi_i - 1)\frac{\partial \psi}{\partial y}\right.$$

$$\left. - 2T\frac{\partial^5 \psi}{\partial y \partial z^4}\right]\delta\frac{\partial \psi}{\partial y} = 0$$

For an arbitrary variation $\delta(\partial\psi/\partial y)$, the above can only be

true if

$$\frac{\partial F}{\partial z} + 2\frac{\partial F}{\partial y} + 2(\chi_i - 1)\frac{\partial \psi}{\partial y} - 2T\frac{\partial^5 \psi}{\partial y \partial z^4} = 0 \qquad (3\text{-}2)$$

By Equations (32) and (30),

$$\frac{\partial F}{\partial z} = \frac{\partial \psi}{\partial z} + 2\chi_i \frac{\partial \psi}{\partial y} + T\frac{\partial^5 \psi}{\partial z^5}$$

$$\frac{\partial F}{\partial y} = \frac{\partial^2 u}{\partial y \partial z} + T\frac{\partial^5 \psi}{\partial y \partial z^4}$$

The above are substituted into Equation (3-2) with the result that

$$\frac{\partial \psi}{\partial z} + 4\chi_i \frac{\partial \psi}{\partial y} + T\frac{\partial^5 \psi}{\partial z^5} - 2\frac{\partial \psi}{\partial y} + 2\frac{\partial^2 u}{\partial y \partial z} = 0$$

If this expression is differentiated once with respect to z and use is made of Equation (30),

$$\frac{\partial^2 u}{\partial z^2} = \frac{\partial \psi}{\partial z} + 2\chi_i \frac{\partial \psi}{\partial y}$$

then we arrive at the expression

$$T\frac{\partial^6 \psi}{\partial z^6} + 4\chi_i \frac{\partial^2 \psi}{\partial y \partial z} + 4\chi_i \frac{\partial^2 \psi}{\partial y^2} + \frac{\partial^2 \psi}{\partial z^2} = 0$$

This is exactly the original perturbation Equation (9) with P=1. It is therefore true that any function ψ, together with a corresponding function F, that satisfies the boundary conditions and maximizes T in (33) is a solution of the governing set of equations.

APPENDIX 4

Orthogonal Functions Satisfying No-Slip Boundary Conditions*

In order to solve the variational expression (34), it is necessary to construct a Fourier Series of orthogonal functions that satisfy, term by term, the boundary conditions

$$\psi = \frac{\partial \psi}{\partial z} = \frac{\partial^4 \psi}{\partial z^4} = \frac{\partial^5 \psi}{\partial z^5} = 0 \quad \text{at } z = -1/2,\ 1/2$$

It may be shown that functions G satisfying the equation

$$\frac{d^4 G}{dz^4} = \alpha^4 G \tag{4-1}$$

and the boundary conditions

$$G = \frac{dG}{dz} = 0 \qquad \text{at } z = -1/2,\ 1/2 \tag{4-2}$$

are orthogonal, and <u>incidentally</u> satisfy the conditions

---

* This section follows a discussion of Chandrasekhar (1961, Appendix V).

$$\frac{d^4G}{dz^4} = \frac{d^5G}{dz^5} = 0 \qquad \text{at } z = -1/2,\ 1/2 \qquad (4\text{-}3)$$

If α_i is a characteristic value associated with a function G_i satisfying (4-1) and (4-2), then

$$\frac{d^4G_i}{dz^4} = \alpha_i{}^4 G_i$$

Now suppose the above is multiplied through by a function G_j (belonging to a characteristic value α_j), and integrated between the boundaries:

$$\int_{-\frac{1}{2}}^{\frac{1}{2}} G_j \frac{d^4G_i}{dz^4} = \alpha_i{}^4 \int_{-\frac{1}{2}}^{\frac{1}{2}} G_iG_j$$

Using the boundary conditions (4-2) and integration by parts, the preceding may be rewritten:

$$\int_{-\frac{1}{2}}^{\frac{1}{2}} \frac{d^2G_j}{dz^2} \frac{d^2G_i}{dz^2} = \alpha_i{}^4 \int_{-\frac{1}{2}}^{\frac{1}{2}} G_jG_i$$

Since, in general, α_i will not be equal to α_j, it is evident that

$$\int_{-\frac{1}{2}}^{\frac{1}{2}} G_iG_j = \delta_{ij}$$

The functions G_i are therefore orthogonal.

Equation (4-1) is readily solved. Applying the boundary conditions (4-2), one may find sets of even and odd solutions C_m and S_m:

$$C_m \equiv \frac{\cos\lambda_m z}{\cos\lambda_m/2} - \frac{\cosh\lambda_m z}{\cosh\lambda_m/2}$$

$$S_m \equiv \frac{\sin\mu_m z}{\sin\mu_m/2} - \frac{\sinh\mu_m z}{\sinh\mu_m/2} \qquad (4-4)$$

where the λ_m's and μ_m's are roots of the equations

$$\tanh \lambda/2 + \tan \lambda/2 = 0$$

and

$$\coth \mu/2 - \cot \mu/2 = 0$$

Tabulated values of λ and μ may be found in Chandrasekhar (1961), page 636.

As the functions C and S satisfy (4-1), it is evident that if either vanishes at the boundaries, then d^4C/dz^4 and d^4S/dz^4 also vanish. Similarly, if (4-1) is differentiated once, then the condition

$$\frac{dG}{dz} = 0 \qquad \text{at boundaries}$$

implies that

$$\frac{d^5G}{dz^5} = 0 \qquad \text{at boundaries}$$

Therefore, the functions S and C constitute orthogonal sets that satisfy the boundary conditions (4-2) and (4-3).

APPENDIX 5

Inertial Stability of Ekman Layer Flow

The perturbation equations for two-dimensional disturbances aligned with the $\hat{x}$ axis in incompressible Ekman layer flow consist of three momentum equations and the continuity equation:

$$\left(\frac{\partial}{\partial t} + \bar{V}\frac{\partial}{\partial y} - \nu\nabla^2\right)u = fv - \overline{U_z}\, w$$

$$\left(\frac{\partial}{\partial t} + \bar{V}\frac{\partial}{\partial y} - \nu\nabla^2\right)v = -fu - \frac{\partial p}{\partial y} - \bar{V}_z w$$

$$\left(\frac{\partial}{\partial t} + \bar{V}\frac{\partial}{\partial y} - \nu\nabla^2\right)w = -\frac{\partial p}{\partial z}$$

$$\frac{\partial v}{\partial y} + \frac{\partial w}{\partial z} = 0$$

where u, v, and w are the perturbation cartesian velocity components, and p is the perturbation pressure normalized by the fluid density. The quantities $\bar{U}$ and $\bar{V}$ are the cartesian components of the unperturbed Ekman flow:

$$\bar{U} = U_g(1 - \cos z e^{-z})$$

$$\bar{V} = U_g \sin z e^{-z}$$

Here, the vertical coordinate z has been non-dimensionalized by the Ekman depth

$$\delta \equiv \left(\frac{2\nu}{f}\right)^{1/2}$$

A streamfunction may be defined from the continuity equation:

$$v \equiv -\frac{\partial \psi}{\partial z} \qquad\qquad w \equiv \frac{\partial \psi}{\partial y}$$

The three momentum equations may be combined into a sixth-order partial differential equation for the streamfunction:

$$\left(\frac{\partial}{\partial t} + \bar{V}\frac{\partial}{\partial y} - \nu\nabla^2\right)^2\nabla^2\psi = -f^2\frac{\partial^2\psi}{\partial z^2}$$

$$- f\frac{\partial}{\partial z}\left(\overline{U_z}\frac{\partial \psi}{\partial y}\right) \qquad (5\text{-}1)$$

$$- \left(\frac{\partial}{\partial t} + \bar{V}\frac{\partial}{\partial y} - \nu\nabla^2\right)\frac{\partial}{\partial z}\left(\overline{V_z}\frac{\partial \psi}{\partial y}\right)$$

According to the assumptions outlined in Chapter 6-d, we take both $\bar{V}$ and $\overline{U_z}$ to be constants equal to the mean of each quantity over the non-dimensional depth H:

$$\bar{V} \simeq \frac{1}{H}\int_0^H U_g \sin z e^{-z} dz = \frac{U_g}{2H}\left[1 - e^{-H}(\sin H + \cos H)\right] \qquad (5\text{-}2)$$

$$\overline{U_z} \simeq \frac{1}{H}\int_0^H \frac{\partial u}{\partial z}\,dz = \frac{\bar{U}(H)}{H} = \frac{U_g(1-\cos H e^{-H})}{\delta H} \simeq \frac{U_g}{\delta H} \qquad (5\text{-}3)$$

The last approximation in (5-3) above is made assuming that $e^{-H} << 1$. This assumption is supported by Lilly's (1966) complete eigenanalysis, which indicates that the parallel disturbances extend well above the nominal boundary layer depth.

We choose a coordinate system that moves in the $\hat{y}$ direction at the constant velocity $\bar{V}$, so that in this frame, Equation (5-1) reduces to:

$$(\frac{\partial}{\partial t} - \nu\nabla^2)^2\nabla^2\psi = -f^2\frac{\partial^2\psi}{\partial z^2} - f\overline{U_z}\frac{\partial^2\psi}{\partial y\partial z}$$

If we normalize the time variable t by the Coriolis parameter, and both spatial coordinates by a quantity $H(2\nu/f)^{1/2}$, in which H is a non-dimensional vertical depth, then the preceding becomes:

$$(\frac{\partial}{\partial t} - \frac{1}{2H^2}\nabla^2)^2\nabla^2\psi = -\frac{\partial^2\psi}{\partial z^2} - \frac{\overline{U_z}}{f}\frac{\partial^2\psi}{\partial y\partial z}$$

Substituting expression (5-3) for $\overline{U_z}$ and $2\nu/\delta^2$ for f, the above may be written:

$$(\frac{\partial}{\partial t} - \frac{1}{2H^2}\nabla^2)^2\nabla^2\psi = -\frac{\partial^2\psi}{\partial z^2} - \frac{Re}{2H}\frac{\partial^2\psi}{\partial y\partial z} \qquad (5\text{-}4)$$

where the Reynolds number is defined:

$$Re \equiv \frac{U_g \delta}{\nu}$$

Equation (5-4) may be solved as a characteristic value problem for the critical value of Re, provided that the time dependence and boundary conditions are defined. For simplicity, we use rigid, free-slip boundary conditions at the non-dimensional vertical coordinates 0 and 1. These are:

$$\psi \ , \ \frac{\partial^2 \psi}{\partial z^2} \ , \ \frac{\partial^4 \psi}{\partial z^4} = 0 \qquad \text{at } z=0,1 \tag{5-5}$$

The marginal state is defined as $\partial/\partial t = 0$, unless the instabilities begin as oscillations. This possibility may be excluded entirely following arguments exactly parallel to those expounded in Appendix 2. (Equation (2-1) has the same form as (5-4), except that the term multiplied by N^2 is missing in the latter instance.)

For the marginal state, then, (5-4) becomes:

$$\frac{1}{4H^4} (\nabla^2)^3 \psi = - \frac{\partial^2 \psi}{\partial z^2} - \frac{Re}{2H} \frac{\partial^2 \psi}{\partial y \partial z} \tag{5-6}$$

In order to solve the above for the characteristic

value of the critical Reynolds number, it is necessary to estimate the height H at which to place the upper boundary. As discussed in Chapter 6-d, we take this height to be the level below which the kinetic energy available to the disturbances from the constant mean shear is identical to that available from the actual shear.

The available kinetic energy is (see Chapter 6):

$$AKE \equiv \overline{U^2} - \overline{U}^2$$

For the approximate shear used in the stability analysis,

$$\overline{U} = \delta z \overline{U_z} = \frac{U_g}{H} z$$

Then,

$$\overline{U^2} = \frac{1}{H} \int_0^H \frac{U_g^2}{H^2} z^2 dz = \frac{1}{3} U_g^2$$

and

$$\overline{U}^2 = \left[\frac{1}{H} \int_0^H \frac{U_g}{H} z \, dz \right]^2 = \frac{1}{4} U_g^2$$

For the approximated flow, then,

$$AKE_1 = \overline{U^2} - \overline{U}^2 = \frac{1}{12} U_g^2 \qquad (5\text{-}7)$$

In the actual Ekman flow, the component of flow in the $\hat{x}$ direction is:

$$u = U_g[1 - \cos z e^{-z}]$$

The mean-square flow is then:

$$\overline{U^2} = \frac{1}{H}\int_0^H U_g^2[1 - \cos z e^{-z}]^2 dz$$

$$= U_g^2\left[1 - \frac{5}{8H} + \frac{1}{H}(e^{-H}(\cos H - \sin H) - \frac{1}{4} e^{-2H}(1 + \right.$$

$$\left. + \frac{1}{2}(\cos 2H - \sin 2H))\right]$$

and the square-mean flow is:

$$\overline{U}^2 = \left[\frac{1}{H}\int_0^H U_g[1 - \cos z e^{-z}]dz\right]^2$$

$$= U_g^2\left[(1 - \frac{1}{2H})^2 - (1 - \frac{1}{2H})\frac{e^{-H}}{H}(\sin H - \cos H)\right.$$

$$\left. + \frac{e^{-2H}}{4H^2}(1 - \sin 2H)\right]$$

The available kinetic energy of the Ekman flow is then:

$$AKE_2 = \overline{U^2} - \overline{U}^2 = U_g^2 \left[\frac{3}{8H} - \frac{1}{4H^2} - \frac{1}{2H^2} e^{-H}(\sinH - \cosH) \right.$$

$$- \frac{e^{-2H}}{4H^2} (1 - \sin2H)$$

$$\left. - \frac{1}{4H} e^{-2H}(1 + \frac{1}{2} (\cos2H - \sin2H)) \right] \qquad (5\text{-}8)$$

The level below which the approximate value of the available kinetic energy is equal to the real value is defined by equating (5-7) with (5-8). If we assume that the value of H is greater than about 3 ($e^{-H} << 1$), we may neglect the transcendental terms of the resulting equation. (This assumption will be justified a posteri.) The equation for H becomes approximately:

$$\frac{2}{3} H^2 - 3H + 2 = 0$$

or

$$H = \frac{1}{4} [9 \pm \sqrt{33}]$$

We choose the larger of the above roots to be consistent with the assumption $e^{-H} << 1$, and also because this larger

value is in good agreement with Faller's (1965) observation that the vertical velocity of boundary layer disturbances vanishes at roughly 4δ. (Also see the numerical results of Lilly, 1966.) Therefore, we take

$$H \simeq 3.69$$

We use this value of H in Equation (5-6) together with the boundary conditions (5-5) and obtain the critical value of the Reynolds number.

Equation (5-6) has exactly the form of Equation (10) for inertial instability in neutrally stratified shear flow. The third-order variational solution of the latter is given by Equation (24), which will also yield solutions to (5-6) if we take

$$T = \frac{1}{4H^4}$$

$$\chi_{ii} = \frac{Re}{2H}$$

Since T is $O(10^{-3})$, the third-order variational method will be accurate to within about 0.8% (see Table 2, Chapter 4). The resulting critical Reynolds number is:

$$Re_c = 54.5$$

This corresponds to a wavelength of 2.19H (= 8.07δ dimensionally). The mean normal component of the flow in the Ekman layer between the lower boundary and H = 3.69δ is:

$$\overline{V} = .14\ U_g$$

Since the instability does not contain an oscillatory component, this value represents the phase speed of the disturbances in this simplified treatment.

APPENDIX 6

Convergence of the Variational Results and Comparison with Those of Walton (1975)

It is of interest to compare the results obtained using the variational method with the asymptotic solutions of Walton (1975), which are valid when $T^{1/6} << 1$. In order to extend the region of validity of the variational solution to encompass sufficiently small values of T, so that an overlap is obtained with Walton's results, it is necessary to carry more terms of the Fourier series in order that the rapidly varying structure functions associated with the low viscosity flow are adequately described. As T becomes very small, the presence of the boundaries has a decreasing effect on the inertial circulations, and the difference between the results obtained using free-slip boundaries and those using no-slip boundaries becomes minimal.

The convergence of the variational method for small values of T is tested by comparing solutions obtained using successively higher numbers of terms in the Fourier series. We compare eigenvalues associated with Fourier series of 4, 6, 8, and 10 terms respectively. The ratio of the $N^{\underline{th}}$ order approximation of χ_i to the approximation of two orders lower is illustrated in Figures A6-1 and A6-2 for free-slip and no-slip boundaries respectively.

(Note the different scales along the ordinates.)

Reasonably good convergence is indicated for values of T as small as 10^{-8} for both sets of solutions; it is felt that the 10^{th} order approximation to χ_i is correct to three significant figures in the range of T illustrated. While the quality of the free-slip solution improves monotonically for increasing T, it appears that the no-slip solution has a maximum rate of convergence for a definite value of T, which decreases as the order of the approximation increases. This phenomenon is interpreted as an indication that the structural complexity of the no-slip solution increases when the flow becomes highly viscous, thus necessitating a longer Fourier series. Both sets of solutions favor higher wavenumbers as the viscosity of the flow becomes very small.

Having acquired some confidence in the rate of convergence of the solutions when T is very small, we are now in a position to compare the variational solutions with the asymptotic results of Walton. In the range of T for which the latter are valid, the type of boundary condition has little influence on the solutions and, in fact, Walton's method only requires the boundaries to be rigid and does not distinguish between free-slip and no-slip boundaries.

Figures A6-3 and A6-4 illustrate both Walton's results and those obtained using the variational method to 10^{th} order. (The no-slip boundary condition was used in the latter since the rate of convergence is slightly better in this range of T. The free-slip solutions are very nearly identical.) Walton's results should deteriorate as T increases, while the variational solutions improve. Since the two results converge as T decreases, one may infer that the 10^{th} order variational result is indeed valid down to at least $T = 10^{-8}$.

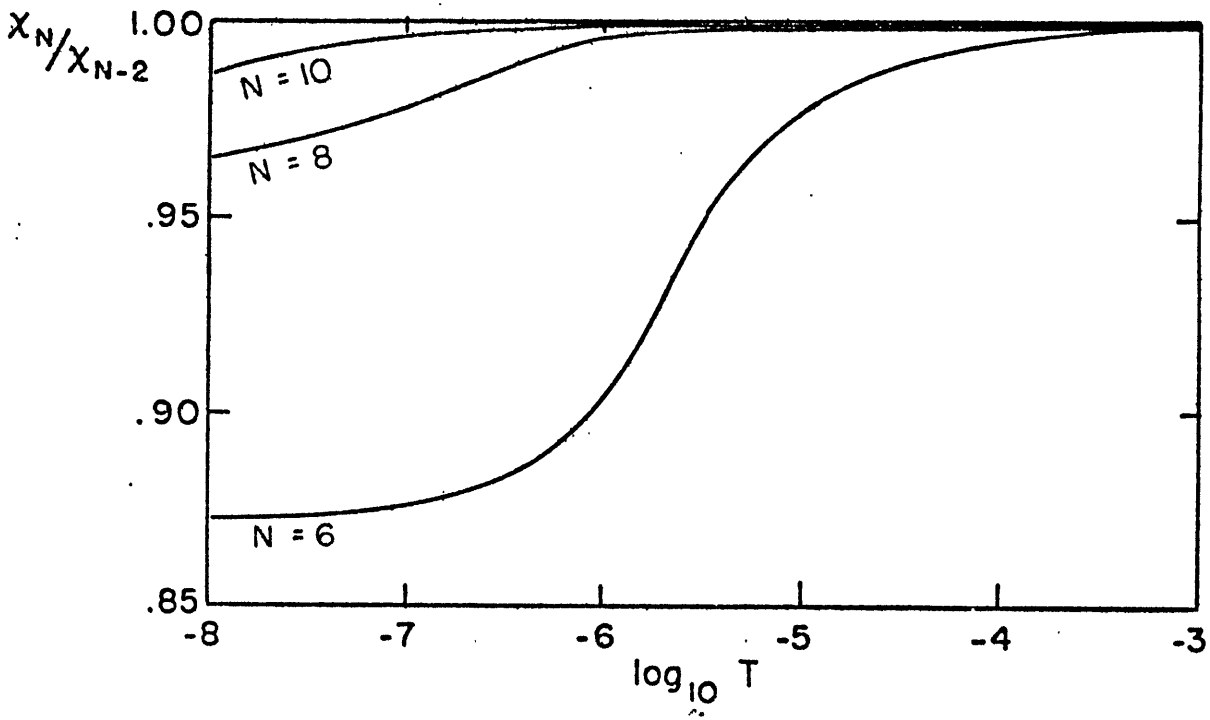

Figure A 6-1: Ratio of the N^{th} order approximation of χ_i with the approximation of two orders lower for various values of N. Boundaries are free-slip.

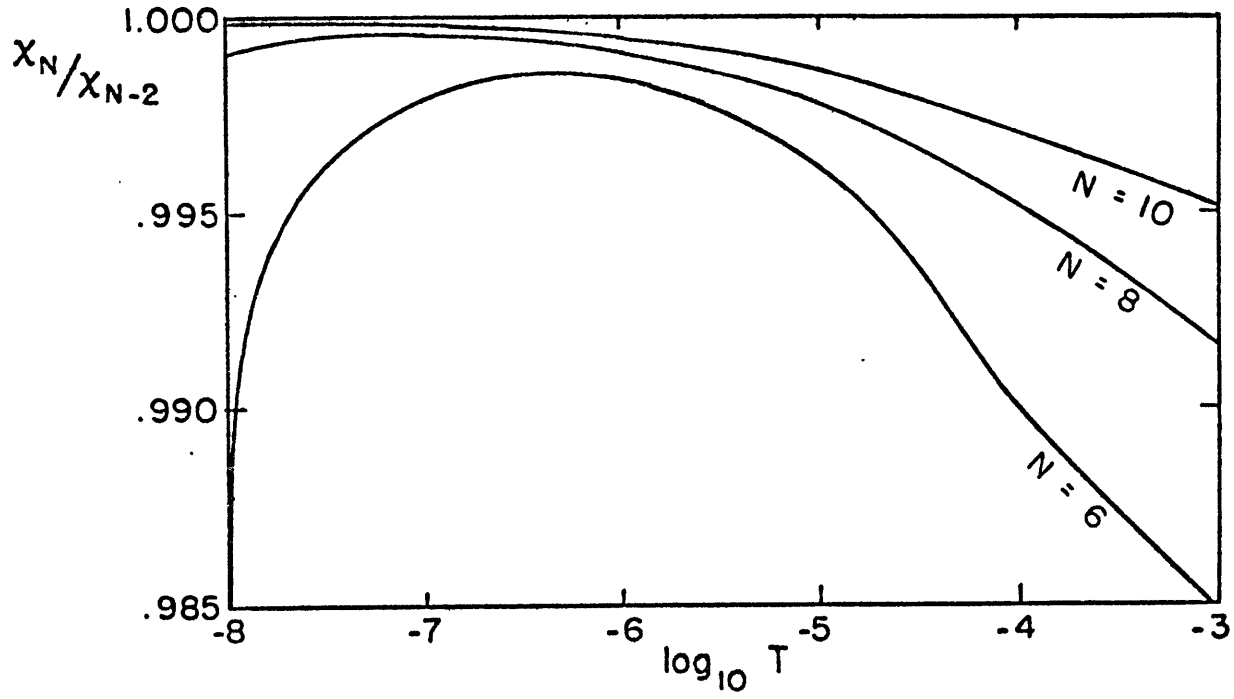

Figure A 6-2: Same as figure A 6-1 but for no-slip boundaries.

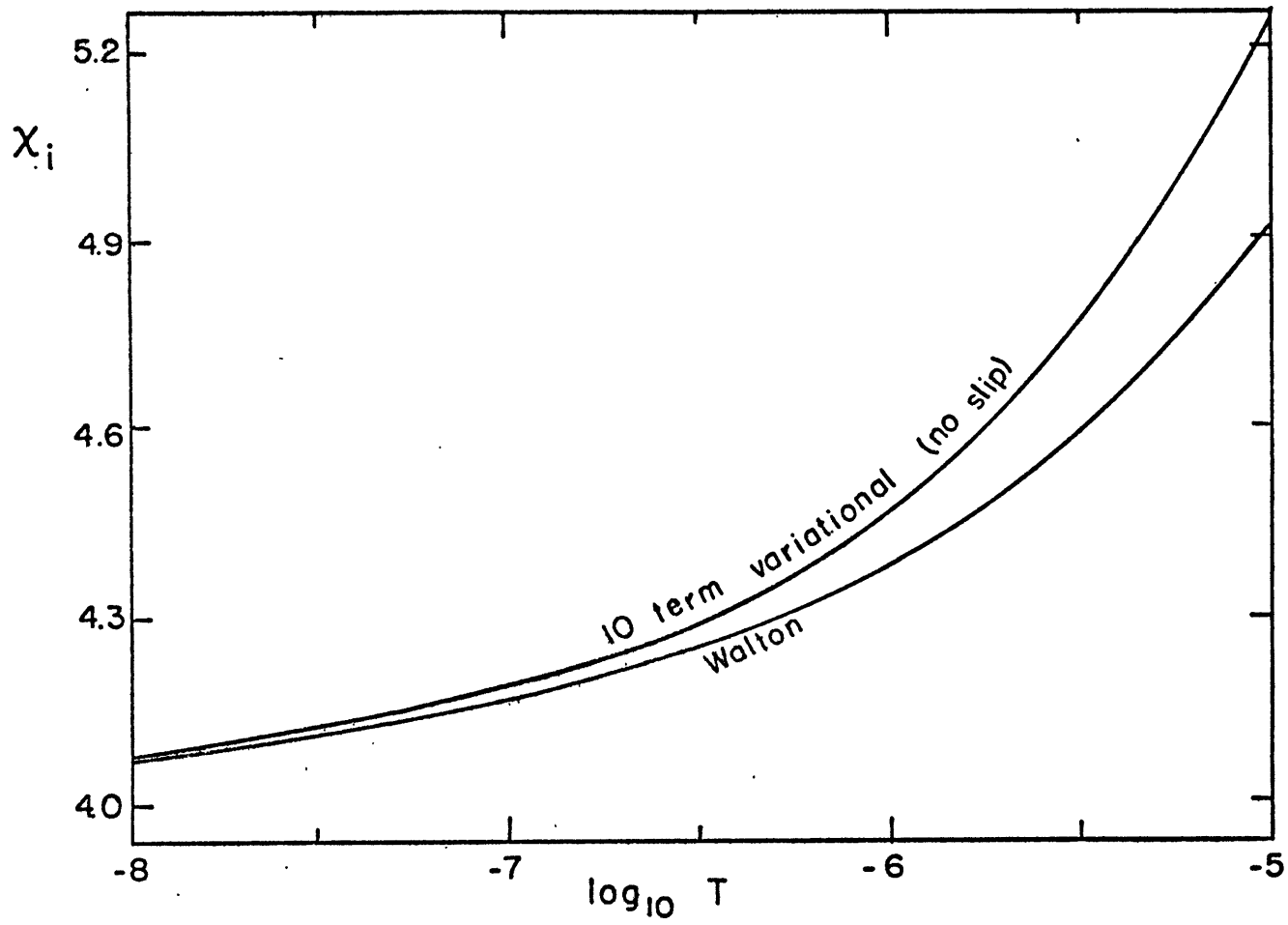

Figure A 6-3: Comparison of the asymptotic solution for the inertial stability parameter χ_1 obtained by Walton with the corresponding 10^{th} order variational solution.

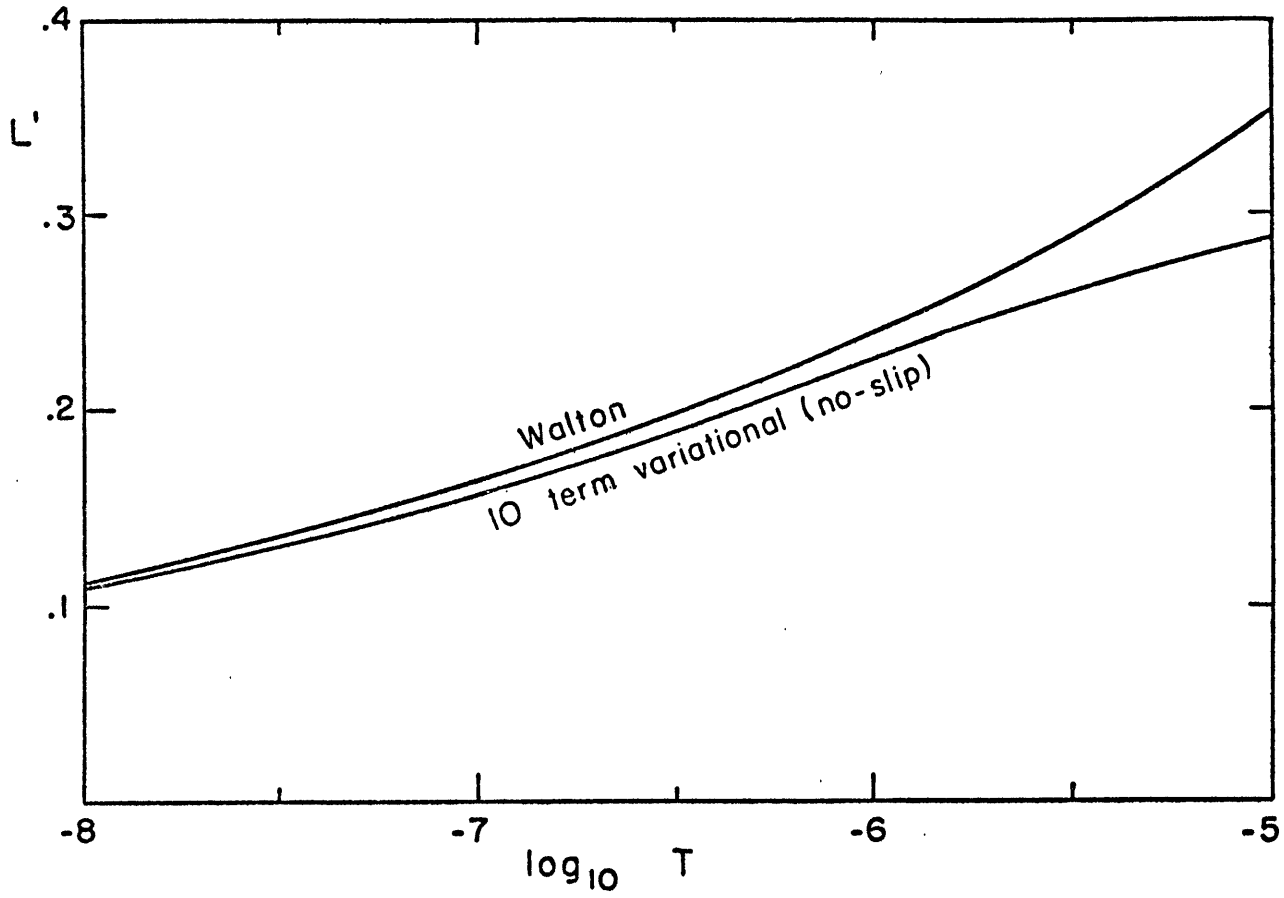

Figure A 6-4: Non-dimensional wavelength L' at which instability first begins, associated with the characteristic values of χ_1 illustrated in figure A 6-3.

BIBLIOGRAPHY

Andre, M.J., 1949: "Distribution of instability weather types with respect to summer cold fronts in the United States", Bull. Amer. Met. Soc., 30, pgs. 228-230.

Boucher, R.J. and R. Wexler, 1961: "The motion and predictability of precipitation lines", J. Meteor., 18, pgs. 160-171.

Breiland, J.G., 1958: "Meteorological conditions associated with the development of instability lines", J. Meteor., 15, pgs. 297-302.

Brown, J.A., 1969: "A numerical investigation of hydrodynamic instability and energy conversions in the quasi-geostrophic atmosphere", Part I - J. Atmos. Sci., 26, pgs. 352-365; Part II - J. Atmos. Sci., 26, pgs. 366-375.

Browning, K.A. and F.H. Ludlam, 1962: "Airflow in convective storms", Q.J.R.M.S., 88, pgs. 117-135.

Byers, H.R., 1951: "Thunderstorms", in Compendium of Meteorology, Amer. Met. Soc., Waverly Press Inc., Baltimore.

Byers, H.R. and R.R. Braham, 1949: "The Thunderstorm", U.S. Govt. Print. Off., Washington, D.C., 287 pp.

Carlson, T.N. and F.H. Ludlam, 1968: "Conditions for the occurrence of severe local storms", Tellus, 20, pgs. 203-226.

Chandrasekhar, S., 1961: Hydrodynamic and Hydromagnetic Stability, Oxford University Press, London.

Charney, J.G., 1947: "The dynamics of long waves in a baroclinic westerly current", J. Meteor., 4, pgs. 135-162.

Clark, T.L. and R. List, 1971: "Dynamics of a falling particle zone", J. Atmos. Sci., 28, pgs. 718-727.

Cotton, W.; R.A. Pielke, and P.T. Gannon, 1976: "Numerical experiments on the influence of the mesoscale circulation on the cumulus scale", J. Atmos. Sci., 33, pgs. 252-261.

Eisen, P.A., 1972: "A mesoscale study of the Oklahoma squall line of 8 and 9 June, 1966", M.S. Thesis, Penn. State Univ. Dept. of Met., 88 pgs.

Enlich, R.M. and R.L. Mancuso, 1968: "Objective analysis of environmental conditions associated with severe thunderstorms and tornadoes", Mon. Wea. Rev., 96, pgs. 342-350.

Faller, A.J., 1965: "Large eddies in the atmospheric boundary layer and their possible role in the formation of cloud rows", J. Atmos. Sci., 22, pgs. 176-184.

Fankhauser, J.C., 1969: "Convective processes resolved by a mesoscale rawinsonde network", J. App. Met., 8, pgs. 778-798.

Fujita, T., 1955: "Results of detailed synoptic studies of squall lines", Tellus, 7, pgs. 405-436.

Fulks, J.R., 1951: "The instability line", in Compendium of Meteorology, Amer. Met. Soc., Waverly Press Inc., Baltimore.

Gordon, N.D., 1978: "Numerical simulation of a long-lasting mesoscale convective line", Ph.D. Thesis, Mass. Inst. of Tech. Dept. of Met.

Greenspan, H.P., 1968: The Theory of Rotating Fluids, Cambridge University Press, London.

Houze, R.A., Jr., 1975: "Squall lines observed in the vicinity of the Researcher during Phase III of GATE", Preprints of the 16th Radar Meteorology Conference, Houston, pgs. 206-209, Amer. Met. Soc.

Houze, R.A., Jr., 1977: "Structure and dynamics of a tropical squall-line system", Mon. Wea. Rev., 105, pgs. 1540-1567.

Hoxit, L.R. and C.F. Chappell, 1975: "An analysis of the mesoscale circulations which produced the April 3, 1974 tornadoes in Northern Indiana", Ninth Conference on Severe Local Storms, Norman, Oklahoma, pgs. 256-263, Amer. Met. Soc.

Kuettner, J., 1971: "Cloud bands in the earth's atmosphere", Tellus, 23, pgs. 404-426.

Kuo, H-L, 1949: "Dynamic instability of two-dimensional nondivergent flow in a barotropic atmosphere", J. Meteor., 6, pgs. 105-122.

Kuo, H-L, 1954: "Symmetrical disturbances in a thin layer of fluid subject to a horizontal temperature gradient and rotation", J. Meteor., 11, pgs. 399-411.

Lilly, D.K., 1966: "On the instability of Ekman boundary flow", J. Atmos. Sci., 23, pgs. 481-494.

Ludlam, F.H., 1963: "Severe Local Storms: A Review" in Meteorological Monograph 5, No. 27, Amer. Met. Soc.

McGinley, J.A. and Y.K. Sasaki, 1975: "The role of symmetric instabilities in thunderstorm development on drylines", Ninth Conference on Severe Local Storms, Norman, Oklahoma, pgs. 173-180, Amer. Met. Soc.

McIntyre, M.E., 1969: "Diffusive destabilization of the baroclinic circular vortex", Geo. Fluid Dyn., 1, pgs. 19-58.

McLean, G.S., 1961: "Observations of severe convective activity in a squall line", Bull. Amer. Met. Soc., 42, pgs. 252-264.

Moncrieff, M.W. and M.J. Miller, 1976: "The dynamics and simulation of tropical cumulonimbus and squall lines", Q.J.R.M.S., 102, pgs. 373-394.

Newton, C.W., 1950: "Structure and mechanism of the prefrontal squall line", J. Meteor., 7, pgs. 210-222.

Newton, C.W., 1963: "Dynamics of Severe Convective Storms", in Meteorological Monograph 5, No. 27, Amer. Met. Soc.

Newton, C.W., 1966: "Circulations in large sheared cumulonimbus", Tellus, 18, pgs. 700-713.

Paine, P.A. and M.L. Kaplan, 1976: "An equivalent potential vorticity theory applied to the analysis and prediction of severe storm dynamics", Preprints of the 6th conference on weather forecasting and analysis, Albany, pgs. 98-105, Amer. Met. Soc.

Pellew, A. and R.V. Southwell, 1940: "On maintained convective motion in a fluid heated from below", Proc. Roy. Soc. of London, A, 176, pgs. 312-343.

Pestaina-Haynes, M. and G.L. Austin, 1976: "Comparison between maritime tropical (GATE and Barbados) and continental mid-latitude (Montreal) precipitation lines", J. App. Meteor., 15, pgs. 1077-1082.

Porter, J.M.; L. L. Means, J.E. Hovde, and W.B. Chappell, 1955: "A synoptic study of squall lines in the north-central United States", Bull. Amer. Met. Soc., 36, pgs. 390-396.

Ramaswamy, C., 1956: "On the sub-tropical jet stream and its role in the development of large-scale convection", Tellus, 8, pg. 26.

Rayleigh, 1880: "On the stability of certain fluid motions", Scientific Papers Vol. I, Dover, pgs. 474-487.

Rayleigh, 1916: "On the dynamics of revolving fluids", Proc. of the Roy. Soc. of London, A, 93.

Raymond, D.J., 1977: "Instability of the low level jet and severe storm formation", Preprints of the 10th conference on severe local storms, Omaha, pgs. 515-520, Amer. Met. Soc.

Sanders, F. and R.J. Paine, 1975" "The structure and dynamics of an intense mesoscale convective storm in Oklahoma", J. Atmos. Sci., 32, pgs. 1563-1579.

Sanders, F. and K.A. Emanuel, 1977: "The momentum budget and temporal evolution of a mesoscale convective system", J. Atmos. Sci., 34, pgs. 322-330.

Sasaki, Y.K., 1973: "Mechanism of squall line formation as suggested from variational analysis of hourly surface observations", Preprints of the 8th conference on severe local storms, Denver, pgs. 300-307, Amer. Met. Soc.

Schaefer, V.J. and W.E. Hubert, 1955: "A case study of jet stream clouds", Tellus, 7, pgs. 301-307.

Skaggs, R.H., 1967: "On the association between tornadoes and 500 mb indicators of jet streams", Mon. Wea. Rev., 95, pgs. 107-110.

Solberg, H., 1933: "Le mouvement d'inertie de L'atmosphère stable et son role dans la théorie des cyclones," Memoir presented to the Meteorological Association of the U.G.G.I. Lisbon, Dupont Press, Paris.

Stone, P.H., 1966: "On non-geostrophic baroclinic stability", J. Atmos. Sci., 23, pgs. 390-400.

Stone, P.H., 1971: "Baroclinic stability under non-hydrostatic conditions", J. Fluid Mech., 45, pgs. 659-671.

Stone, P.H., 1972: "On non-geostrophic baroclinic stability Part III. The momentum and heat transports", J. Atmos. Sci., 29, pgs. 419-426.

Stokes, J., 1976: "Heat, Moisture, and momentum budgets for an Oklahoma squall line", M.S. Thesis, Mass. Inst. of Tech.

Tatro, P.R. and E.L. Mollo-Christensen, 1967: "Experiments on Ekman layer instability", J. Fluid Mech., 28, pgs. 531-543.

Tracton, M.S., 1973: "The role of cumulus convection in the development of extratropical cyclones", Mon. Wea. Rev., 101, pgs. 573-593.

Walton, I.C., 1975: "The viscous nonlinear symmetric baroclinic instability of a zonal shear flow", J. Fluid Mech., 68, pgs. 757-766.

Williams, G.P., 1968: "Thermal convection in a rotating fluid annulus, Part 3: Suppresion of the frictional constraint on lateral boundaries", J. Atmos. Sci., 25, pgs. 1034-1045.

Woodcock, A., 1941: "Soaring over the open sea", Sci. Mon. 55, pgs. 226-232.

Yanai, M. and T. Tokioka, 1969: "Axially symmetric meridional motions in the baroclinic circular vortex: a numerical experiment", J. Met. Soc. Japan, 47, pgs. 183-198.

Zipser, E.J., 1977: "Mesoscale and convective-scale downdrafts as distinct components of squall-line structure", Mon. Wea. Rev., 105, pgs. 1568-1589.